International Journal of Heat and Mass Transfer 179 (2021) 121656

Contents lists available at ScienceDirect

International Journal of Heat and Mass Transfer

journal homepage: www.elsevier.com/locate/hmt

Review of Databases and Correlations for Saturated Flow Boiling Heat Transfer Coefficient for Cryogens in Uniformly Heated Tubes, and Development of New Consolidated Database and Universal Correlations

Vishwanath Ganesan[a], Raj Patel[a], Jason Hartwig[b], Issam Mudawar[a,*]

[a] Purdue University Boiling and Two-Phase Flow Laboratory (PU-BTPFL), School of Mechanical Engineering, Purdue University, 585 Purdue Mall, West Lafayette, IN 47907, U.S.A.

[b] NASA Glenn Research Center, Fluids and Cryogenics Branch, Cleveland, OH 44135, U.S.A.

ARTICLE INFO

Article history:
Received 17 March 2021
Revised 22 June 2021
Accepted 27 June 2021
Available online 28 July 2021

Keywords:
Heat transfer coefficient
Flow boiling
Cryogens
Saturated boiling
Universal correlations

ABSTRACT

Experiments to determine saturated flow boiling heat transfer coefficient (HTC) for cryogens in uniformly heated, round tubes have been performed throughout the globe during the past sixty years. However, experimental HTC data are either rarely published or made available only for a few cryogens, with majority remaining in the archives of authors, or in obscure technical reports of an organization or other inaccessible sources. In the present study, the Purdue University-Boiling and Two-Phase Flow Laboratory (PU-BTPFL) Cryogen Saturated Flow Boiling HTC Database is consolidated from world literature dating back to 1959. With 2505 local and 747 average data points for LHe I, para-LH_2, LNe, LN_2, LAr, and LCH_4, it represents the largest cryogen saturated flow boiling HTC database assembled to date. This database encompasses the controlled variables of tube diameter, from 0.47 to 14.1 mm, heated length-to-diameter ratio, 0.79 to 470.81, system pressure, 0.01 to 2.99 MPa, reduced pressure, 0.03 to 0.88, mass velocity, 7.89 to 1787.56 kg m^{-2} s^{-1}, and heat flux, 0.01 to 223.2 kW m^{-2}. Using this database, distinct physics unique to cryogens are studied and new dimensionless criteria are developed to classify the data, which are subsequently used to both assess predictive accuracy of seminal HTC correlations and develop new universal cryogen saturated boiling HTC correlations. The new HTC correlations are shown to provide good predictive agreement with the database with an MAE of 26.4% and 34.5%.

1. Introduction

1.1. Applications of Cryogenic Fluids

Cryogenic fluids are used in a range of industries. For example, in the food industry, Liquid Nitrogen (LN_2) is used to fast freeze food and, in the healthcare industry, to preserve tissues and blood and to destroy unhealthy tissues in cryosurgery. Liquid Oxygen (LOX) is widely used in the healthcare industry, especially in life support systems. However, a range of cryogens, especially LOX, Liquid Hydrogen (LH_2), Liquid Methane (LCH_4), and Liquid Helium (LHe), have been used over the years for two primary applications: cooling of superconducting magnets and space, the latter being the primary focus of the present study.

In the field of superconducting magnet cooling, after an initial period of academic research in LHe heat transfer in West Germany [1], United States of America [2], and Japan [3,4] in the early 1970s, the period of 1975-85 saw a surge in LHe flow boiling research in the former Soviet Union [5,6]. Both LH_2 [7-14] and LN_2 [15,16] have been used over the years to cool HTS magnets.

But in recent years, space applications saw appreciable rise in the use of cryogens. Having the lowest critical temperature of any known fluid, LHe is used to chill down Earth-orbiting telescopes and satellites as well as cool space experiments, where ambient space temperature is ~ 2.7 K. And following initial work around 1960, LCH_4 received renewed interest at NASA's Glenn Research Center [17] and Johnson Space Center [18-20] as part of their Propulsion and Cryogenics Advanced Development (PCAD) project [21], where non-toxic propellants such as LOX/LCH_4 were being tested for spacecraft applications. LOX/LCH_4 and LOX/LH_2 are used in ascent stages, descent stages, and in-space fuel depots. Additionally, LH_2 has been proposed for use in several other future

* Corresponding author.
E-mail address: mudawar@ecn.purdue.edu (I. Mudawar).

https://doi.org/10.1016/j.ijheatmasstransfer.2021.121656
0017-9310/

Nomenclature

Bo	boiling number, $q/(Gh_{fg})$
c_1-c_9	empirical constants in HTC correlations
Co	confinement number, $\sqrt{\sigma/((\rho_f-\rho_g)gD^2)}$
$c_{p,f}$	specific heat of liquid at saturated conditions
D	tube inner diameter
D_b	bubble diameter
D_{depart}	bubble departure diameter
f_{sp}	Fanning friction factor corresponding to single-phase flow
F	enhancement factor, defined in Eq. (12)
$Fr_{fo,D}$	liquid-only Froude number based on tube diameter, $G^2/(\rho_f{}^2gD)$
Fr^*	modified Froude number, $Gcos\theta/(\rho_f\sqrt{gD(\rho_f-\rho_g)/\rho_f})$
F_{drag}	drag force on the bubble
F_{lift}	shear lift force on the bubble
G	mass velocity
g	gravitational acceleration
h	enthalpy of fluid; heat transfer coefficient
h_{CB}	convective boiling component of two-phase heat transfer coefficient
h_{NB}	nucleate boiling component of two-phase heat transfer coefficient
h_{sp}	single-phase heat transfer coefficient
$h_{sp,f}$	liquid single-phase heat transfer coefficient
$h_{sp,fo}$	liquid-only single-phase heat transfer coefficient
h_{tp}	two-phase heat transfer coefficient, $q/(T_w - T_{sat})$
$\bar{h}_{tp}$	average two-phase heat transfer coefficient, $q/(\bar{T}_w - T_{sat})$
$h_{cond,\delta}$	heat transfer coefficient associated with conduction across liquid film
$h_{f,in}$	inlet enthalpy of liquid
h_f	enthalpy of saturated liquid
h_{fg}	latent heat of vaporization
$h_{f,out}$	outlet enthalpy of liquid
h_{PB}	pool boiling heat transfer coefficient
j_f	superficial liquid velocity, $G(1\text{-}x_e)/\rho_f$
j_g	superficial vapor velocity, Gx_e/ρ_g
Ja	Jacob number, $c_{p,f}\Delta T_{sat}/h_{fg}$
k_f	thermal conductivity of liquid at saturated conditions
k_w	thermal conductivity of tube wall
L_H	heated length of tube
L_{PH}	pre-heater length
M	molecular weight
MAE	mean absolute error, defined in Eq. (31)
n	exponent dictating transition from nucleate to convective boiling heat transfer, defined in Eq. (10)
$N_{conv.}$	convection number, $(\frac{1-x_e}{x_e})^{0.8}(\frac{\rho_g}{\rho_f})^{0.5}$
Nu_D	Nusselt number based on tube diameter, hD/k_f
P	system pressure
P_{sat}	saturation pressure
ΔP	pressure drop
ΔP_{sat}	saturation pressure difference corresponding to ΔT_{sat}
P_R	reduced pressure, P/P_{crit}
Pr_f	liquid Prandtl number at saturated conditions, $\mu_f c_{p,f}/k_f$
q	heat flux based on tube's inside area
q_{ONB}	onset of nucleate boiling (ONB) heat flux based on tube's inside area
R_b	bubble radius during nucleate boiling, defined in Eq. (6)
$R_{b,crit}$	critical bubble radius during nucleate boiling (0.3 μm as recommended by Steiner and Taborek [31])
R_p	height of surface roughness element
$Re_{f,D}$	liquid Reynolds number based on tube diameter, $GD(1\text{-}x_e)/\mu_f$
$Re_{fo,D}$	liquid-only Reynolds number based on tube diameter, GD/μ_f
$Re_{g,D}$	vapor Reynolds number based on tube diameter, GDx_e/μ_g
$Re_{go,D}$	vapor-only Reynolds number based on tube diameter, GD/μ_g
RMS	root mean squared error, defined in Eq. (32)
S	suppression factor, defined in Eq. (13)
T	temperature
T_f	bulk liquid temperature
T_λ	Lambda point temperature (2.17 K) for Liquid Helium transitioning from LHe I to LHe II
T_{sat}	saturation temperature
ΔT_{sat}	wall superheat, $T_w - T_{sat}$
ΔT^*_{sat}	dimensionless wall superheat, defined in Eq. (27)
T_w	tube wall temperature
$\bar{T}_w$	average tube wall temperature
$T_{w,ONB}$	tube wall temperature at onset of nucleate boiling (ONB)
ΔT_{ONB}	minimum wall superheat for ONB to occur, $T_{w,ONB} - T_{sat}$
t_w	tube wall thickness
$We_{fo,D}$	Weber number based on tube diameter, $G^2D/(\rho_f\sigma)$
x	flow quality
x_e	thermodynamic equilibrium quality, $(h - h_f)/h_{fg}$
X_{tt}	Lockhart–Martinelli parameter based on turbulent liquid-turbulent vapor flows, $(\frac{1-x_e}{x_e})^{0.9}(\frac{\rho_g}{\rho_f})^{0.5}(\frac{\mu_f}{\mu_g})^{0.1}$
$x_{e,in}$	inlet thermodynamic equilibrium quality based on pressure at inlet of heated length, $(h_{in} - h_{f,in})/h_{fg,in}$
$x_{e,out}$	outlet thermodynamic equilibrium quality determined from $x_{e,in}$, energy balance for entire heated length, and pressure at outlet of heated length, $(h_{out} - h_{f,out})/h_{fg,out}$
y	wall normal axis
z	axial location
z_0	axial location where $x_e = 0$
$\Delta z_{sat}/L_H$	saturation length ratio, defined in Eq. (29)

Greek symbols

α	void fraction
δ	liquid film thickness; boundary layer thickness
μ	dynamic viscosity
ν	specific volume
ρ	density
σ	surface tension
θ	percentage of data points predicted within ±30%; angle of inclination from horizontal plane
ξ	percentage of data points predicted within ±50%
$\Pi_{1\text{-}\alpha}$	liquid holdup dimensionless group, defined in Eq. (12)
Π_G	flow induced suppression dimensionless group, defined in Eq. (13)
Π_{xe}	bubble motion induced suppression dimensionless group, defined in Eq. (13)
$\Pi'_{1\text{-}xe}$	correction term for boiling suppression due to flow quality, defined in Eq. (14)

Subscripts

A	accelerational component
CB	convective boiling
crit	fluid's critical point
DB	Dittus-Boelter single-phase HTC correlation [30]
exp	experimental
f	liquid
fo	liquid-only
F	frictional component
film	liquid film
G	gravitational component
GN	Gnielinski single-phase HTC correlation [33]
g	vapor
H	heated section
in	inlet of heated length
max	maximum
NB	nucleate boiling
ONB	onset of nucleate boiling
PB	pool boiling
PH	pre-heater section
out	outlet of heated length
pred	predicted
sat	saturated conditions
sp	single-phase
tp	two-phase
w	tube wall

advanced propulsion systems such as nuclear thermal propulsion [22] and hybrid-electric aircraft [23], where it would be used as both propellant and coolant. Fig. 1 shows examples of the space applications of cryogens.

While almost all cryogens exist in unique states, this is not the case with LH_2 and LHe. LH_2 usually exists in two molecular spin states, orthohydrogen and parahydrogen, which exhibit significantly different thermal properties such as specific heat and thermal conductivity. Since the operating temperature of LH_2 is ~ 20.4 K for space applications of interest, it is predominantly parahydrogen (0.2% ortho- and 99.8% para-) as compared to orthohydrogen (75% ortho- and 25% para) at 300 K. Likewise, LHe exists in two states, LHe I (above the lambda temperature, T_λ of 2.17 K) and LHe II (below the lambda temperature T_λ). Since the operating temperature of LHe in space applications of interest to the present study is above 2.17 K, emphasis is placed here entirely on LHe I. Hereafter and throughout the present study LH_2 parahydrogen and LHe I will be referred to simply as LH_2 and LHe, respectively.

Use of LCH_4 in space applications is complicated by the fact that, while this cryogen exists in single unique state, is sometimes used as one constituent of Liquified Natural Gas (LNG) [24,25], a mixture comprised of (by mole fraction) ~89.7% LCH_4, ~6% liquid ethane, ~3% liquid propane, with the balance including liquid isobutane, liquid butane, and LN_2. In the present study, focus will be placed on analysis of data for pure LCH_4 rather than LNG.

1.2. Experimental Issues Unique to Cryogens

Cryogens constitute a unique class of fluids which are clearly distinguishable from water and refrigerants by virtue of their low saturation temperatures, as shown in Fig. 2 (calculated using REFPROP 10 [26], which has the most accurate thermophysical property database). Because of these low temperatures, two unique issues exist in experimental investigation of flow boiling of cryogens that are often ignored when working with other near-room temperature fluids, namely (1) choice of temperature sensors and (2) choice of test tube material.

Cryogens pose major challenges in experimental temperature measurements. This especially is the case where values of wall superheat, $T_w - T_{sat}$, or wall-to-fluid temperature difference, $T_w - T_f$, are about or below 0.5 K, which is less commonly encountered with water and refrigerants. In these situations, measurements errors might cause Nusselt number for cryogens to exhibit erroneous trends in the form of large artificial spikes or even unphysical values below zero. These large errors can be explained as follows.

Assuming an uncertainty in wall temperature measurements of dT_w, the experimentally determined Nusselt number can be expressed as

$$Nu_D = \frac{hD}{k_f} = \frac{q}{T_w + dT_w - T_f}\frac{D}{k_f} = \frac{1}{1 + \frac{dT_w}{T_w - T_f}}\frac{q}{T_w - T_f}\frac{D}{k_f}. \quad (1)$$

Hence, for situations where $dT_w >> (T_w - T_f)$, the calculated Nusselt number will exhibit very large measurement uncertainly, which increases with increasing dT_w and/or decreasing $T_w - T_f$. This is particularly the case for LHe, LH_2, and Liquid Neon (LNe), which possess extremely low saturation temperatures of 4.2 K, 20.3 K, and 27.1 K, respectively, at atmospheric pressure. Such large Nusselt number errors are clearly evident in the database of Lewis et al. [14], whose local wall temperature data for LH_2 measured using copper-Constantan thermocouples showed high scatter/variance, as confirmed later by Steiner and Schlünder [27]. Similar errors are also evident in nucleate boiling data for LH_2 by Core et al. [12], whose wall temperatures were measured using Chromel-Alumel thermocouples. Interestingly, owing to much larger saturation temperature, LN_2 data from Lewis et al. [14] using copper-Constantan thermocouples showed relatively less scatter in the local wall temperature measurements. Overall, selection of appropriate temperature sensors is vitally important when making heat transfer measurements with cryogens which has led to using semiconductor-based devices such as constant current silicon diodes or variable current Cernox sensors in place of thermocouples for low normal boiling point cryogens in recent experiments.

Cryogens also pose additional challenges in designing the test section for experiments. Cryogen flow boiling data are acquired using either quenching or heating experiments, the latter being the more accurate and therefore preferred method. In the heating experiments, the flow channel is subjected to electric heating to produce a uniform heat flux from channel wall to fluid. Often, small channel wall thickness is adopted to reduce axial conduction along the wall, which is known to alter axial development of boiling behavior along the channel. However, axial conduction is also a function of thermal conductivity of the channel wall, which is less of a concern when working with room temperature fluids. But at cryogenic temperatures (< ~30 K), thermal conductivity for specific metals and metal alloys escalates appreciably, which exasperates axial conduction effects even for thin channel walls. This trend is clearly captured in Fig. 3, which depicts variation of thermal conductivity (calculated using Engineering Equation Solver, EES, 10 [28]) versus wall temperature for commonly used tube materials, where the conductivity is evaluated at saturation temperature corresponding to atmospheric pressure for commonly used cryogens and water. Notice how for low cryogenic temperatures, especially for LHe (4.2 K), LH_2 (20.3 K), and LNe (27.1 K), copper and silver must be avoided as tube materials.

Three important inferences regarding these temperature measurement challenges are:

(1) Investigators must always be mindful of the potential for high uncertainties when acquiring cryogen data.
(2) These high uncertainties create appreciable scatter when aiming to develop a cryogen correlation from experimental data.

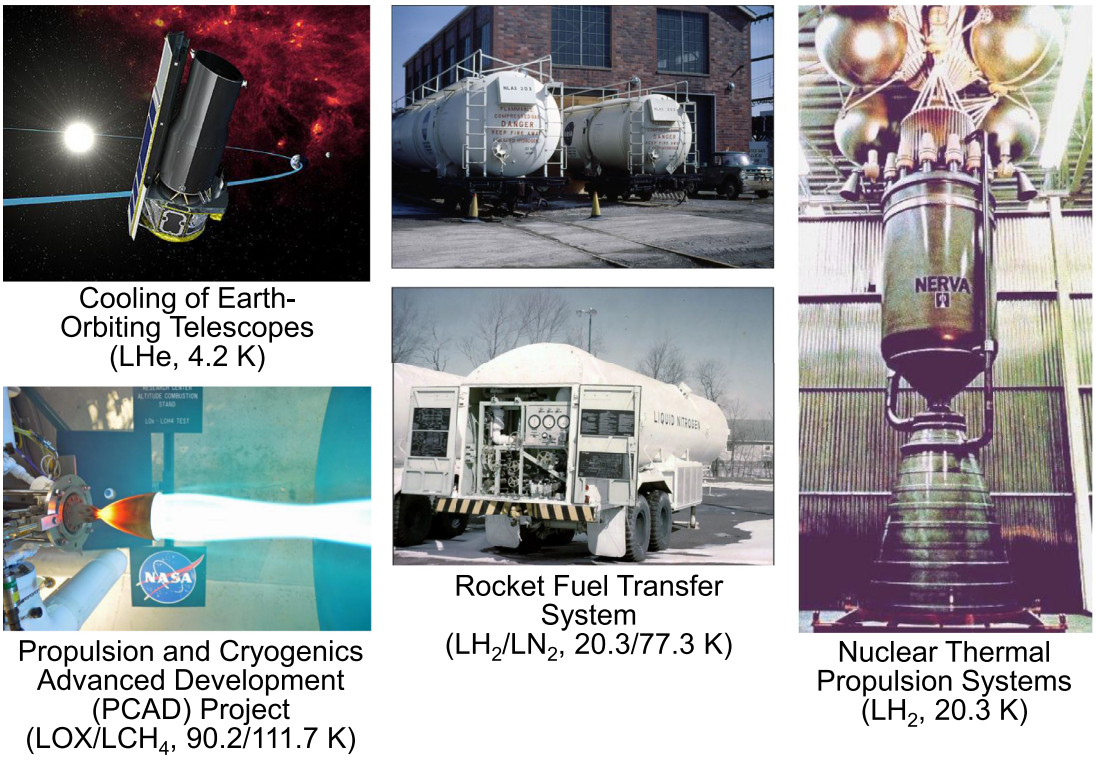

Fig. 1. Examples of space applications of cryogens.

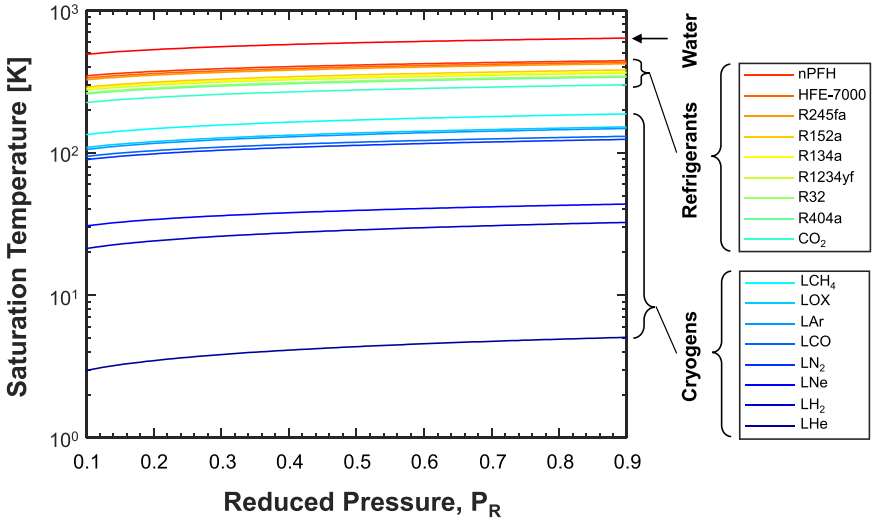

Fig. 2. Classification of coolants into water, refrigerants, and cryogens based on variation of saturation temperature with reduced pressure.

(3) When selecting wall material, investigators must consider the potential for non-uniformity in wall heat flux resulting from elevated wall thermal conductivity at low temperatures.

1.3. Fluid Physics Unique to Cryogens and Heat Transfer Mechanisms

In addition to low saturation temperatures, cryogens also exhibit other general thermophysical property trends, including (a) low surface tension, σ, (b) low latent heat of vaporization, h_{fg}, (c) low liquid viscosity, μ_f, and, to a lesser extent, (d) low liquid-to-vapor density difference, ρ_f - ρ_g [29]. Important consequences of these property trends are relatively high liquid-only Reynolds number based on saturated liquid viscosity and tube diameter, $Re_{fo,D}$, high liquid-only Weber number, also based on saturated liquid density and tube diameter, $We_{fo,D}$, and high modified Froude number, Fr^* (> 6); the impact of all three dimensionless parameters were discussed in regards to critical heat flux (CHF) for cryogens.

Unlike CHF, which is characterized by a unique value for a given set of operating conditions, in the current study, which is focused on saturated flow boiling heat transfer (with $x_e \geq 0$), the heat transfer coefficient (HTC), h, varies along the heated tube. For a given set of operating conditions (*i.e.,* inlet pressure, P_{in}, mass velocity, G, tube diameter, D, and heat flux, q), h is dictated by local conditions, including local pressure, P, and local flow quality, x. In the saturated flow boiling region, h is dominated by one of three unique heat transfer mechanisms, saturated liquid convection, nu-

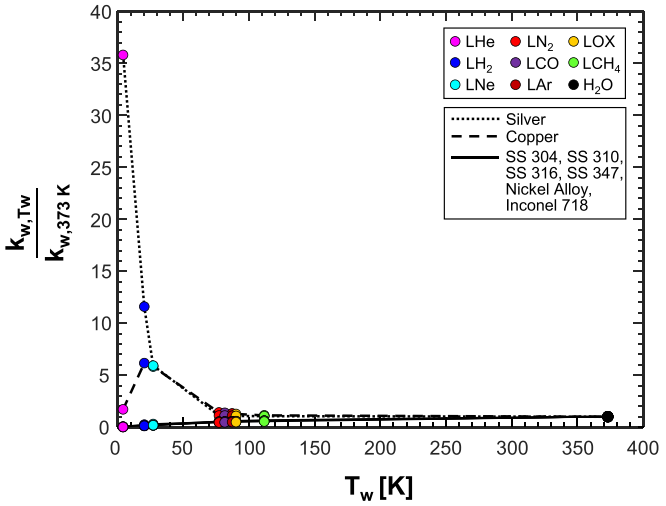

Fig. 3. Variation of thermal conductivity for commonly used wall materials with wall temperature corresponding to saturation temperatures for cryogens and water evaluated at atmospheric pressure.

cleate boiling, and convective boiling, or combinations thereof. Detailed discussions of these mechanisms will follow.

1.3.1. Saturated liquid convection

In saturated flow boiling for cryogenic applications of interest, the heat transfer is forced convection driven. In axial locations before CHF (dryout or departure from nucleate boiling, DNB), the test section wall is fully wetted with liquid. At such locations, a portion of the heat is removed from the wall through forced convective heat transfer in both nucleate boiling and convective boiling dominant regions, which can be estimated by multiplying the single-phase HTC with a suitable two-phase multiplier. Boiling number, *Bo*, and Lockhart-Martinelli parameter, X_{tt}, are two-phase multipliers commonly used to estimate HTC in nucleate boiling and convective boiling regions, respectively.

Because of popular methods of expressing the two-phase HTC in terms of the single-phase HTC, it is of interest to compare the single-phase HTC for different fluids. The magnitude of saturated liquid convective HTC, $h_{sp,f}$, is dictated by the product of ratio of thermal conductivity of liquid to tube diameter, k_f/D, liquid Reynolds number, $Re_{f,D}$, and saturated liquid Prandtl number, Pr_f. $h_{sp,f}$ is therefore influenced by thermophysical property trends unique to cryogens, including comparatively high liquid thermal conductivity, k_f, (except LHe) and low saturated liquid Prandtl number, Pr_f. Figs. 4(a) and 4(b) show, respectively, variations of k_f and Pr_f for commonly used cryogens with reduced pressure, P_R, over the range of 0 to 1. Fig. 4(c) shows the variation of $h_{sp,f}$ with reduced pressure, evaluated using Dittus-Boelter's [30] correlation for $Re_{fo,D} = 10^4$ (turbulent flow), $D = 5$ mm, and $x_e = 0$ (non-boiling saturated liquid region with $T_w < T_{w,ONB}$):

$$h_{sp,f} = 0.023 Re_{f,D}^{0.8} Pr_f^{0.4} \frac{k_f}{D} = 0.023 Re_{fo,D}^{0.8} Pr_f^{0.4} (1 - x_e)^{0.8} \frac{k_f}{D}. \quad (2)$$

Notice how, because of low k_f, as seen in Fig. 4(a), LHe exhibits the lowest $h_{sp,f}$ while, owing to its comparatively high k_f, LCH_4 yields the highest $h_{sp,f}$ among all the cryogens. Also noticeable is how LH_2 has a rather constant $h_{sp,f}$ for low-to-medium pressures ($P_R \leq 0.6$). With regards to other cryogens, there is no clear distinction in $h_{sp,f}$ as compared to regular fluids (excluding water).

1.3.2. Nucleate boiling

Post onset of nucleate boiling (ONB) ($T_w \geq T_{w,ONB}$), at low void fractions, the two-phase HTC, h_{tp}, is dominated by nucleate boiling. Fig. 5(a) shows, for $Re_{fo,D} = 10^4$ and $D = 5$ mm, the variation of heat flux required to initiate ONB, q_{ONB}, with reduced pressure, evaluated using a correlation developed by Steiner and Taborek [31] based on the Karlsruhe data bank [32] for all fluid classes, including LHe, LH_2, and LN_2.

$$q_{ONB} = \frac{2\sigma T_{sat} h_{sp,fo}}{R_{b,crit} \rho_g h_{fg}}, \quad (3)$$

where, $R_{b,crit}$, is the critical bubble radius, which represents the maximum radius of a bubble ($= 2\sigma/\Delta P_{sat}$) undergoing evaporation within the thermal boundary layer, with $R_{b,crit} = 0.3$ μm recommended by Steiner and Taborek [31], and the liquid-only single-phase HTC, $h_{sp,fo}$, based on the Gnielinski [33] correlation.

$$h_{sp,fo} = \frac{\left(4f_{sp,fo}/8\right)\left(Re_{fo,D} - 1000\right)Pr_f}{1 + 12.7\left(4f_{sp,fo}/8\right)^{0.5}\left(Pr_f^{2/3} - 1\right)} \frac{k_f}{D}, \quad (4)$$

where

$$4f_{sp,fo} = \left[0.7904 \ln Re_{fo,D} - 1.64\right]^{-2}. \quad (5)$$

For saturated liquid inlet conditions, the wall superheat at ONB, $\Delta T_{ONB} = T_{w,ONB} - T_{sat}$, is evaluated from $\Delta T_{ONB} = q_{ONB}/h_{sp,fo}$ and its variation with reduced pressure is plotted in Fig. 5(b). Figs. 5(a) and 5(b) show ONB is achieved in cryogens at significantly lower heat fluxes and wall superheats, respectively, compared to other fluid classes. For cryogens, these trends broaden the range of the two-phase region dominated by nucleate boiling compared to convective boiling. An especially interesting trend is observed for LHe, which has q_{ONB} and $\Delta T_{w,ONB}$ values orders of magnitude lower than the other cryogens. This may explain why LHe data were treated separately from other cryogens when developing HTC correlations, which is evident from works by Steiner and Taborek [31] for flow boiling, and Gorenflo and Sokol [34] for pool boiling HTC.

Given the greater importance of nucleate boiling for cryogens, it would be useful to also explore the size of growing bubbles, which could have a strong influence on the transition between the nucleate boiling and convective boiling mechanisms. To do so, an early yet popular model for by Forster and Zuber [35], which has been used to explore bubble nucleation in the nucleate boiling region of flow boiling, is used here, where the bubble radius, R_b, is given by

$$R_b = \frac{\Delta T_{sat}}{h_{fg}\rho_g}\sqrt{\frac{2\pi k_f \rho_f c_{p,f}\sigma}{\Delta P_{sat}}}\,4\sqrt{\frac{\rho_f}{\Delta P_{sat}}} \quad (6)$$

Here the bubble radius, R_b, signifies the limit till which it contributes significantly to convection in the boundary layer due to pushing of the liquid phase across the interface owing to evaporation. Since the wall superheat, ΔT_{sat}, is a response variable to the heating process and not a controlled variable, the variation of bubble radius, R_b is plotted in Fig. 5(c) against reduced pressure for $\Delta T_{sat} = 1$K. Equation (6) is further simplified by expressing ΔP_{sat} in terms of ΔT_{sat} using the Clausius-Clapeyron relation, $\Delta P_{sat}/\Delta T_{sat} = h_{fg}/(T_{sat}\nu_{fg})$. Fig. 5(c) shows that for cryogenic fluids, operating at low wall superheats, the bubbles formed at the heated surface in cryogens are quite small compared to those formed in other fluid classes. Therefore, nucleate boiling will persevere in cryogens over a much longer axial span compared to other fluids and will get enhanced due to lots of small bubbles departing from the wall at higher frequency owing to smaller bubble length scales for cryogens. This finding is consistent with one presented earlier by Ganesan et al. [29], where nucleate boiling in cryogens was shown to commence at lower surface superheat and eventually leading to a larger number of small bubbles forming at and ultimately departing from the surface due to low surface tension and low latent heat of vaporization.

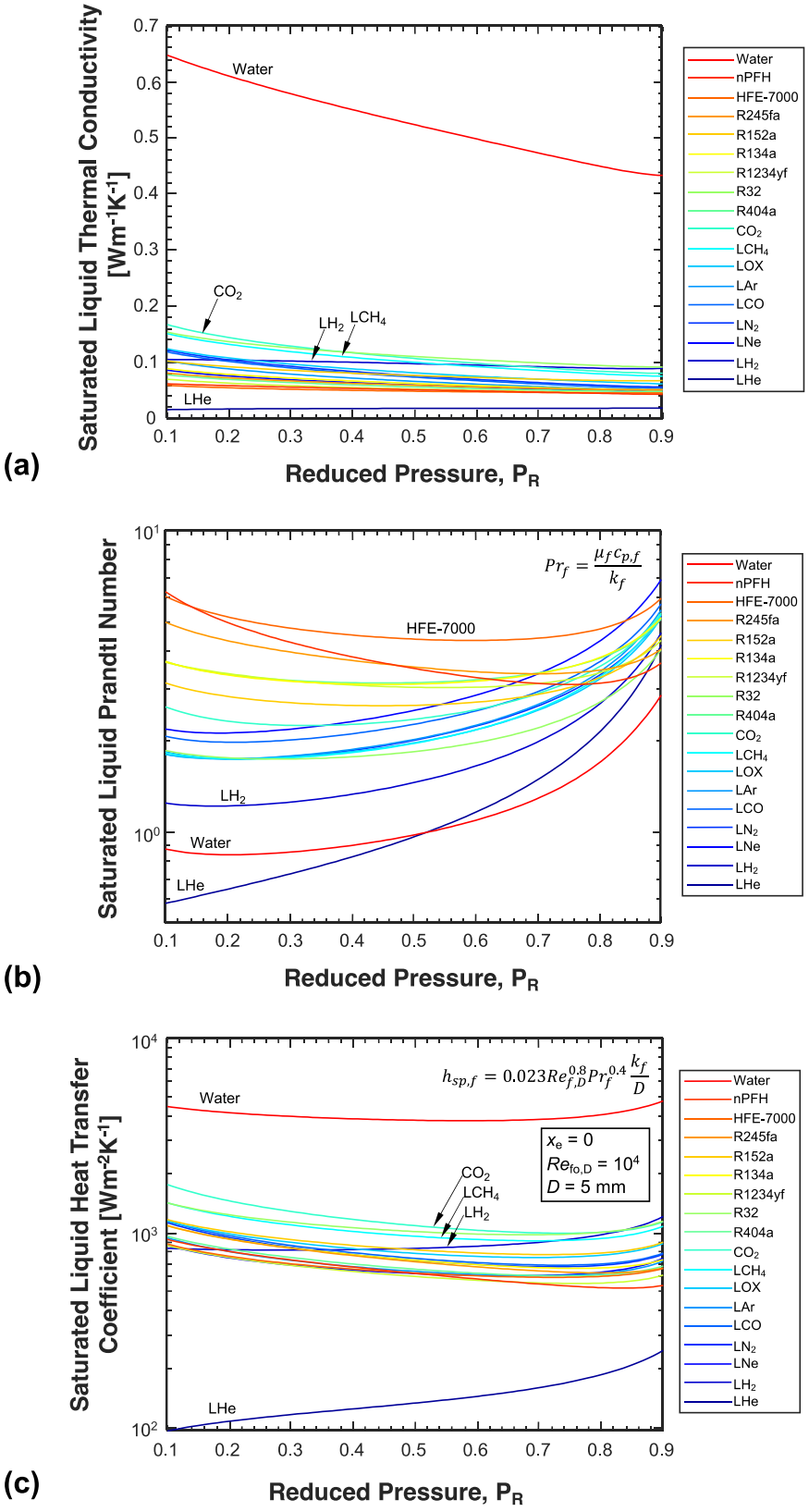

Fig. 4. Variations of (a) saturated liquid thermal conductivity, (b) saturated liquid Prandtl number, and (c) saturated liquid convective heat transfer coefficient with reduced pressure for cryogens compared to those of other fluid classes.

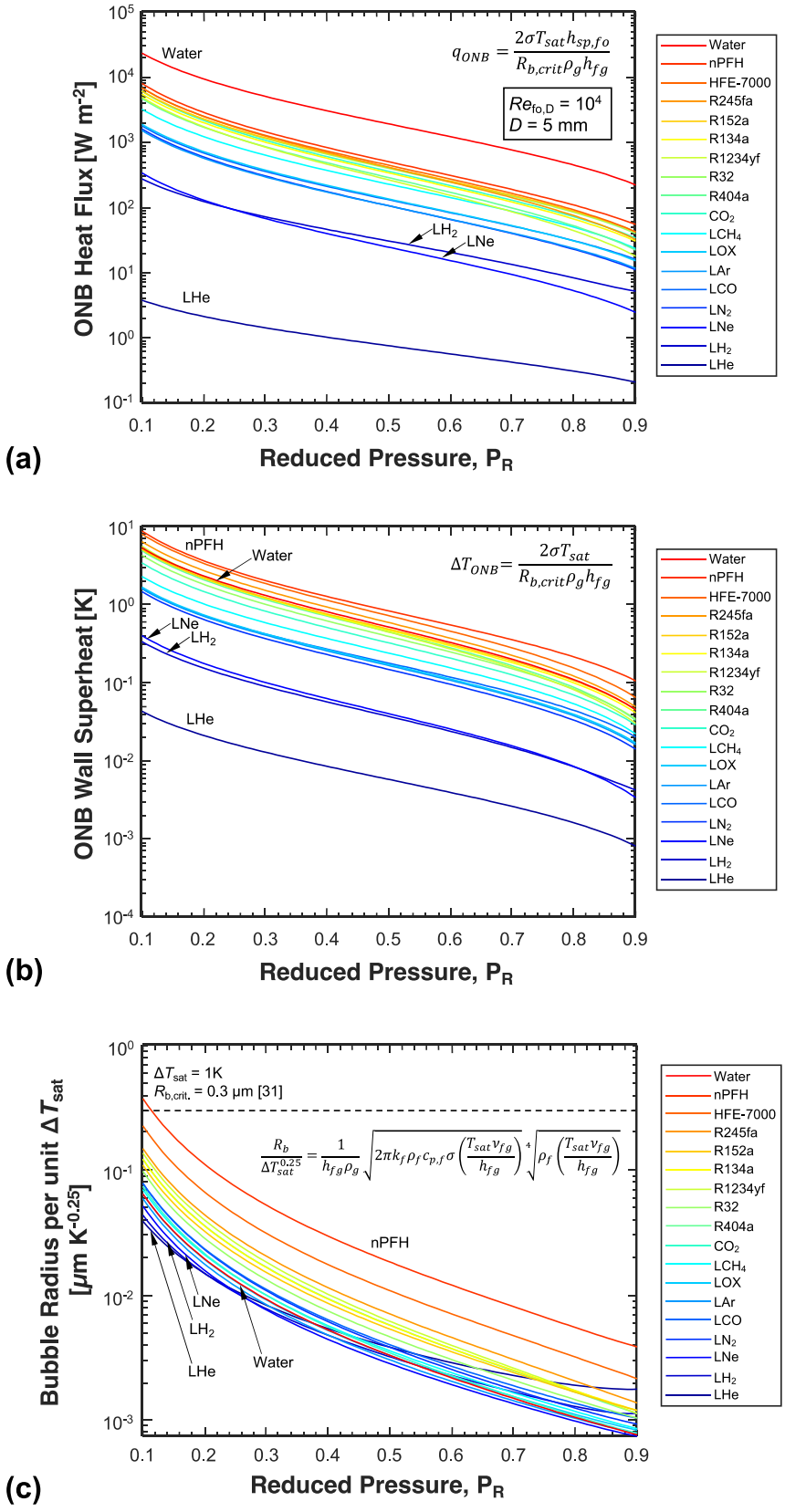

Fig. 5. Variations of (a) ONB heat flux [31], (b) ONB wall superheat [31], and (c) bubble radius [35] with reduced pressure for cryogens compared to those of other fluid classes.

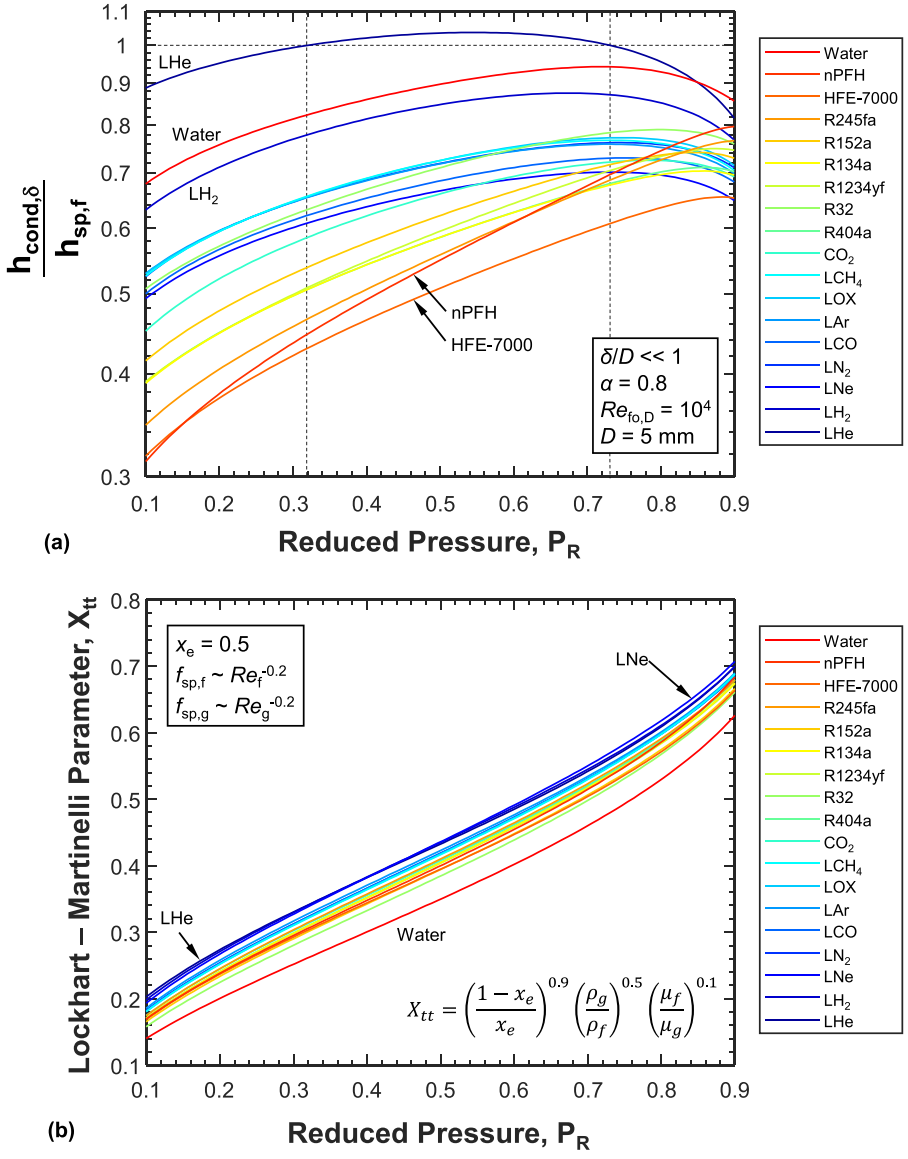

Fig. 6. Variations of (a) conductive-to-convective heat transfer coefficient ratio, $h_{cond,\delta}/h_{sp,f}$, in the annular liquid film and (b) Lockhart-Martinelli parameter, X_{tt}, with reduced pressure for cryogens compared to those of other fluid classes.

1.3.3. Convective boiling

With increasing void fraction in the flow direction comes a point where the flow transitions from bubbly to annular, wherein the bubble nucleation is suppressed, signaling transition from nucleate boiling to convective boiling. Here, under the condition of $\delta_{film}/D << 1$, conduction across the thin annular liquid film begins to gain prominence. To evaluate the contribution of film conduction, the film thickness, δ_{film}, can be related to void fraction, α, according to:

$$1-\alpha = \frac{\pi D \delta_{film}}{\frac{\pi D^2}{4}} = \frac{4\delta_{film}}{D}. \tag{7}$$

After determining δ_{film}, the HTC due to conduction across the liquid film can be evaluated according to

$$h_{cond,\delta} = \frac{k_f}{\delta_{film}} = \frac{4k_f}{(1-\alpha)D}. \tag{8}$$

The void fraction is related to thermodynamic equilibrium quality, x_e, using Zivi's relation [36],

$$\alpha = \left[1 + \left(\frac{1-x_e}{x_e}\right)\left(\frac{\rho_g}{\rho_f}\right)^{2/3}\right]^{-1}. \tag{9}$$

Fig. 6(a) shows variation of the ratio of $h_{cond,\delta}$ to liquid convective HTC $h_{sp,f}$, Eq. (2), in the annular film for $Re_{fo,D} = 10^4$ and $D = 5$ mm, with the value of void fraction set to $\alpha = 0.8$ (typical for transition to annular flow) and the value of x_e in Eq. (2) obtained from Eq. (9). Notice, first, the anomalous behavior of LHe, which exhibits very strong conduction effects, especially for low-to-medium reduced pressures ($0.3 \le P_R \le 0.7$), despite this fluid's exorbitantly low liquid thermal conductivity as seen in Fig. 4(a). This result implies comparatively weak convective heat transfer in the annular liquid film, which, when coupled with the inference from Fig. 5(b) that $\Delta T_{w,ONB}$ for LHe is quite small, hints at nucleate boiling possibly persisting even within the annular flow regime.

Although this behavior is clearly evident for LHe, it will be proven later to prevail for other cryogens to varying degrees.

Fig. 6(a) proves cryogens are associated with a higher HTC ratio, $h_{cond,\delta}/h_{sp,f}$, than most refrigerants. Hence, it is imperative to further explore the ratio $h_{cond,\delta}/h_{sp,f}$ for cryogenic annular flow boiling data before developing a HTC correlation for the same fluids. For turbulent annular flow, $f_{sp,f} \sim Re_{f,D}{}^{-0.2}$ and $f_{sp,g} \sim Re_{g,D}{}^{-0.2}$, the liquid hold-up term (1 - α) in Eq. (7) has been successfully correlated by Lockhart and Martinelli [37] using the parameter X_{tt}, which plays a significant role in estimating the enhancement to the convective boiling HTC. Fig. 6(b) shows variation of X_{tt} with reduced pressure for $x_e = 0.5$. Clearly captured is the trend of cryogens exhibiting relatively higher values of X_{tt} compared to common fluids.

It is evident from trends presented thus far that, for all three heat transfer mechanisms (liquid convection, nucleate boiling, convective boiling), that (1) cryogens behave differently from other common fluids and (2) even among the cryogens, LHe almost always acts as an outlier. These facts suggest heat transfer correlations for cryogens are best pursued separately from those of other fluid classes (*i.e.,* rather than using universal correlations applicable to all fluid classes), with particular attention given to LHe.

To achieve the goal of developing flow boiling HTC correlation for cryogens, data are amassed from the literature and consolidated into a new Purdue University-Boiling and Two-Phase Flow Laboratory (PU-BTPFL) Cryogen Saturated Flow Boiling Heat Transfer Coefficient Database (PU-BTPFL HTC Database for short), which will be discussed in subsequent sections, the largest ever assembled for cryogens. Table 1 provides details of ranges of this database, including controlled variables (P_R, D, G, and q), response variables (local and average HTC, and local α) alongside the largest database for non-cryogenic fluids from Qiu et al. [38]. Also, included in the same table are corresponding values of dimensionless parameters of liquid-only Reynolds number, Weber number, and Froude number, and liquid Prandtl number, Pr_f. This table points to trends quite unique to cryogens, including relatively high $Re_{fo,D}$, high We_{fo}, high $Fr_{fo,D}$, and low Pr_f, which is further evidence that heat transfer correlations for cryogens are best pursued separately from those of other fluid classes.

1.4. Saturated Flow Boiling Heat Transfer

1.4.1. Dominant flow patterns in saturated flow boiling

In flow boiling experiments, the heat transfer mechanism at each location along the tube is dictated by the flow regime existing at that location. Based on the experimentally controlled variables of G, q, $x_{e,in}$, heated length, L_H, and a fixed inlet pressure, P_{in}, a range of flow regimes can be achieved, culminating in a region where saturated flow boiling heat transfer will occur. Fig. 7 shows schematics of all possible permutations of operating conditions for achieving saturated flow boiling region in a uniformly heated tube. Based on either low or high mass velocity, either both bubbly flow and annular flow or bubbly flow alone will be observed, respectively, in the saturated boiling region. Fig. 7(a) highlights the flow patterns present in the saturated boiling region for subcooled inlet conditions ($x_{e,in} < 0$) and both low and high G, assuming of course the tube is sufficiently long. Notice that the saturated boiling region extends from $x_e = 0$ to the location of *Dryout type CHF* for low G or location of *Departure from Nucleate Boiling (DNB) type CHF* for high G. Both cases involve an upstream non-boiling region ($T_w < T_{w,ONB}$), followed by a subcooled boiling region ($T_w \geq T_{w,ONB}$ and $x_e < 0$), within which two-phase HTC begins to increase downstream of the point of Net Vapor Generation (NVG) (where bubbles are able to grow and depart from the surface). For low G (also low q), all possible flow regimes can occur until the dryout location; this is where the saturated boiling region is comprised of clearly defined nucleate boiling dominant region and convective boiling dominant region, the contributions of which to h_{tp} are h_{NB} and h_{CB}, respec-

Table 1
Operational ranges of controlled variables, response variables, and corresponding dimensionless numbers in the present PU-BTPFL Saturated Cryogenic Flow Boiling Heat Transfer Coefficient (HTC) Database and in databases for other common fluids.

Fluid(s)	Controlled Variables				Response Variables			Dimensionless Numbers			
	Reduced Pressure	Tube Inner Diameter	Mass Velocity	Heat Flux	Local [a] two-phase HTC	Average [b] two-phase HTC	Local void Fraction [d]	Liquid-Only Reynolds Number	Liquid-Only Weber Number	Liquid-Only Froude Number	Liquid Prandtl Number
	P_R	D x 10^3 [m]	G [kg m^{-2} s^{-1}]	q x 10^{-3} [W m^{-2}]	h_{tp} x 10^{-3} [W m^{-2} K^{-1}]	$\bar{h}_{tp}$ x 10^{-3} [W m^{-2} K^{-1}]	α	$Re_{fo,D}$ x 10^{-3}	$We_{fo,D}$ x 10^{-3}	$Fr_{fo,D}$	Pr_f
LHe	0.06	0.47	7.89	0.01	0.99	0.53	0	5.16	0.02	0.06	0.57
	0.86	10	636	9.29	123.3	16.89	0.93	457.26	141.69	1417.2	3.06
LH_2	0.12	3	75.47	1.03	29.42	3.84	0	65.3	1.28	30.31	1.23
	0.54	8	1787.6	130.74	29.42	225.78	0.4	779.77	361.55	33716	1.52
LNe	0.06	4	111	0.39	5.4	-	0.74	3.88	0.01	0.23	2.36
	0.06	4	131	33.09	21.2		0.87	4.58	0.01	0.31	2.36
LN_2	0.03	0.53	27.08	0.21	0.73	1.76	0	3.98	0	0.01	1.75
	0.88	14.1	1743	223.2	58.85	5.35	0.98	146.55	6.73	1210.4	4.61
LAr	0.03	14	117.04	0.22	0.49	-	0.35	7.96	0.01	0.06	1.89
	0.40	14	460	98.99	9.67		0.92	73.36	0.85	1.33	2.09
LCH_4	0.06	6	116.49	4.99	5.77	-	0.17	8.84	0.02	1.5	1.80
	0.13	6	273.89	61.99	17.79		0.83	20.77	0.13	8.31	1.84
CO_2, FC72, Propane, R11, R113, R123, R1234yf, R1234ze, R134a, R152a, R22, R236fa, R245fa, R32, R600a and water[c]	0.0046	0.15	19	-		0.29	0	0.03	0	0.02	0.91
	0.77	6.5	1608	-		297.56	1	55.27	3.14	439.11	8.92

[a] From 2505 local HTC data points from current database.
[b] From 747 average HTC data points from current database.
[c] From 16,593 HTC data points by Qiu et al. [38] with flow quality, x, and void fraction ranging from 0 to 1.
[d] Evaluated using Zivi's relation, Eq. (9).

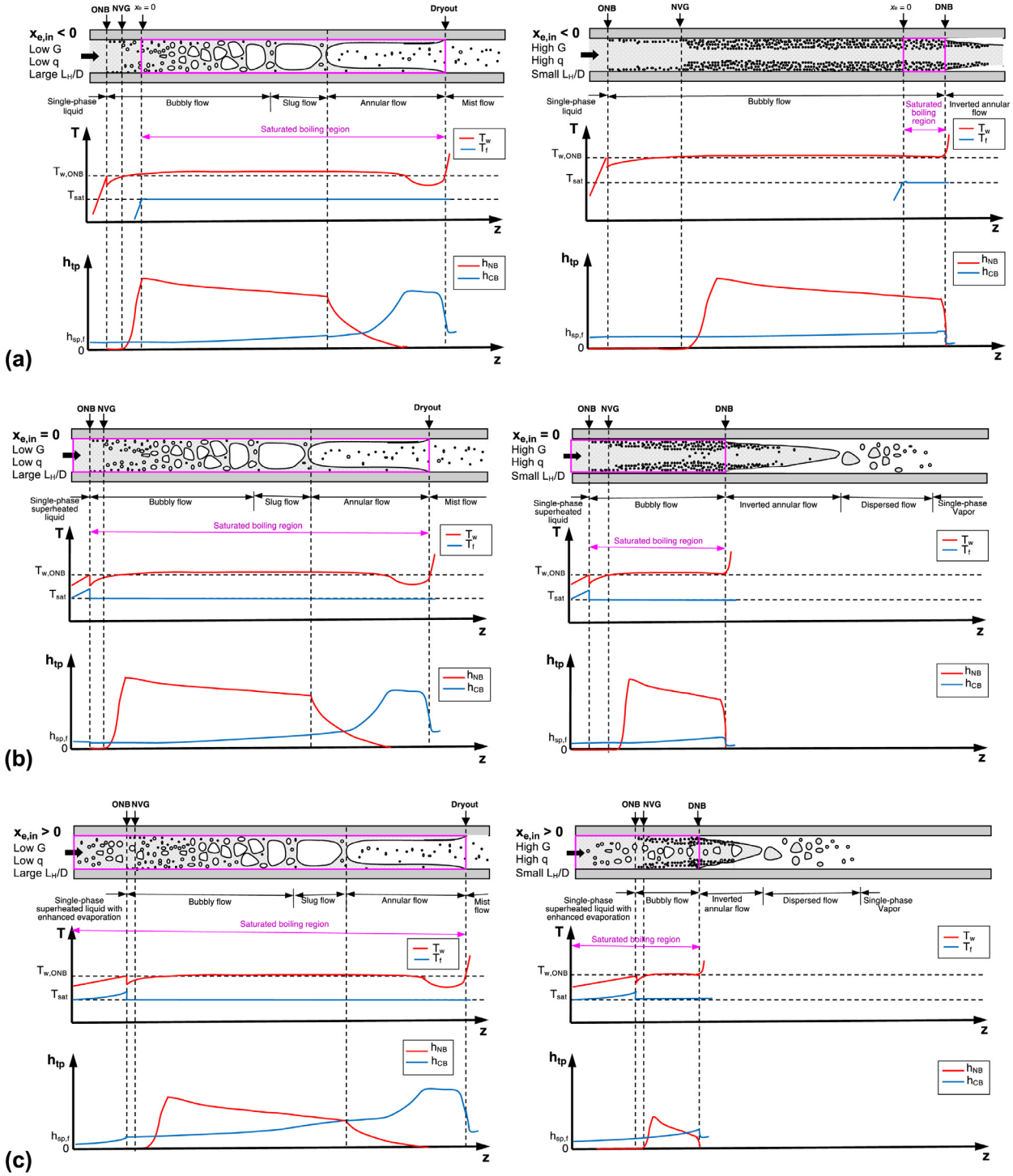

Fig. 7. Schematics of flow regimes and variations of wall and bulk fluid temperature, and of nucleate boiling and convective boiling components of the two-phase heat transfer coefficient along a uniformly a heated tube for (a) subcooled inlet conditions ($x_e < 0$), (b) saturated liquid inlet conditions ($x_e = 0$), and (c) two-phase mixture inlet conditions ($x_e > 0$).

tively. However, for the high G case (also generally high q), the saturated boiling region is dominated entirely by nucleate boiling.

Fig. 7(b) highlights the flow patterns present in the saturated boiling region for saturated liquid inlet conditions ($x_{e,in} = 0$) and both low and high G. Here, the saturated boiling region extends from ONB to the CHF location. For low G (also low q), the flow regimes in the saturated boiling region are fairly similar to those of the subcooled inlet case and terminate at the dryout point. For high G, the saturated boiling region is shorter and dominated by bubbly flow, which persists to the DNB location.

Fig. 7(c) shows dominant flow patterns for two-phase mixture inlet conditions ($x_{e,in} > 0$) and both low and high G. Despite nucleate boiling at the wall being delayed until $T_w \geq T_{w,ONB}$, the presence of vapor bubbles at the inlet enhances convection in the upstream region. For low G, the saturated boiling region, unlike the previous subcooled and saturated inlet cases, now encompasses

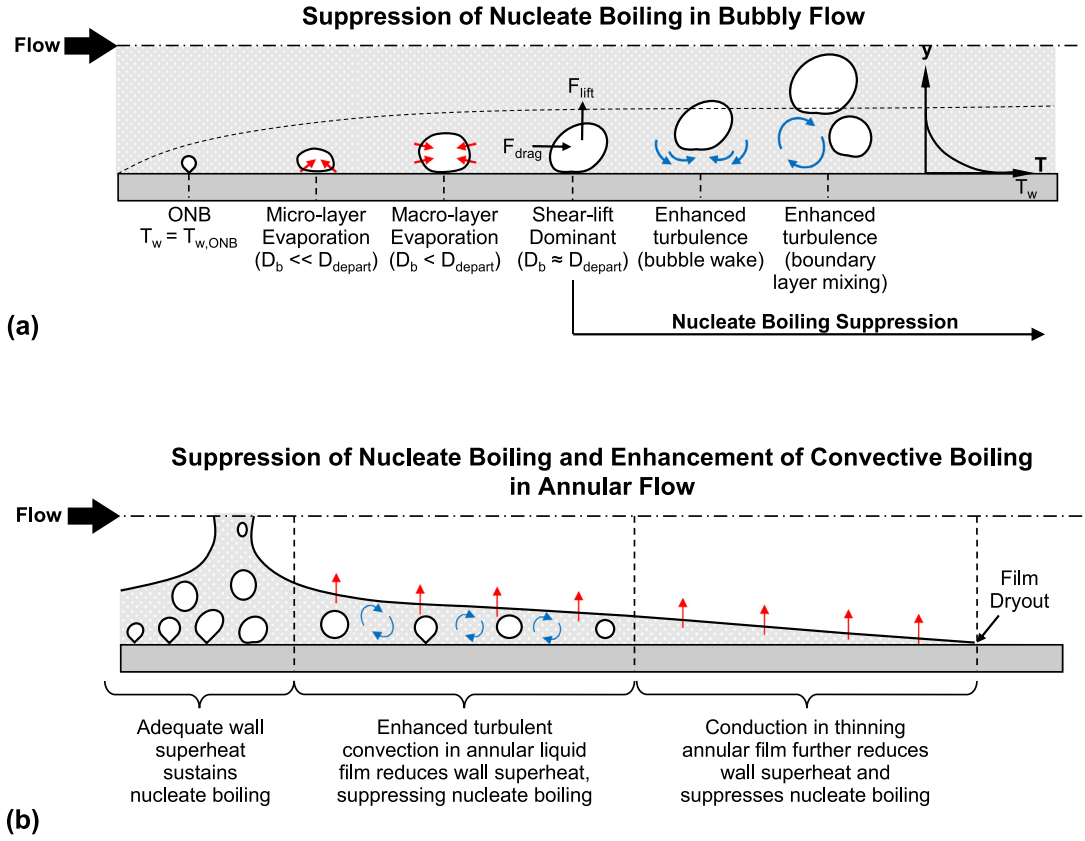

Fig. 8. Schematic of heat transfer mechanisms aiding in suppression of nucleate boiling and enhancement of convective boiling in (a) bubbly flow and (b) annular flow.

the entire inlet region. But here too, the saturated boiling region extends to the dryout point. For high G, the saturated boiling region also encompasses the entire inlet region and terminates at the DNB location.

1.4.2. Suppression of nucleate boiling and enhancement of convective boiling

Overall, the most prevalent flow regimes in the saturated flow boiling region are bubbly flow and annular flow. For bubbly flow the dominant heat transfer mechanism is nucleate boiling, and for annular flow, convective boiling. Despite the dominance of these mechanisms in their respective flow regimes, bubble nucleation and convection are present in both regimes and their interplay is influenced by two well-known flow boiling phenomena: *Boiling Suppression* and *Convection Enhancement*, which are commonly employed when developing boiling correlations.

Fig. 8 illustrates important heat transfer phenomena that contribute to suppression of nucleate boiling and enhancement of convection in the bubbly flow and annular flow regimes. Fig. 8(a) shows the phenomena that contribute to boiling suppression within the bubbly flow regime. Shown is behavior of a single representative bubble, which in fact is duplicated by multiple bubbles. Within the liquid boundary layer along the heated wall, very small bubbles are first formed where $T_w = T_{w,ONB}$. Thereafter, the bubble nucleation and growth are aided by evaporation of the thin micro-layer at the heated wall beneath the bubble. As the bubble grows within the thermal boundary layer, further bubble growth is achieved due to macro-layer evaporation around the bubble interface. However, the same growth begins to increase the magnitude of two forces exerted on the bubble: axial drag force and normal shear-lift force, which contribute to departure of the bubble once it reaches its departure diameter ($D_b = D_{depart}$). The bubble departure in turn enhances turbulence by creating a liquid wake at the wall, which improves surface cooling and decreases wall temperature, thereby serving to suppress nucleate boiling. With further penetration of the bubbles into the bulk flow, further suppression of nucleate boiling is achieved by enhanced turbulence due to boundary layer mixing caused by liquid from the bulk region being drawn toward the wall to replace the departed bubble.

Fig. 8(b) illustrates the heat transfer phenomena that contribute to suppression of boiling and enhancement of convection in the annular flow regime. As the annular regime begins to develop, any wall superheat upstream that might be adequate for sustaining bubble nucleation, begins to diminish because of turbulent convection in the annular film. As the wall temperature decreases and becomes less than $T_{w,ONB}$, nucleate boiling ceases to exist in the annular regime. Farther downstream, interfacial evaporation of the film precipitates substantial thinning of the film until its eventual dryout. With decreasing flow rate of the film, turbulence effects are suppressed, and heat transfer becomes dominated by conduction, which further decreases the wall superheat and prevents any further bubble nucleation.

Hence, it is evident from the above discussion that the nucleate boiling and convective boiling mechanisms contribute the most heat transfer to the bubbly and annular flow regimes, respectively, with intermediate flow regimes having partial contributions of both mechanisms. This observation has served as basis for formulating functional relations for the two-phase HTC, h_{tp}. For example, in 1952, Rohsenow [39] proposed an additive formulation to represent h_{tp} as a function of the nucleate boiling (NB) HTC, h_{NB}, in the bubbly flow regime and the convective boiling (CB) HTC, h_{CB}, in the annular flow regime.

$$h_{tp} = \left(h_{NB}^{n} + h_{CB}^{n}\right)^{1/n}. \tag{10}$$

Where the empirical exponent n is used to tackle the transition from the nucleate boiling to the convective boiling mechanisms in

intermediate regimes. Later, Schrock and Grossman [40], Chen [41], and Gungor and Winterton [42] proposed setting $n = 1$, which implies a smooth transition from one heat transfer mechanism to the other. On the other hand, Shah [43] and Klimenko [44] proposed setting $n = \infty$ with $h_{tp} = \max\{h_{NB}, h_{CB}\}$, implying a sharper transition and overall dominance of only one of the two mechanisms. Table 2 provides a summary of prior seminal saturated flow boiling HTC correlations employing different h_{tp} formulations with varied values of n.

1.4.3. Convective boiling heat transfer coefficient (HTC), h_{CB}

Based on the heat transfer mechanism dominant in annular flow, Fig. 8(b), the convective boiling HTC, h_{CB}, is determined using analogy between turbulent annular liquid film flow having hydraulic diameter $4\delta_{film}$ (assuming $\delta_{film}/D << 1$), with heat transferred from the wall at T_w and interface at temperature T_{sat}; and single-phase turbulent liquid flow having diameter D, with heat transferred from the wall at T_w and mean fluid temperature at T_f. Using this analogy, combined with Eq. (7),

$$h_{CB} = Nu_{D,sp,f}\frac{k_f}{4\delta_{film}} = h_{sp,f}\frac{D}{4\delta_{film}} = h_{sp,f}\frac{1}{1-\alpha}, \tag{11}$$

where, $h_{sp,f}$ is the single-phase liquid HTC evaluated using either Eq. (2) or Eq. (4) (after replacing $Re_{fo,D}$ with $Re_{f,D}$). This formulation implies h_{CB} for annular flow may be expressed in general in terms of the *enhancement factor, F*, according to

$$h_{CB} = h_{sp,f}\frac{1}{\Pi_{1-\alpha}} = h_{sp,f}F, \tag{12}$$

where $F = 1/\Pi_{1-\alpha}$ and $\Pi_{1-\alpha}$ is a dimensionless function of the liquid hold-up parameter (1- α) (term first introduced by Lockhart and Martinelli [37] as a measure of the extent of phase separation). The enhancement factor, F, is generally correlated to $1/X_{tt}$ [40,41,49] in addition to other multipliers like density ratio and reduced pressure (used to account for fluid property variations with pressure for a given fluid or for multiple fluids) as indicated in Table 2.

Note that as α increases axially in the annular flow regime, $1/X_{tt}$ also increases (by virtue of increasing x_e), and so does h_{CB}, as indicated by Eq. (11). This provides validation of observed experimental trends that are captured by Eq. (12). Similarly, even in the low void fraction region (bubbly flow), where it was observed that convection effects are enhanced with increasing x_e, Eq. (12) obeys the expected physics, thereby validating its applicability in determining the HTC for intermediate regimes (between bubbly and annular) using Eq. (10).

Predictions of Eq. (11), which is a first-guess approximation for h_{CB} is put to test in Fig. 9 showing its variation in the annular film over the entire range of reduced pressure, P_R. For $Re_{fo,D} = 10^4$ and $D = 5$ mm, with the value of void fraction set to $\alpha = 0.8$ (typical for transition to annular flow) and the value of x_e in Eq. (2) obtained from Eq. (9), h_{CB} showed significant convergence among values for the different cryogens, excepting those for LHe, which exhibited appreciably lower values for h_{CB}. It is evident that, compared to other cryogens, LHe exhibits very poor convective boiling, which implies that, in the annular flow regime, it is unable to lower the surface temperature to completely suppress the boiling. This is consistent with observations made for LHe in section 1.3.3 hinting at nucleate boiling possibly persisting even within the annular flow regime. This anomalous behavior of LHe from the rest of the fluid classes (including cryogens) strongly suggests treating it separately when developing HTC correlation.

1.4.4. Nucleate boiling heat transfer coefficient (HTC), h_{NB}

The nucleate boiling HTC, h_{NB}, is strongly dependent on heat flux, q, and pressure, P. The dependence on q is the outcome of nucleation and increased number of active nucleation sites and intensified bubble growth rate and departure frequency with increasing q and wall superheat, ΔT_{sat}. On the other hand, h_{NB} increases with increasing P as a result of decreasing surface tension (due to increasing T_{sat}) and latent heat of vaporization. These trends are also reflected in a number of prior correlations for pool boiling HTC, h_{PB} [*e.g.,* 35,50,34]. From Fig. 8(a), it is observed that nucleate boiling in the bubbly flow regime is suppressed with increases in G, and/or x_e. This points to the following functional relation dependence of h_{NB} on *Suppression Factor, S*, in which the dependence on q (or ΔT_{sat}) and P is included in h_{PB}.

$$h_{NB} = f\left(q, P, \frac{1}{G}, \frac{1}{x_e}\right) = f\left(\Delta T_{sat}, P, \frac{1}{G}, \frac{1}{x_e}\right) = h_{PB}S\left(\frac{1}{\Pi_G}, \frac{1}{\Pi_{x_e}}\right), \tag{13}$$

where Π_G and Π_{xe} are dimensionless function of G and x_e, respectively. This functional form of Eq. (13) was employed by Chen [41], Liu and Winterton [48], and Steiner and Taborek [31] who used earlier pool boiling correlations (for h_{PB}) by Forster and Zuber [35], Cooper [50], and Gorenflo and Sokol [34], respectively, as summarized in Table 3, along with relations for S provided in Table 2. Notice how by setting $n = 3$, Steiner and Taborek [31] assumed an asymptotic-to-sharp transition between the nucleate boiling and convective boiling mechanisms, therefore avoiding the notion of suppression, which is equivalent to setting $S = 1$.

An alternate functional relationship for h_{NB} that does not make use of pool boiling HTC correlations is formulated by re-arranging Eq. (13) and introducing the single-phase liquid HTC, $h_{sp,f}$, as,

$$h_{NB} = f\left(q, P, \frac{1}{G}, \frac{1}{x_e}\right) = f\left(Bo, P_R, \frac{1}{G}, \frac{1}{x_e}\right) = f\left(Bo, P_R, h_{sp,f}, \frac{1}{\Pi'_{1-x_e}}\right), \tag{14}$$

where, the effect of G is absorbed in both Bo (which decreases with increasing G) and $h_{sp,f}$ (which increases with increasing G) and similarly the effect of x_e is absorbed in both $h_{sp,f}$ (which decreases with increasing x_e) and dimensionless group $\Pi'_{1\text{-}xe}$ (which decreases with increasing x_e). Here, $\Pi'_{1\text{-}xe}$ is introduced as a correction to the term $(1\text{-}x_e)^{0.8}$ in $h_{sp,f}$ (see Eq. (2)) so as to predict the true trend of h_{NB} with respect to x_e. Since h_{NB} decreases with increasing G and increasing x_e, it is imperative for the exponent to G in Bo to be greater than the exponent of G in $h_{sp,f}$. Similarly, the exponent of $(1\text{-}x_e)$ in $h_{sp,f}$ needs to be greater than the exponent of $(1\text{-}x_e)$ in $\Pi'_{1\text{-}xe}$. The consequence of not obeying the latter constraint will lead to a case where as $x_e \to 1$, $h_{NB} \to \infty$, which is physically untrue. The functional form of Eq. (14) was employed by Schrock and Grossman [40], Shah [43], Gungor and Winterton [42], and Kim and Mudawar [49]. A summary of the functional relationships used in these correlations for determining h_{NB} and its associated correction ($\Pi'_{1\text{-}xe}$) for boiling suppression due to increasing x_e is provided in Table 2. An important check by the present authors on the effects of G and x_e on h_{NB} for all correlations which absorb the terms governing suppression effects showed that, excepting the Schrock and Grossman [40] correlation, which does not account for suppression with increased x_e, all three other correlations do obey the observed physics of decreasing h_{NB} with increasing x_e. On the other hand, only the Schrock and Grossman [40] and Gungor and Winterton [42] correlations capture the physics of h_{NB} decreasing with increasing G. Meanwhile, Klimenko's [44] correlation predicts sharp transition in the heat transfer mechanism ($h_{NB} \sim G^0$ and $h_{NB} \sim x_e^0$) and therefore does not obey the expected notion of boiling suppression.

By combining Eqs. (10), (12), and (13) using pool boiling based formulation, and Eqs. (10), (12), and (14), for an alternative formulation independent of pool boiling correlations, two distinct func-

Table 2
Summary of prior seminal saturated flow boiling HTC correlations*.

Author(s)	Equation(s)	Remarks
Schrock & Grossman [40]	$h_{tp} = h_{NB} + h_{CB}$ $\frac{h_{NB}}{h_{sp,fo}} = 7391.3Bo$ $\frac{h_{CB}}{h_{sp,fo}} = F = 1.11(\frac{1}{X_{tt}})^{2/3}$ where $h_{sp,fo} = 0.023Re_{fo,D}^{0.8}Pr_f^{1/3}\frac{k_f}{D}$	Fluid: water Vertical upflow Smooth transition of HTC mechanism: $n = 1$ in Eq. (10) Functional relationship for h_{NB}: Using Bo and $h_{sp,fo}$ in Eq. (14) with $\Pi'_{1-x_e} = 1$ (assumes no boiling suppression due to increase in x_e)
Chen [a,b,c] [41]	$h_{tp} = h_{NB} + h_{CB}$ $\frac{h_{NB}}{h_{PB}} = S$ $\frac{h_{CB}}{h_{sp,f}} = F$ where $h_{sp,f} = 0.023Re_{f,D}^{0.8}Pr_f^{0.4}\frac{k_f}{D}$ $h_{PB} = 0.0015Re_b^{0.62}Pr_f^{0.33}\frac{k_f}{R_b}$ $Re_b = \frac{\pi}{Pr_f}(\frac{\rho_f}{\rho_g}Ja)^2$ $R_b = \frac{\Delta T_{sat}}{h_{fg}\rho_g}\sqrt{\frac{2\pi k_f \rho_f c_{p,f}\sigma}{\Delta P_{sat}}}\sqrt[4]{\frac{\rho_f}{\Delta P_{sat}}}$ For $1/X_{tt} \le 0.1$, $F = 1$ For $1/X_{tt} > 0.1$, $F = 2.35(0.213 + \frac{1}{X_{tt}})^{0.736}$ $S = \frac{1}{1+2.53\times10^{-6}(Re_{f,D}F^{1.25})^{1.17}}$	Fluids: water, methanol, cyclohexane, pentane, heptane, benzene Vertical flows (upflow and downflow) Smooth transition of HTC mechanism: $n = 1$ in Eq. (10) Functional relationship for h_{NB}: Using h_{PB} and S in Eq. (13)
Shah [d] [43]	$\frac{h_{tp}}{h_{sp,f}} = \max\{\frac{h_{NB}}{h_{sp,f}}, \frac{h_{CB}}{h_{sp,f}}\}$ where $h_{sp,f} = 0.023Re_{f,D}^{0.8}Pr_f^{0.4}\frac{k_f}{D}$ $\frac{h_{CB}}{h_{sp,f}} = F = 1.8/N^{0.8}$ For vertical flow, $N = N_{conv.}$ For horizontal flow, if $Fr_{fo,D} \ge 0.04$, $N = N_{conv.}$ if $Fr_{fo,D} < 0.04$, $N = 0.38(Fr_{fo,D})^{-0.3}\ N_{conv.}$ For $N > 1$ if $Bo > 3 \times 10^{-5}$, $\frac{h_{NB}}{h_{sp,f}} = 230Bo^{0.5}$ if $Bo < 3 \times 10^{-5}$, $\frac{h_{NB}}{h_{sp,f}} = 1 + 46Bo^{0.5}$ For $0.1 < N \le 1$ $\frac{h_{NB}}{h_{sp,f}} = FBo^{0.5}\exp(2.74N^{-0.1})$ For $N \le 0.1$ $\frac{h_{NB}}{h_{sp,f}} = FBo^{0.5}\exp(2.47N^{-0.15})$ where $F = 14.7$, if $Bo \ge 11 \times 10^{-4}$ $F = 15.43$, if $Bo < 11 \times 10^{-4}$	Fluids: water, R11, R12, R22, R113, R505, cyclohexane, ammonia, n-butyl alcohol, isopropyl alcohol, aqueous solutions of potassium carbonate Also tested by Shah [45] for LHe, LH_2, LNe, LN_2, and LAr Vertical flows (upflow and downflow) and horizontal flow Sharp transition of HTC mechanism: $n = \infty$ in Eq. (10) Functional relationship for h_{NB}: Using Bo and $h_{sp,f}$ in Eq. (14) with $\Pi'_{1-x_e} = 1$ for $N > 1$ and $\Pi'_{1-x_e} = N_{conv.}$ for $N \le 1$
Gungor & Winterton [e] [42]	$\frac{h_{tp}}{h_{sp,f}} = E + \frac{h_{NB}}{h_{sp,f}} + \frac{h_{CB}}{h_{sp,f}}$ $\frac{h_{NB}}{h_{sp,f}} = 3000EBo^{0.86}$ $\frac{h_{CB}}{h_{sp,f}} = F = 1.12E(\frac{x_e}{1-x_e})^{0.75}(\frac{\rho_f}{\rho_g})^{0.41}$ where $h_{sp,f} = 0.023Re_{f,D}^{0.8}Pr_f^{0.4}\frac{k_f}{D}$ For vertical flow, $E = 1$ For horizontal flow, if $Fr_{fo,D} \ge 0.05$, $E = 1$ if $Fr_{fo,D} < 0.05$, $E = Fr_{fo,D}^{(0.1-2Fr_{fo,D})}$	Fluids: water, R11, R12, R113, R114, R22, ethylene Glycol, n-butanol, tthanol Vertical Flows (upflow and downflow) and horizontal flow Smooth transition of HTC mechanism: $n = 1$ in Eq. (10) Functional relationship for h_{NB}: Using Bo and $h_{sp,f}$ in Eq. (14) with $\Pi'_{1-x_e} = 1$
Klimenko [f] [44]	$h_{tp} = \max\{h_{NB}, h_{CB}\}$ $h_{NB} = C(\frac{qLa_D}{h_{fg}\rho_g\alpha_f})^{0.6}(\frac{PLa_D}{\sigma})^{0.54}Pr_f^{-0.33}(\frac{k_w}{k_f})^{0.12}\frac{k_f}{La_D}$ $h_{CB} = 0.087(\frac{G}{\rho_f}[1 + x_e(\frac{\rho_f}{\rho_g} - 1)]\frac{La_D}{\nu_f})^{0.6}Pr_f^{1/6}(\frac{\rho_g}{\rho_f})^{0.2}(\frac{k_w}{k_f})^{0.09}\frac{k_f}{La_D}$ where $C = 6.1 \times 10^{-3}$ for cryogenic fluids $La_D = \sqrt{\frac{\sigma}{g(\rho_f - \rho_g)}}$	Fluids: water, R11, R12, R113, R114, R22, NH_3, propane, butane, pentane, peptane, isooctane, benzene, cyclohexane, methanol, ethanol, LHe, LH_2, LNe, LN_2, LAr Vertical flows (upflow and downflow) and horizontal flow Sharp transition of HTC mechanism: $n = \infty$ in Eq. (10) Functional relationship for h_{NB}: Assumes no boiling suppression with $h_{NB} \sim G^0$, $x_e{}^0$
Liu & Winterton [48]	$h_{tp}^2 = h_{NB}^2 + h_{CB}^2$ $\frac{h_{NB}}{h_{PB}} = S = E_{NB}[1 + 0.055(1 + x_e Pr_f(\frac{\rho_f}{\rho_g} - 1))^{0.035}Re_{fo,D}^{0.16}]^{-1}$ $\frac{h_{CB}}{h_{sp,fo}} = F = E_{CB}[1 + x_e Pr_f(\frac{\rho_f}{\rho_g} - 1)]^{0.35}$ where $h_{sp,fo} = 0.023Re_{fo,D}^{0.8}Pr_f^{0.4}\frac{k_f}{D}$ $h_{PB} = 55P_R^{0.12}(-\log_{10}P_R)^{-0.55}q^{2/3}M^{-0.5}$ For vertical flow, $E_{NB} = E_{CB} = 1$ For horizontal flow, if $Fr_{fo,D} \ge 0.05$, $E_{NB} = E_{CB} = 1$ if $Fr_{fo,D} < 0.05$, $E_{CB} = Fr_{fo,D}^{(0.1-2Fr_{fo,D})}$ $E_{NB} = Fr_{fo,D}^{0.5}$	Fluids: water, R11, R12, R113, R114, R22, ethylene glycol, n-butanol, ethanol Vertical flows (upflow and downflow) and horizontal flow Asymptotic transition of HTC mechanism: $n = 2$ in Eq. (10) Functional relationship for h_{NB}: Using h_{PB} and S in Eq. (13)

(*continued on next page*)

Table 2 (*continued*)

Author(s)	Equation(s)	Remarks
Steiner & Taborek [31]	$h_{tp}^3 = h_{NB}^3 + h_{CB}^3$ $\frac{h_{NB}}{h_{NB,o}} = F_P[q/q_o]^n[D/D_o]^{-0.4}[R_p/R_{p,o}]^{0.133}F_M$ $\frac{h_{CB}}{h_{sp,fo}} = F = [(1-x_e)^{1.5} + 1.9x_e^{0.6}(\frac{\rho_f}{\rho_g})^{0.35}]^{1.1}$ where $h_{sp,fo} = \frac{(f_{sp,f}/8)(Re_{fo,D}-1000)Pr_f}{1+12.7(f_{sp,f}/8)^{0.5}(Pr_f^{2/3}-1)}\frac{k_f}{D}$ $f_{sp,f} = [0.7904\ln Re_{fo,D} - 1.64]^{-2}$ Standard reference conditions: $P_{R,o} = 0.1$, $R_{p,o} = 1\mu m$, $D_o = 0.01m$, and, For LHe, $q_o = 1000$ W/m^2, $h_{NB,o} = 1990$ W/m^2-K, $F_M = 0.86$ For LH_2, $q_o = 10{,}000$ W/m^2, $h_{NB,o} = 12{,}220$ W/m^2-K, $F_M = 0.35$ For LNe, $q_o = 10{,}000$ W/m^2, $h_{NB,o} = 8920$ W/m^2-K, $F_M = 0.98$ For LN_2, $q_o = 10{,}000$ W/m^2, $h_{NB,o} = 4380$ W/m^2-K, $F_M = 0.8$ For LAr, $q_o = 10{,}000$ W/m^2, $h_{NB,o} = 3870$ W/m^2-K, $F_M = 1.15$ For LCH_4, $q_o = 20{,}000$ W/m^2, $h_{NB,o} = 8060$ W/m^2-K, $F_M = 0.93$ For $P_R < 0.95$, $F_P = 2.816P_R^{0.45} + (3.4 + 1.7/(1-P_R^7))P_R^{3.7}$ For LH_2, LNe, LN_2, LAr, $n = 0.7 - 0.13\exp(1.105P_R)$ For LHe and LCH_4, $n = 0.8 - 0.1\exp(1.75P_R)$	Fluids: water, R11, R12, R113, R22, benzene, n-pentane, n-heptane, cyclohexane, methanol, n-butanol, ammonia, LHe, LH_2, LN_2 Vertical upflow Asymptotic-to-sharp transition of HTC mechanism: n = 3 in Eq. (10) Functional relationship for h_{NB}: Using h_{PB} (= h_{NB}) and S in Eq. (13) with S = 1 (assumes no boiling suppression)
Kim & Mudawar [49]	$h_{tp}^2 = h_{NB}^2 + h_{CB}^2$ $\frac{h_{NB}}{h_{sp,f}} = [2345(Bo\frac{P_H}{P_F})^{0.7}P_R^{0.38}(1-x_e)^{-0.51}]$ $\frac{h_{CB}}{h_{sp,f}} = F = [5.2(Bo\frac{P_H}{P_F})^{0.08}We_{fo,D}^{-0.54} + 3.5(\frac{1}{X_{tt}})^{0.94}(\frac{\rho_g}{\rho_f})^{0.25}]$ where $h_{sp,f} = 0.023Re_{f,D}^{0.8}Pr_f^{0.4}\frac{k_f}{D}$ For uniformly heated round tube, $P_H = P_F = D$	Fluids: water, FC72, R11, R113, R123, R1234yf, R1234ze, R134a, R152a, R22, R236fa, R245fa, R32, R404A, R407C, R410A, R417A, CO_2 Vertical flows (upflow and downflow) and horizontal flow Asymptotic transition of HTC mechanism: n = 2 in Eq. (10) Functional relationship for h_{NB}: Using Bo, P_R, and $h_{sp,f}$ in Eq. (14) with $\Pi'_{1-x_e} = 1\text{-}x_e$

* Correlations for pool boiling HTC, h_{PB}, used in this table are provided separately in Table 3.
[a] See Appendix 1 for complete derivation for Nu_{NB}.
[b] h_{tp} evaluated iteratively by initially assuming local wall temperature, T_w, until convergence.
[c] ΔP_{sat} is found using the Clausius–Clapeyron relation, $\Delta P_{sat}/\Delta T_{sat} = h_{fg}/(T_{sat}v_{fg})$.
[d] Correlation equations approximating the original graph [46] are presented in Shah [43].
[e] Improved version of the correlation by Gungor and Winteron [47].
[f] Wall thermal conductivity, k_w, evaluated at T_w using EES 10 [28] and used explicitly in this study.

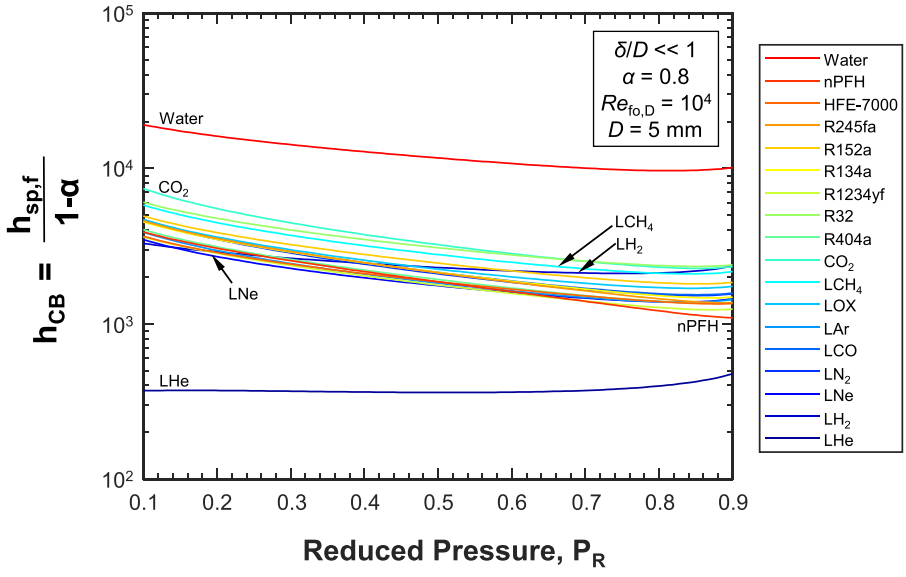

Fig. 9. Variations of convective boiling heat transfer coefficient, h_{CB}, (first-guess approximation, Eq. (11)) with reduced pressure for cryogens compared to those of other fluid classes.

tional forms of two-phase HTC correlations are,

$$h_{tp}^n = h_{PB}^n\left[S\left(\frac{1}{\Pi_G}, \frac{1}{\Pi_{x_e}}\right)\right]^n + h_{sp,f}^n\left[F\left(\frac{1}{\Pi_{1-\alpha}}\right)\right]^n \quad (15)$$

and

$$\frac{h_{tp}^n}{h_{sp,f}^n} = \left[f\left(Bo, P_R, \frac{1}{\Pi'_{1-x_e}}\right)\right]^n + \left[F\left(\frac{1}{\Pi_{1-\alpha}}\right)\right]^n, \quad (16)$$

respectively. Given its reliance on pool boiling HTC correlations, Eq. (15) includes a standalone relation for boiling suppression factor, *S*. On the other hand, without reliance on pool boiling correlations, Eq. (16) absorbs the suppression factor terms within the h_{NB} term.

Notice in Table 2 how the correlations of Shah [43], Gungor and Winterton [42], and Liu and Winterton [48] show influence of flow orientation on the convective boiling component of two-phase HTC at low Froude numbers ($Fr_{fo,D} < 0.05$). Since cryogenic flows are generally associated with high values of Froude number (see Table 1), the effect of orientation on saturated boiling HTC for cryogens is deemed inconsequential, especially for LH_2, an infer-

Table 3
Summary of prior seminal correlations for pool boiling HTC, h_{PB}, correlations later incorporated into correlations for nucleate boiling component of two-phase HTC, h_{NB} (see Table 2).

Author(s)	Equation(s)	Remarks	Functional form of h_{PB}
Forster & Zuber [a,b] [35]	$h_{PB} = 0.0015 Re_b^{0.62} Pr_f^{0.33} \frac{k_f}{R_b}$ where $Re_b = \frac{\pi}{Pr_f}(\frac{\rho_f}{\rho_g} Ja)^2$ $R_b = \frac{\Delta T_{sat}}{h_{fg}\rho_g}\sqrt{\frac{2\pi k_f \rho_f c_{p,f}\sigma}{\Delta P_{sat}}}\sqrt[4]{\frac{\rho_f}{\Delta P_{sat}}}$	Fluids: water, *n*-pentane, benzene, ethanol Employed by Chen [41]	$h_{PB} = f(\Delta T_{sat}, P)$
Cooper [50]	$h_{PB} = C P_R^{0.12-0.2\log_{10}R_p}(-\log_{10}P_R)^{-0.55} q^{2/3} M^{-0.5}$ where For stainless-steel tubes: $C = 55$	Fluids: water, R22, R21, R13, R12, R11, SF_6, R13B1, R115, R114, R226, R113, RC318, benzene, *n*-butane, ethanol, propane, methanol, ethane, LHe I, LHe II, LH_2, LD_2, LN_2, LNe, LOX, LCH_4 Employed by Liu & Winterton [48]	$h_{PB} = f(q, P, M, R_p)$
Gorenflo & Sokol [34]	$\frac{h_{PB}}{h_{PB,o}} = F_P[\frac{q}{q_o}]^n[\frac{R_p}{R_{p,o}}]^{0.133}$ where $F_P = 1.2P_R^{0.27} + 2.5P_R + \frac{P_R}{1-P_R}$ $n = 0.9 - 0.3P_R^{0.3}$ Reference conditions: $P_{R,o} = 0.1$, $R_{p,o} = 1\mu m$, and, For LHe, $q_o = 1000$ W/m^2, $h_{PB,o} = 2000$ W/m^{2}K For LH_2, $q_o = 20{,}000$ W/m^2, $h_{PB,o} = 9500$ W/m^2-K For LNe, $q_o = 20{,}000$ W/m^2, $h_{PB,o} = 9500$ W/m^2-K For LN_2, $q_o = 20{,}000$ W/m^2, $h_{PB,o} = 10{,}000$ W/m^2-K (copper surface) For LN_2, $q_o = 20{,}000$ W/m^2, $h_{PB,o} = 5000$ W/m^2-K (stainless-steel surface) For LAr, $q_o = 20{,}000$ W/m^2, $h_{PB,o} = 9500$ W/m^2-K For LOX, $q_o = 20{,}000$ W/m^2, $h_{PB,o} = 9500$ W/m^2-K For LCH_4, $q_o = 20{,}000$ W/m^2, $h_{PB,o} = 9500$ W/m^2-K	Fluids: water, R11, R12, R113, R22, benzene, *n*-pentane, *n*-heptane, cyclohexane, methanol, *n*-butanol, ammonia, LHe, LH_2, LN_2 Employed by Steiner & Taborek [31]	$h_{PB} = f(q, P, R_p)$

[a] h_{PB} evaluated iteratively by initially assuming local wall temperature, T_w, until convergence.
[b] ΔP_{sat} is found using the Clausius–Clapeyron relation, $\Delta P_{sat}/\Delta T_{sat} = h_{fg}/(T_{sat}\nu_{fg})$.

ence also made in a recent study by the present authors on flow boiling CHF for cryogens [29]. The main implication of high $Fr_{fo,D}$ is strong dominance of inertial effects over gravity/buoyancy effects, rendering the flow physics, hence HTC, independent of flow orientation.

Although the two-phase HTC functional forms of Eqs. (15) and (16) are general in nature, as they are designed to mostly segregate heat transfer mechanisms associated with two specific limiting flow regimes, bubbly and annular, close inspection of Fig. 7(c) shows presence of high vapor content at the inlet significantly alters the heat transfer mechanism within both these flow regimes. Since the fluid physics and associated HTC mechanisms are fundamentally different for two-phase mixture inlet with high quality, it imperative to make a distinction between this case and the rest of the HTC data when developing an HTC correlation. This notion will be carefully addressed in a subsequent section.

Finally, for saturated flow boiling in tubes with constant heat flux below CHF, Eqs. (15) and (16) can also be used to correlate average HTC, $\bar{h}_{tp}$, which is obtained by harmonically averaging the local HTC, h_{tp}, over the heated length,

$$\frac{1}{\bar{h}_{tp}} = \frac{1}{L_H - z_0}\int_{Z_0}^{L_H}\frac{1}{h_{tp}}dz, \tag{17}$$

where, for subcooled inlet conditions, z_0 is the location from tube inlet where $x_e = 0$, and z_0 is set to zero for saturated liquid and two-phase mixture inlet conditions. Supporting text deriving Eq. (17) for saturated flow boiling with constant heat flux is provided in Appendix 2.

1.5. Objectives of Present Study

The present study is motivated by (i) the lack of a unified, comprehensive and reliable heat transfer coefficient (HTC) database for saturated flow boiling of cryogens in a uniformly heated tube, and (ii) the lack of an accurate correlation universally valid for different cryogens. Following are key objectives of the study:

(1) Amass from the world literature cryogenic saturated flow boiling HTC data (both local and average) for saturated flow boiling of cryogens in uniformly heated tubes.
(2) Using systematic criteria, assess the accumulated data on a point-by-point basis to exclude any that are inaccurate or missing vital information such as operating conditions.
(3) Compile the data into a new consolidated database - Purdue University-Boiling and Two-Phase Flow Laboratory (PU-BTPFL) Cryogen Saturated Flow Boiling Heat Transfer Coefficient Database (PU-BTPFL HTC Database for short) - after applying the exclusion criteria.
(4) Carefully segregate the data based on fluid (LHe, LH_2, LNe, LN_2, LAr, LCH_4), flow orientation (vertical upflow, vertical downflow, horizontal flow), inlet state (subcooled liquid, saturated liquid, two-phase mixture), and tube material.
(5) Identify new physics-based classifiers that aid in understanding of physics unique to cryogens prior to correlation development.
(6) Assess the performance of prior seminal HTC correlations using the PU-BTPFL HTC Database.
(7) Using the PU-BTPFL HTC Database, develop new 'Universal HTC Correlation' for saturated flow boiling of cryogens.
(8) Ascertain the accuracy of the new correlation for each cryogen and against each primary variable (mass velocity, heat flux, system pressure or reduced pressure, diameter, and local quality).
(9) Identify 'gaps' in the available data which warrant further experimental investigation.
(10) Recommend a methodology for acquiring future HTC data in a manner that is conducive to refining HTC correlations and/or mechanistic models.

2. Compilation of Saturated Flow Boiling HTC Database for Cryogens

As indicated earlier, the present study involves exhaustive data mining of saturated flow boiling HTC data for cryogens from all literature sources available to the present authors. This includes (1) major cryogen journals (*e.g.,* Cryogenics (Elsevier), Advances in Cryogenic Engineering (Springer), (2) major cryogen conferences (*e.g.,* International Cryogenic Engineering Conference, Cryogenic Engineering Conference (early papers published in Advances in Cryogenic Engineering)), (3) NASA and NIST technical reports, and (4) other sporadic publications, reports and theses from across the globe.

Three kinds of HTC data can be extracted from any given reference: (1) local HTC data with prescribed local quality conditions, *i.e.,* $h_{tp} = f\,(q,\ P,\ D,\ G,\ x_e)$, (2) local HTC data with prescribed inlet conditions, *i.e.,* $h_{tp} = f\,(q,\ P_{in},\ D,\ G,\ x_{e,in},\ z)$, and (3) average HTC data with prescribed inlet conditions, *i.e.,* $\bar{h}_{tp} = f\,(q,\ P_{in},\ D,\ G,\ x_{e,in},\ L_H)$. In order to ensure the HTC data belong to the saturated flow boiling region, only local HTC data with $x_e \geq 0$ and average HTC data with $x_{e,in} \geq 0$ are considered. Unless HTC data are explicitly specified in a given reference, the HTC information is determined from wall temperature distribution along the heated tube for local HTC data and average wall temperature information for average HTC data. Furthermore, any data point missing heat flux or quality information is excluded from consideration. In order to exclude any post-CHF (DNB or Dryout type), two inspection methods are used: (1) ensuring, for a given heat flux, that any local wall temperature data are void of excursions indicative of CHF occurrence, and (2) ensuring that any HTC data do not include significant deterioration with increasing heat flux (for both local and average HTC data) or quality (for local HTC data).

The data mining effort was complicated by difficulty acquiring certain references because of such factors as (a) lack of availability from international interlibrary services, (b) reluctance of a few investigators to share their own data, and (c) lack of English translated versions of foreign literature containing data. Additionally, avoidance of duplicate data was a thorough and time-consuming effort, necessitated by the fact that many published works lacked clear indication of sources for the data presented. Overall, the possibility of data duplication in the HTC database was prevented by careful point-by-point inspection of the acquired data.

After completing the initial data mining effort and making certain of absence of duplicate data, efforts shifted to excluding data that did not strictly conform to the following uniformity requirements:

(1) Only single component cryogens, *i.e.,* excluding data for binary or higher order mixtures.
(2) Only forced convection driven tubes; data for boiling in capillary tubes, thermosyphons, and natural circulation driven two-phase flow are excluded.
(3) Flow in only straight circular tubes; data for non-circular tubes (*e.g.,* rectangular, square, annular, rod, bundle), helical tubes or U-bends are excluded.
(4) Flow in only stationary tubes; data for rotating tubes are excluded.
(5) Flow not involving use of swirl flow promotor (*e.g.,* twisted tape and wire coil inserts) within the tube or upstream of the tube's inlet.
(6) Flow not involving use of abnormal tube inlet or outlet (*e.g.,* orifice plate, inlet expansion, outlet expansion).
(7) Flow in tubes whose inner walls are not modified (*e.g.,* finned or coated) for the purpose of enhancing heat transfer performance.
(8) Flow in tubes whose inner walls are not altered for the purpose of enhancing nucleation.
(9) Only data for vertical upflow, vertical downflow, and horizontal flow; data for inclined tubes are excluded.
(10) Only uniformly heated circular tubes; data for axially or circumferentially nonuniform wall heat flux are excluded.
(11) Only data obtained from heating experiments; data obtained from quenching experiments, which are prone to appreciable measurement error resulting mostly from fast temperature transients, are excluded.
(12) Only steady-state data; transient data are excluded.
(13) Only fully wetted tube data; horizontal flow boiling data corresponding to the stratified and stratified-wavy flow regimes are excluded.
(14) Only data presented by original authors with documented values for every parameter necessary for correlating the data (*e.g.,* heat flux, operating pressure, mass velocity, local quality, tube geometry, *etc.*).

This exclusion strategy, details of which are summarized in Table 4, resulted in an initial database suitable for developing correlations (also future models) for the saturated flow boiling HTC specific to cryogens. However, it is important to note that the above do not constitute a complete list for data exclusion, as other considerations, achieved through further assessment of the amassed data as discussed in a later section, preclude inclusion of certain additional datapoints. These additional exclusions are used in pursuit of the final Purdue University-Boiling and Two-Phase Flow Laboratory (PU-BTPFL) Cryogen Saturated Flow Boiling Heat Transfer Coefficient Database, referred to hereafter for brevity as PU-BTPFL HTC Database.

3. Assessment of World HTC Data

Pursuant to application of the exclusion criteria discussed in the previous section, further assessment of world cryogen HTC data is broadly classified into two categories based on implementation of (i) physics-based data exclusion criteria and (ii) additional physics-based data classifiers.

3.1. Physics-Based Data Exclusion Criteria

3.1.1. Subcritical boiling verification

When acquiring flow boiling data in experiments, it is crucial that operating conditions be maintained below the critical point everywhere along the tube. For common fluids, critical pressure and critical temperature are comparatively much higher than those for cryogens and experiments are conveniently performed below the critical point. However, cryogens, especially fluids like LHe, LH_2, and LNe, possess extremely low critical temperatures of 5.2 K, 33.1 K, and 44.4 K, respectively, while that for LN_2 is 126.2 K, which is still much lower than that for common fluids. These low critical temperatures greatly increase the likelihood for wall temperature to exceed the critical temperature, especially for LHe, LH_2, and LNe. Hence, the criterion of $T_w < T_{crit}$ is applied to the amassed data to make certain they obey subcritical conditions. It is observed that few LHe data by Bredy [92] and almost all LH_2 data by Core et al. [12] and von Glahn and Lewis [98] fail to obey this criterion and are therefore excluded from the HTC database. Table 5 provides details of data points violating this criterion, which are observed only for local HTC with prescribed inlet conditions.

3.1.2. Energy balance verification for average HTC data

The flow boiling data sought after in the present study must fall in the range of $0 \leq x_e \leq 1$. As seen from Eqs. (15) and (16), the

Table 4
Data exclusion strategy for single component saturated boiling HTC data for sub-critical cryogenic flow boiling in uniformly heated straight circular tubes.

Reference	Deviation from standard flow configuration [a]	Missing data	Miscellaneous factors	Remarks
(a) Complete Exclusion				
Dean & Thompson [52]	•			Annular circular test section with heater in the core
Walters [53]		•		Only overall range for mass velocity provided
Lewis et al. [14]		•	•	Abnormally high scatter reported for LH_2 HTC data owing to experimental uncertainties; only outer wall temperature provided for LH_2 and LN_2 data
Jones & Altman [54]	•			Circular test section with a U-bend
Chi [55]		•		Only overall range of operating conditions provided
Glickstein & Whitesides [56]		•		Only overall range for pressure provided and local quality information missing
Keilin [57]		•		Only overall range for mass velocity provided for certain data points
Hynek et al. [58]	•	•		Certain tests performed using twisted tapes; local quality information missing for certain data points
Jergel & Stevenson [59]	•			Rectangular channel test section with only a small fraction of test section heated
Jergel & Stevenson [60]	•			Rectangular channel test section with only a small fraction of test section heated
Jergel et al. [61]	•			Rectangular channel test section with only a small fraction of test section heated
Jergel & Hlasnik [62]	•			Rectangular channel test section with only a small fraction of test section heated
Antipov et al. [63]	•			Boiling in capillary tube
Papell & Hendricks [64]		•		Local quality information missing
Papell & Hendricks [65]			•	Duplicate data from Papell & Hendricks [64]
Petukhov et al. [66]		•		Only overall range for mass velocity and inlet quality provided for certain data points
Subbotin et al. [67]		•		Only overall range for mass velocity provided and local quality information missing for certain data points; certain data points provided for decreasing heat flux
Steiner [68]		•		Test section information missing
Umekawa & Ozawa [69]	•			Natural circulation driven two-phase flow in a closed loop
Lu [70]	•			Rectangular channel test section with discrete heat sources
Klimenko & Sudarchikov [71]		•	•	Only overall range for pressure and inlet quality provided for certain data points; HTC data highly influenced by thermal oscillations
Benkheria et al. [72]	•			Thermosyphon two-phase flow
Qi et al. [73]		•		Only overall range for inlet quality provided
Yun et al. [74]	•		•	Horizontal flow boiling in stratified and stratified-wavy flow regime [c]; certain tests performed with circular test section containing wire coil inserts
Fu et al. [75]			•	Transient boiling data
Zhang & Fu [76]		•		Heat flux and local wall temperature information missing
Fu et al. [77]		•		Boiling from a surface that has been altered to enhance nucleation
Fu et al. [78]	•			Rectangular channel test section with three-sided heating
Chen & Shi [24]			•	Tests performed using Liquified Natural Gas (LNG)
Mustafi [79]	•			Boiling initiated in helically shaped pre-heater
Trejo et al. [18]	•			Square and rectangular channel test sections
Deng et al. [80]	•			Two-phase flow in heated U-tubes
Yoneda et al. [81]	•			Rectangular channel test section with one-sided heating
Tatsumoto et al. [82]	•			Annular circular test section with heater in the core
Sudarchikov [83]		•		Local quality information missing
Trejo et al. [19]	•			Rectangular channel test section
Liu et al. [84]		•		Local HTC information provided in the form $h_{min.}/h_{avg.}$
An et al. [85]		•		Pressure and inlet quality information missing
Tatsumoto et al. [15]			•	Average HTC data with subcooled inlet and saturated outlet
Tatsumoto et al. [16]			•	Average HTC data with subcooled inlet and saturated outlet
(b) Partial Exclusion [b]				
Core et al. [12]			•	Abnormally high scatter reported for LH_2 HTC data owing to experimental uncertainties
Wright & Walters [13]		•	•	Only outer wall temperature provided; high uncertainty in thermal conductivity of copper at ~ 25K; local HTC data extracted and provided in Steiner & Schlünder [27] rejected due to aforementioned issues
Johannes [86]		•		Thermocouple position information missing for certain data points
Hilderbrandt [1]		•	•	Only overall range for mass velocity provided for certain data points; certain data points provided for decreasing heat flux
Giarrantano et al. [2]		•		Heat flux and local quality information missing for certain data points
Ogata & Sato [4]		•	•	Certain data points provided for decreasing heat flux; only overall range for mass velocity and pressure provided for certain data points
Jones & Johnson [87]		•	•	Only overall range for inlet quality provided for certain data points

(*continued on next page*)

Table 4 (*continued*)

Reference	Deviation from standard flow configuration [a]	Missing data	Miscellaneous factors	Remarks
Klein [88]		•	•	Certain data points provided for decreasing heat flux; heat flux information missing for certain data points
Steiner & Schlünder [27]			•	Certain data points difficult to extract due to strong overlap and similarity of symbols
Klimenko & Sudarchikov [89]		•		Local quality information missing for certain data points
Petukhov et al. [5]	•			Certain tests performed using rotating test section
Subbotin et al. [90]			•	Certain data points provided for decreasing heat flux
Klimenko et al. [91]		•		Heat flux information missing for certain data points
Klimenko et al. [51]		•	•	Mass velocity and heat flux information missing for certain data points; horizontal flow boiling in stratified flow regime [c]
Bredy et al. [92]		•	•	Local quality information missing for certain data points; certain data points difficult to extract due to strong overlap
Panek et al. [93]			•	Certain data points difficult to extract due to strong overlap
Giarrantano et al. [94]		•		Only overall range for mass velocity and inlet quality provided for certain data points; duplicate data from Jones & Johnson [87]
Zhang et al. [95]		•		Only overall range for local quality provided for certain data points
Chen et al. [96]		•		Local quality information unclear for certain data points
Matsumoto et al. [11]			•	Certain data points provided for decreasing heat flux
Zhang et al. [97]		•		Only overall range for pressure provided for certain data points

[a] Standard flow configuration is a uniformly heated straight circular tube with heat applied externally to single-component fluid.
[b] Select data points are excluded while remaining data are used in the present study.
[c] Asymmetrical wetting of test section (top-dry and bottom-wet) leads to exorbitantly high wall superheat and drastically low HTC values at the top as compared to the bottom wetted portion.

Table 5
Summary of data points excluded from the HTC databases.

Reference	Total HTC data points	Constant pressure assumption violation			Critical Condition	Energy balance violation	Acceptable HTC data points
		High $\Delta P_{max}/P$ [a] Low *Co*	High $\Delta P_{max}/P$ [b] High *Co*	ΔP_{max} out of bounds [c]	$T_w > T_{crit.}$ [d]	$x_{e,out} > 1$ [e]	
Local HTC database with prescribed inlet conditions *							
Liquid Helium							
(a) Horizontal Flow							
Bredy [92]	15				8		7
Liquid Hydrogen							
(a) Vertical Upflow							
Core et al. [12]	6				5		1
von Glahn & Lewis [98]	11				11		0
Liquid Nitrogen							
(a) Vertical Upflow							
Grigoriev et al. [100]	18			18			0
Qi et al. [103]	31	20	4	7			0
(b) Horizontal Flow							
Chen et al. [96]	179	32					147
Total	**260**	**52**	**4**	**25**	**24**		**155**
Average HTC database with prescribed inlet conditions **							
Liquid Helium							
(a) Vertical Upflow							
Grigoriev et al. [99]	51					1	50
Grigoriev et al. [100]	33					1	32
Liquid Hydrogen							
(a) Horizontal Flow							
Wright & Walters [13]	19	8					11
Liquid Nitrogen							
(a) Vertical Upflow							
Grigoriev et al. [100]	89		48	41			0
Total	192	8	48	41		2	93

* Local thermodynamic equilibrium quality is determined from prescribed inlet qualities, using the energy balance equation, $x_e = x_{e,in} + 4Bo\frac{z}{D}$.
[a] Data with $\Delta P_{max}/P > 0.2$ and $Co \leq 1.5$.
[b] Data with $\Delta P_{max}/P > 0.2$ and $Co > 1.5$.
[c] High *Co* data (> 1.5 and in some cases > 3) with high pressure drop causing pressure to go out of bounds for evaluation of thermophysical properties in REFPROP 10 [26].
[d] Condition violated only by LHe and LH_2 local HTC data with prescribed inlet conditions.
** All average HTC data have $x_{e,in} = 0$ except for those from Wright and Walters [13], where $x_{e,in} > 0$.
[e] For average HTC data with prescribed inlet conditions, $x_{e,out}$ is determined from prescribed inlet conditions using the energy balance equation, Eq. (18).

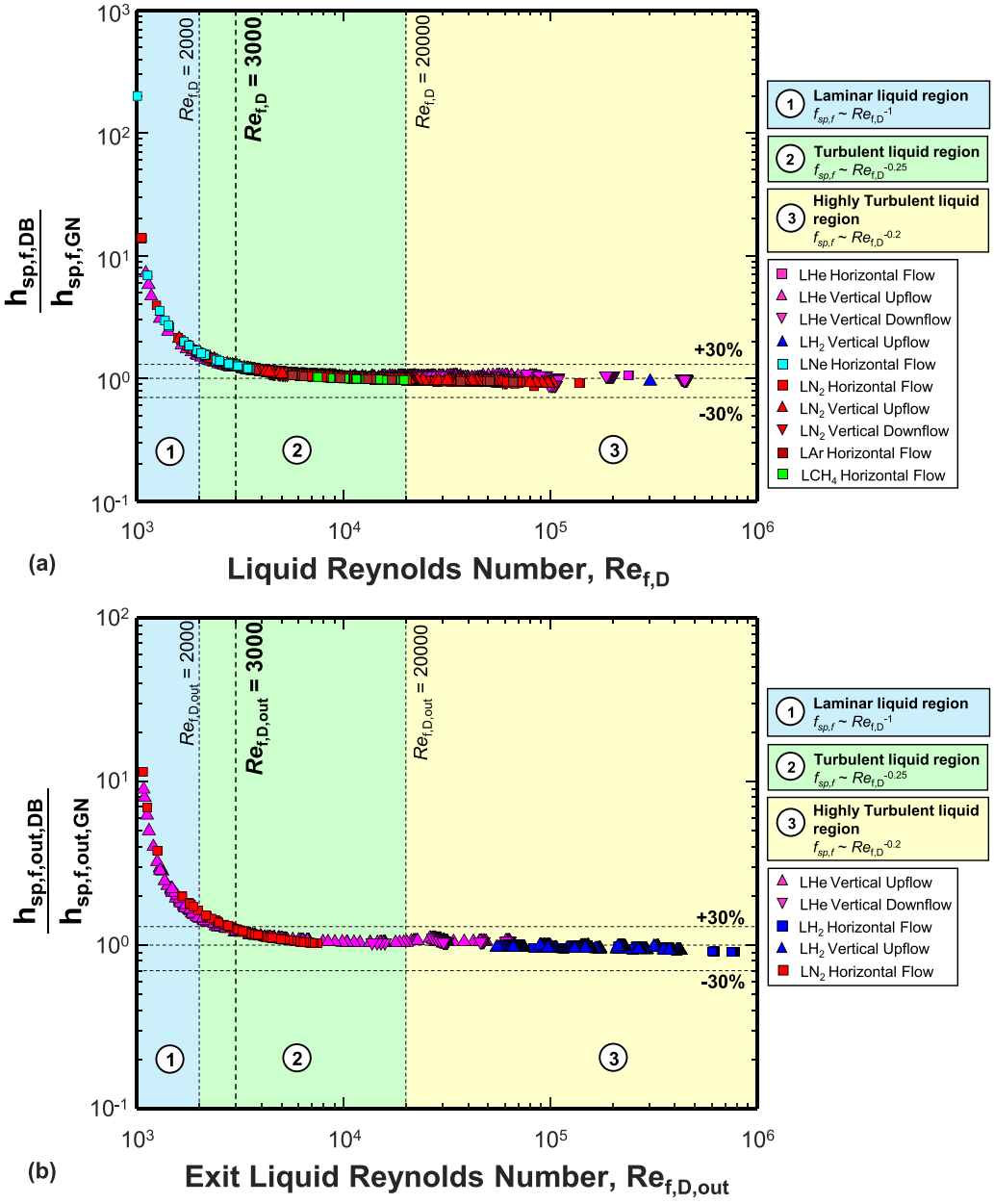

Fig. 10. Variations of ratio of single-phase liquid heat transfer coefficient data using Dittus-Boelter [30] and Gnielinski [33] HTC correlations with liquid Reynolds number using (a) local Reynolds number for local HTC data and (b) exit Reynolds number for average HTC data.

local flow boiling HTC is a function of local x_e. Hence, no further verification is required for the local HTC data as local x_e information is both available and bounded by the constraint $x_e \leq 1$. However, for average flow boiling HTC data, obtained by harmonically averaging local HTC measurements along the heated length, it is mandatory to check that local x_e is indeed between 0 and 1 along the entire heated tube. As discussed in section 2, only average HTC data with $x_{e,in} \geq 0$ and showing no indication of CHF are considered. Hence, it is sufficient to establish that $x_{e,out} \leq 1$, where $x_{e,out}$ is found using an energy balance (with constant pressure assumption),

$$x_{e,out} = x_{e,in} + 4Bo\frac{L_H}{D}. \tag{18}$$

It is observed that only two data points by Grigoriev et al. [99,100] violate this criterion. Table 5 provides details of these data points.

3.1.3. Constant pressure verification for HTC data with prescribed inlet conditions

The majority of reviewed studies were found to lack mention of whether the reported system pressure is the measured inlet or outlet pressure. Since the local two-phase HTC is a function of local pressure, the system pressure reported in the studies is considered to be the local pressure for local HTC evaluation, and inlet pressure for average HTC evaluation. Hence, for data with prescribed local quality information, there is no need for pressure drop analysis. However, for local and average HTC data with prescribed inlet conditions, pressure drop along the tube directly influences the evaluation of local x_e using Eq. (18), which is based on the assumption of constant pressure. This fact renders verification of constant pressure imperative for both local and average HTC data with prescribed inlet conditions. Fortunately, some authors do provide pressure drop data along with the heat transfer data. It is found for most studies providing pressure drop data that maximum pres-

sure drop along the tube is quite small (*e.g.,* $\Delta P_{max}/P < 0.1$ as suggested by Katto and Yokoya [101]), which allows using the constant pressure assumption. Such low pressure drops along with absence of mention whether quoted system pressure was measured at the inlet, locally, or at the exit, provide ample justification for using system pressure alone for determining values for saturated thermophysical properties when correlating HTC data. This approach is used throughout the present correlation effort, where either inlet or local pressures are provided.

To systematically verify the assumption of constant pressure, the present authors employed a conservative (high) estimate for ΔP_{max} between the inlet and outlet of the heated tube for both local and average HTC data with prescribed inlet conditions. For axial locations where $x_e < 0$, which is the case only for local HTC data with subcooled inlet (as average HTC data are bounded by the constraint $x_{e,in} \geq 0$), the portion of pressure drop associated with single-phase liquid is calculated using Colebrook's friction factor relation [102], with any applicable gravitational pressure drop included as well,

$$\frac{dP_{sp,f,F}}{dz} = \frac{2}{D} f_{sp,f} \frac{G^2}{\rho_f}, \tag{19}$$

$$\frac{1}{\sqrt{4f_{sp,f}}} = -2\log_{10}\left(\frac{R_p}{3.7D} + \frac{2.51}{Re_{fo,D}\sqrt{4f_{sp,f}}}\right), \tag{20}$$

and

$$\frac{dP_{sp,f,G}}{dz} = \rho_f g sin\theta. \tag{21}$$

Whereas, for axial locations where $x_e \geq 0$, two-phase relations are used, which include those for friction, acceleration and gravity. The accelerational and gravitational gradients are determined, respectively, according to

$$\frac{dP_{tp,A}}{dz} = G^2 \frac{d}{dz}\left\{\frac{x_e^2}{\alpha\rho_g} + \frac{(1-x_e)^2}{(1-\alpha)\rho_f}\right\} \tag{22}$$

and

$$\frac{dP_{tp,G}}{dz} = \left(\alpha\rho_g + (1-\alpha)\rho_f\right) g sin\theta, \tag{23}$$

where the void fraction α is calculated using Zivi's [36] relation, Eq. (9).

Finally, total pressure drop ΔP is determined by integrating the pressure gradient relations for the single-phase and two-phase regions over the respective axial span for each data point. Notice that, for the two-phase region, frictional pressure gradient is bound on the lower side by that for pure saturated liquid and on the upper side pure saturated vapor, both calculated using Colebrook's friction factor relation [102], *i.e.,*

$$0 \leq \frac{\Delta P_{tp,F} - \Delta P_{sp,f,F}}{\Delta P_{sp,g,F} - \Delta P_{sp,f,F}} \leq 1, \tag{24}$$

Therefore, a conservative high estimate for total pressure drop, ΔP_{max}, is found by replacing the two-phase frictional pressure drop for axial locations where $x_e > 0$ by that corresponding to single-phase saturated vapor.

$$\frac{dP_{sp,g,F}}{dz} = \frac{2}{D} f_{sp,g} \frac{G^2}{\rho_g} \tag{25}$$

and

$$\frac{1}{\sqrt{4f_{sp,g}}} = -2\log_{10}\left(\frac{R_p}{3.7D} + \frac{2.51}{Re_{go,D}\sqrt{4f_{sp,g}}}\right) \tag{26}$$

Owing to the conservative nature of the maximum pressure drop (which definitely exceeds the actual pressure drop), the constant pressure assumption suggested by Katto and Yokoya [101] is slightly relaxed to $\Delta P_{max}/P < 0.2$. A key advantage of this method is lack of reliance on the myriad of possible models or correlations for calculating the two-phase frictional pressure gradient.

Overall, the criterion $\Delta P_{max}/P < 0.2$ is found to be valid for almost all cases, excepting a few LN_2 data points by Chen et al. [96], and LH_2 data points by Wright and Walters [13], and all LN_2 data points by Grigoriev et al. [100] and Qi et al. [103], which, in addition to having $\Delta P_{max}/P > 0.2$, also exhibit high confinement number, $Co > 1.5$, a characteristic of micro-channels having very small diameter. Table 5 provides additional details on data points violating the constant pressure assumption and therefore excluded from the HTC database.

3.1.4. Turbulent flow verification

As seen in Table 1, the vast majority of available experimental data for cryogens are associated with high values of liquid-only Reynolds numbers, $Re_{fo,D}$, therefore turbulent flow. When aiming to develop flow boiling HTC correlations for cryogens, it is imperative to assume that the boiling suppression and convection enhancement mechanisms discussed earlier and illustrated in Fig. 8 would be different for laminar versus turbulent flows. Therefore, laminar data are expected to show appreciable departure from correlations intended for turbulent flow, hence the need to exclude laminar data from the cryogen flow boiling HTC database. This fact is further substantiated by revisiting Table 2 and examining the single-phase HTC correlations used in prior flow boiling HTC correlations. It is seen that either the Dittus-Boelter [30] correlation, Eq. (2), or the Gnielinski [33] correlation, Eqs. (4) and (5), are used, both being applicable to only turbulent flow. However, the Dittus-Boelter correlation is recommended for $Re_{f,D} \geq 10^4$, compared to $Re_{f,D} \geq 3000$ for the Gnielinski correlation. Hence, it is imperative to check the cryogen flow boiling HTC database for deviations related to range of Reynolds number. Fig. 10 shows this deviation by plotting $h_{sp,f,DB}/h_{sp,f,GN}$, ratio of single-phase liquid HTC based on the Dittus-Boelter correlation to that of the Gnielinski correlation (with $h_{sp,f,GN}$ calculated by replacing $Re_{fo,D}$ in Eqs. (4) and (5) by $Re_{f,D}$), versus liquid Reynolds number, $Re_{f,D}$. For local HTC data, Fig. 10(a), local values of $h_{sp,f,DB}/h_{sp,f,GN}$ are plotted versus local $Re_{f,D}$, whereas for average HTC data, Fig. 10(b), exit values are used for both the HTC ratio, $h_{sp,f,out,DB}/h_{sp,f,out,GN}$, and liquid Reynolds, $Re_{f,D,out}$. It is evident from both Fig. 10(a) and 10(b) that the two correlations predict the single-phase HTC to within ±30% for Reynolds numbers above 3000. Tables 6(a) and 6(b) provide a summary local HTC data points (both with and without prescribed inlet conditions) and average HTC data points, respectively, that have been excluded for failing to obey this criterion. For the average HTC data, the criterion is modified to $Re_{f,D,min} \geq 3000$, signifying that the lowest value that liquid Reynolds number can have at the tube exit is above 3000.

3.1.5. Distinction of boiling from non-boiling data

Recall that a key objective of this study is to develop correlations specific to flow boiling. Therefore, it is essential that any non-boiling data be excluded before correlating HTC data. As shown earlier in Fig. 7(a), nucleate boiling initiation is not dictated by $x_e = 0$, but rather by ONB ($T_w \geq T_{w,ONB}$). Although local HTC data with prescribed local quality information and obeying $x_e > 0$ will almost always be in the two-phase region, the region with $x_e \approx 0$ need to be checked carefully for possible non-boiling data. For local and average HTC data with prescribed subcooled ($x_e < 0$) inlet conditions (Figs. 7(a)), the constraint $x_e \geq 0$ alone ensures that the HTC data are associated with saturated boiling. For local and average HTC data with prescribed saturated liquid ($x_e = 0$) inlet conditions (Fig.7(b)), $x_{e,in} = 0$ is a necessary but not sufficient condition for saturated boiling. For local and average HTC data with prescribed two-phase mixture ($x_e > 0$) inlet conditions (Fig. 7(c)),

Table 6a
Summary of additional data points excluded from HTC databases. (a) Exclusions of local HTC data.

Reference	Total HTC data points	Low Reynolds number data		Non-boiling data		Acceptable HTC data points
		$Re_{f,D} < 1000$ [a]	$1000 < Re_{f,D} < 3000$ [b]	$\frac{h_{tp}}{h_{sp,f}} \leq 1.1$ [c]	$\frac{T_w - T_{sat}}{T_{w,max} - T_{sat}} \geq 0.9$ [d,e]	
Local HTC database with prescribed local conditions						
Liquid Neon						
(a) Horizontal Flow						
Mohr & Runge [104]	136	17	92			27
Liquid Nitrogen						
(a) Vertical Upflow						
Qi et al. [103]	306	1	14			291
(b) Horizontal Flow						
Steiner & Schlünder [27]	509	6	19	4	9	471
Klein [88]	124		4			120
Muller et al. [105]	120			2	8	110
Liquid Argon						
(a) Horizontal Flow						
Muller et al. [105]	140		20	1	2	117
Total	**1335**	**24**	**149**	**7**	**19**	**1136**
Local HTC database with prescribed inlet conditions [f]						
Liquid Helium						
(a) Vertical Upflow						
Ogata & Sato [4]	46			3	4	39
Keilin et al. [106]	99		1			98
Grigoriev et al. [99]	50		2	18	1	29
Grigoriev et al. [100]	35	2	33			0
Romanov et al. [6]	61				5	56
Yarmak & Zhukov [107]	25			7		18
(b) Vertical Downflow						
Giarratano et al. [2]	144			4		140
Liquid Nitrogen						
(a) Vertical Upflow						
Xu et al. [108]	18		1			17
(b) Horizontal Flow						
Zhang et al. [95]	229		21	11		197
Chen et al. [96]	147	1	30	4	1	111
Total	854	3	88	47	11	705

[a] Liquid Reynolds number is bounded by the constraint $Re_{f,D} > 1000$ to be used in the Gnielinski's [33] HTC correlation.
[b] Based on criteria indicated in Fig. 10(a) which allow a maximum deviation of ±30% between $Re_{f,D}$ predicted according to Dittus-Boelter [30] and Gnielinski [33].
[c] Single-phase liquid HTC, $h_{sp,f}$, is evaluated using Gnielinski's [33] correlation.
[d] Maximum wall temperature, $T_{w,max}$, is defined in Eq. (28).
[e] All data points that satisfy the criterion, $\frac{h_{tp}}{h_{sp,f}} \leq 1.1$ also satisfy $\frac{T_w - T_{sat}}{T_{w,max} - T_{sat}} \geq 0.9$, hence, only unique data points are tabulated.
[f] Local x_e is determined from prescribed inlet qualities using the energy balance equation, $x_e = x_{e,in} + 4Bo\frac{z}{D}$.

all upstream data will involve saturated boiling. The same rationale can be applied to average HTC data with one of the three prescribed inlet conditions, to exclude data having significant non-boiling region.

To distinguish boiling from non-boiling data, a dimensionless wall superheat parameter, ΔT^*_{sat}, is defined as

$$\Delta T^*_{sat} = \frac{T_w - T_{sat}}{T_{w,max} - T_{sat}}, \tag{27}$$

where, $T_{w,max}$, is the maximum wall temperature possible without initiating any boiling. For saturated boiling HTC region, $T_{w,max}$ for non-boiling data can be defined as

$$T_{w,max} = T_{sat} + \frac{q}{h_{sp,fo}}, \tag{28}$$

where $h_{sp,fo}$ is evaluated using the Gnielinski [33] correlation, Eqs. (4) and (5). Since, for a fixed heat flux, the two-phase HTC, h_{tp}, is orders of magnitude greater than the single-phase HTC, $h_{sp,f}$, the additional criterion of $\Delta T^*_{sat} < 1$ must be satisfied for local HTC data to be associated with boiling. Figs. 11(a) and 11(b) show variations of two-phase to single-phase HTC ratio with ΔT^*_{sat} for local and average HTC data, respectively. These figures show a 10% underrelaxing of this criterion is allowed to allow for measurement uncertainty. They reveal two classes of violations associated with non-boiling data, $h_{tp}/h_{sp,f} < 1$ and $\Delta T^*_{sat} > 1$, which imply $T_w > T_{w,max}$. Hence, with the 10% underrelaxation, these constraints are revised slightly as $h_{tp}/h_{sp,f} \leq 1.1$ and $\Delta T^*_{sat} \geq 0.9$; the latter being dominant as it contains all data of the former. A similar analysis is applied to the average HTC data, where the local wall temperature in Eq. (27) is replaced with average wall temperature, $\bar{T}_w$, and $T_{w,max}$, which is independent of local flow quality remains the same as in Eq. (28). Additionally, the value of $h_{sp,f}$ in the $h_{tp}/h_{sp,f} \leq 1.1$ criteria is modified to $h_{sp,f,min}$, which is evaluated at tube exit. Tables 6(a) and 6(b) provide a summary of local HTC data points (with and without prescribed inlet conditions) and average HTC data points, respectively, which have been excluded for failing to obey these criteria.

Fig. 12 shows a summary of cryogenic HTC data deemed acceptable after being subjected to the aforementioned physics-based exclusion criteria of constant pressure assumption, turbulent flow, and boiling existence. Fig. 12(a) shows histograms of the data

Table 6b
Summary of additional data points excluded from HTC databases. (b) Exclusions of average HTC* data with prescribed inlet conditions.

Reference	Total HTC data points	Low Reynolds number data		Non-boiling data		Acceptable HTC data points
		$Re_{f,D,min} < 1000$ [a]	$1000 < Re_{f,D,min} < 3000$ [b]	$\frac{\tilde{h}_{tp}}{h_{sp.f.min}} \leq 1.1$ [c]	$\frac{\tilde{T}_w - T_{sat}}{T_{w,max} - T_{sat}} \geq 0.9$ [d,e]	
Liquid Helium						
(a) Vertical Upflow						
Hilderbrandt [1]	78	6	46			26
Grigoriev et al. [99]	50	2	10	12	2	24
Grigoriev et al. [100]	32	5	12			15
Liquid Hydrogen						
(a) Vertical Upflow						
Tatsumoto et al. [7]	44			13	1	30
Shirai et al. [8]	100			17	1	82
Tatsumoto et al. [10]	325			85	6	234
(b) Horizontal Flow						
Tatsumoto et al. [9]	166			94	2	70
Liquid Nitrogen						
(a) Vertical Upflow						
Petukhov et al. [5]	6	6				0
(b) Horizontal Flow						
Zhang et al. [95]	81		12	12	4	53
Chen et al. [96]	34	4	12	6	1	11
Total	**916**	**23**	**92**	**239**	**17**	**545**

* Local and exit x_e is determined from prescribed inlet conditions using the energy balance equation, $x_e = x_{e,in} + 4Bo\frac{z}{D}$.
[a] Liquid Reynolds number is bounded by the constraint $Re_{f,D} > 1000$ to be used in Gnielinski's [33] HTC correlation.
[b] Based on criteria indicated in Fig. 10(b) to allow a maximum error of ±30% between $Re_{f,D}$ predicted according to Dittus-Boelter [30] and Gnielinski [33].
[c] Minimum single-phase liquid HTC, $h_{sp,f,min}$, is evaluated at outlet using Gnielinski's [33] correlation.
[d] Maximum wall temperature, $T_{w,max}$, is defined in Eq. (28).
[e] All data points that satisfy the criterion $\frac{\tilde{h}_{tp}}{h_{sp.f.min}} \leq 1.1$ also satisfy $\frac{\tilde{T}_w - T_{sat}}{T_{w,max} - T_{sat}} \geq 0.9$, hence, only unique data points are tabulated.

based on maximum pressure drop ratio and confinement number. It can be seen that all the data (local and average HTC data with prescribed inlet conditions) satisfy the constant pressure criteria of $0 \leq \Delta P_{max}/P \leq 0.2$, and almost all of the data are associated with $0 \leq \Delta P_{max}/P \leq 0.1$. Additionally, almost all of the data are associated with confinement numbers below 0.6, while only a few LN_2 data points exceed this value. Notice that, since *Co* is inversely proportional to *D*, high *Co* values are also reflected in high pressure drop across the tube. To this end, the criterion proposed by Kew and Cornwell [109] of $Co = 0.5$ is relaxed to $Co = 0.6$ to distinguish macro-scale from micro-scale behavior. Fig. 12(b) shows a Reynolds number map of $Re_{g,D}$ versus $Re_{f,D}$ separated into four quadrants of (i) laminar liquid – laminar vapor ($Re_{f,D} < 2000$ and $Re_{g,D} < 2000$), (ii) laminar liquid – turbulent vapor ($Re_{f,D} < 2000$ and $Re_{g,D} \geq 2000$), (iii) turbulent liquid – laminar vapor ($Re_{f,D} \geq 2000$ and $Re_{g,D} < 2000$), and (iv) turbulent liquid – turbulent vapor ($Re_{f,D} \geq 2000$ and $Re_{g,D} \geq 2000$). Notice that the vast majority of the local and average HTC data belong to the turbulent liquid – turbulent vapor quadrant, and the remaining data in the turbulent liquid – laminar vapor quadrant. The physics dictating the presence of a data point in either of these quadrants is governed by two independent parameters, $Re_{fo,D}$ and $(1\text{-}x_e)$, used in defining Re_f, and $Re_{go,D}$ and x_e in defining Re_g. Hence, for data points with sufficiently high *G*, a data point in the turbulent liquid – laminar vapor quadrant in indicative of low quality, which is representative of data in the nucleate boiling dominant regime as shown earlier in Fig. 7. For both local and average HTC data with Reynolds numbers based on exit conditions for the latter, Fig. 12(b) clearly shows existence of a large fraction of the LHe data in the turbulent liquid – laminar vapor quadrant, indicative of nucleate boiling dominant region wherein both q_{ONB} and $\Delta T_{w,ONB}$ for LHe are orders of magnitude smaller than those of the other cryogens. Finally, Fig. 12(c) shows histograms for HTC ratio and dimensionless wall superheat, ΔT^*_{sat}, for both local and average HTC data, confirming the HTC database are void of any non-boiling data.

3.2. Physics-Based Data Classifiers

3.2.1. Primary classifiers

Cryogen two-phase HTC data can be classified based on fluid (LHe, LH_2, LNe, LN_2, LAr, LCH_4), flow orientation (vertical upflow, downflow, horizontal flow), and confinement number, *Co* (micro-scale, macro-scale). The classification based on fluid is especially significant in regard to LHe based on the earlier discussion proving this fluid exhibits anomalous behavior compared to other cryogens. The classification based on orientation is significant in that it is a controlled variable in flow boiling experiments incorporated in prior HTC correlations using the Froude number, $Fr_{fo,D}$ for horizontal flows. The classification based on confinement number is relevant to the ability to distinguish physics for micro-channels from those of conventional macro-channels. However, because only a small fraction of LN_2 data exhibits micro-scale tendency ($Co > 0.6$) and almost all other HTC data for LN_2 as all other cryogens exhibiting macro-scale behavior, this classifier is deemed relatively inconsequential as far as the cryogenic flow boiling HTC database is concerned. Discussed below are additional physics-based classifiers that help in understanding the HTC mechanisms unique to cryogens and aid in correlation development.

3.2.2. Saturation length ratio

As seen from Fig. 7, the classification based on inlet quality is of paramount importance to flow boiling behavior along the entire tube. This is especially true for the case of two-phase mixture inlet with high vapor content, which can significantly alter the heat transfer mechanism in both nucleate boiling and convective boiling regions. Unfortunately, inlet quality information is not always provided for cryogenic two-phase HTC data, which led the present authors to draw a distinction between those data with prescribed inlet conditions and those without. This distinction required developing a criterion for classifying data based on availability or absence of inlet quality information. A dimensionless term, saturation

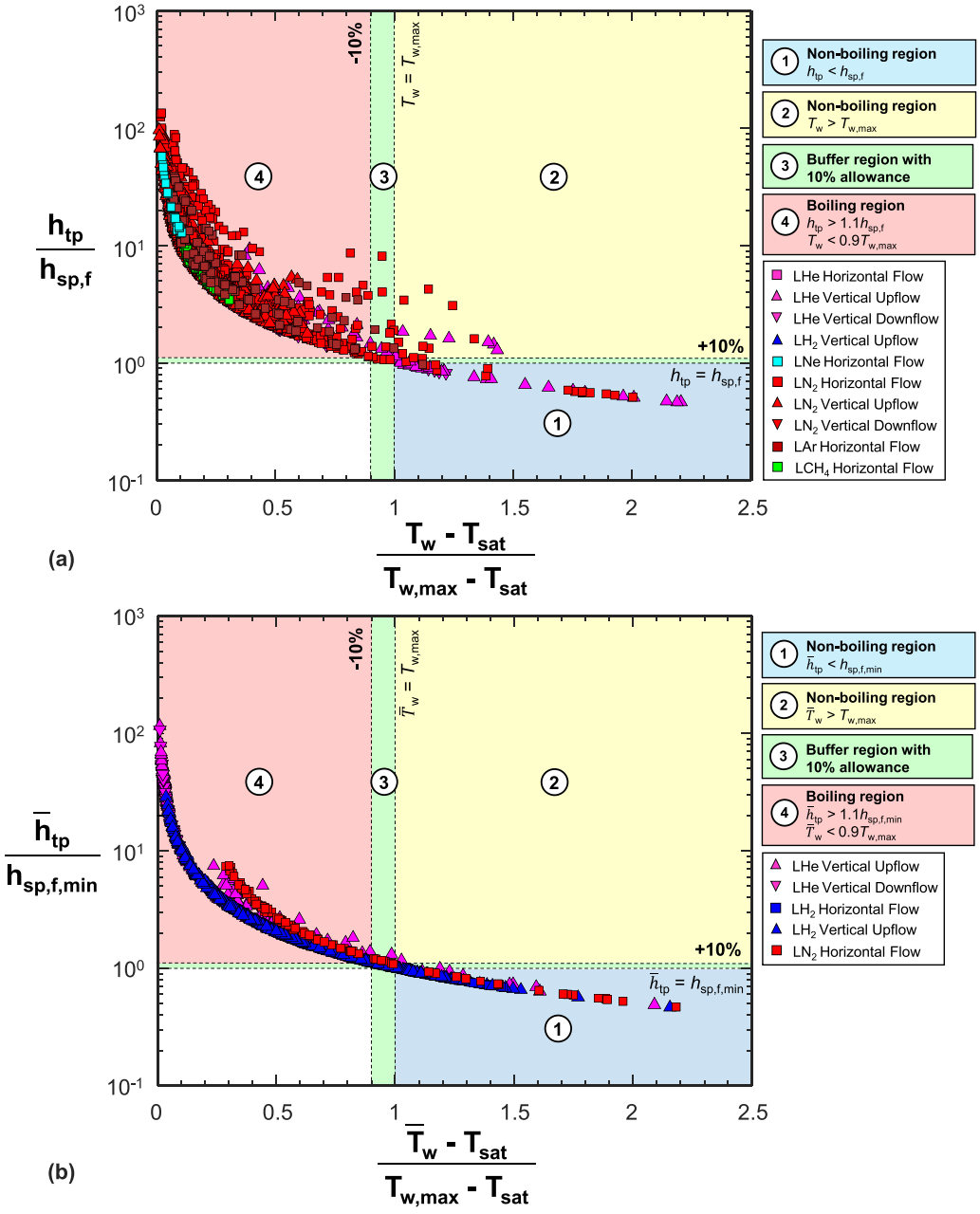

Fig. 11. Technique for identifying non-boiling data points from (a) local HTC data and (b) average HTC data.

length ratio ($\Delta z_{sat}/L_H$), is proposed here, which is defined as,

$$\frac{\Delta z_{sat}}{L_H} = \frac{z - z_0}{L_H} = \frac{x_e}{4Bo}\left(\frac{D}{L_H}\right). \tag{29}$$

where, z_0 corresponds to the location from inlet where local x_e becomes zero, and L_H is the heated length of the tube. The advantage of using the saturation length ratio is that it is independent of inlet quality while providing a measure of two-phase mixture inlet quality. To help illustrate variations of the saturation length ratio based on inlet condition, it is assumed the heated tube is preceded by a hypothetical preheating section of length L_{PH} providing either zero heat flux for the subcooled inlet case or heat flux $q_{PH} = q$ for the two-phase mixture inlet case. Fig. 13(a) shows, for subcooled inlet conditions, that the saturation length ratio obeys the inequality $0 < \Delta z_{sat}/L_H < 1$. For the saturated liquid inlet, Fig. 13(b), the saturation length ratio obeys the inequality $0 \leq \Delta z_{sat}/L_H \leq 1$. Fig. 13(c) shows, for two-phase mixture inlet conditions, that the saturation length ratio obeys the inequality, $0 \leq \Delta z_{sat}/L_H < 1 + L_{PH}/L_H$. It is important to note that for two-phase mixture inlet, the saturation length ratio can be both less than 1 and greater than 1. Since the saturation length ratio is proportional to local quality, as seen in Eq. (29), it can be hypothesized that for two-phase mixture inlet with low vapor content, $\Delta z_{sat}/L_H < 1$, and two-phase mixture with high vapor content, $\Delta z_{sat}/L_H > 1$. Hence, with an allowance of +10% (designed to account for an increase in x_e, and thus $\Delta z_{sat}/L_H$, due to local pressure drop ($\Delta P_{max}/P \leq 0.2$)), an underrelaxed criterion to distinguish two-phase mixture inlet data with high vapor content from the rest is set as $\Delta z_{sat}/L_H > 1.1$. Table 7 provides a summary of data within the cryogenic boiling HTC database that obey this criterion. All the reported data either have prescribed two-phase mixture inlet conditions or have been referenced as involving use of a preheater and/or throttle valve or orifice in the experimental setup upstream of the heated section, thereby enabling production of high vapor content to the inlet

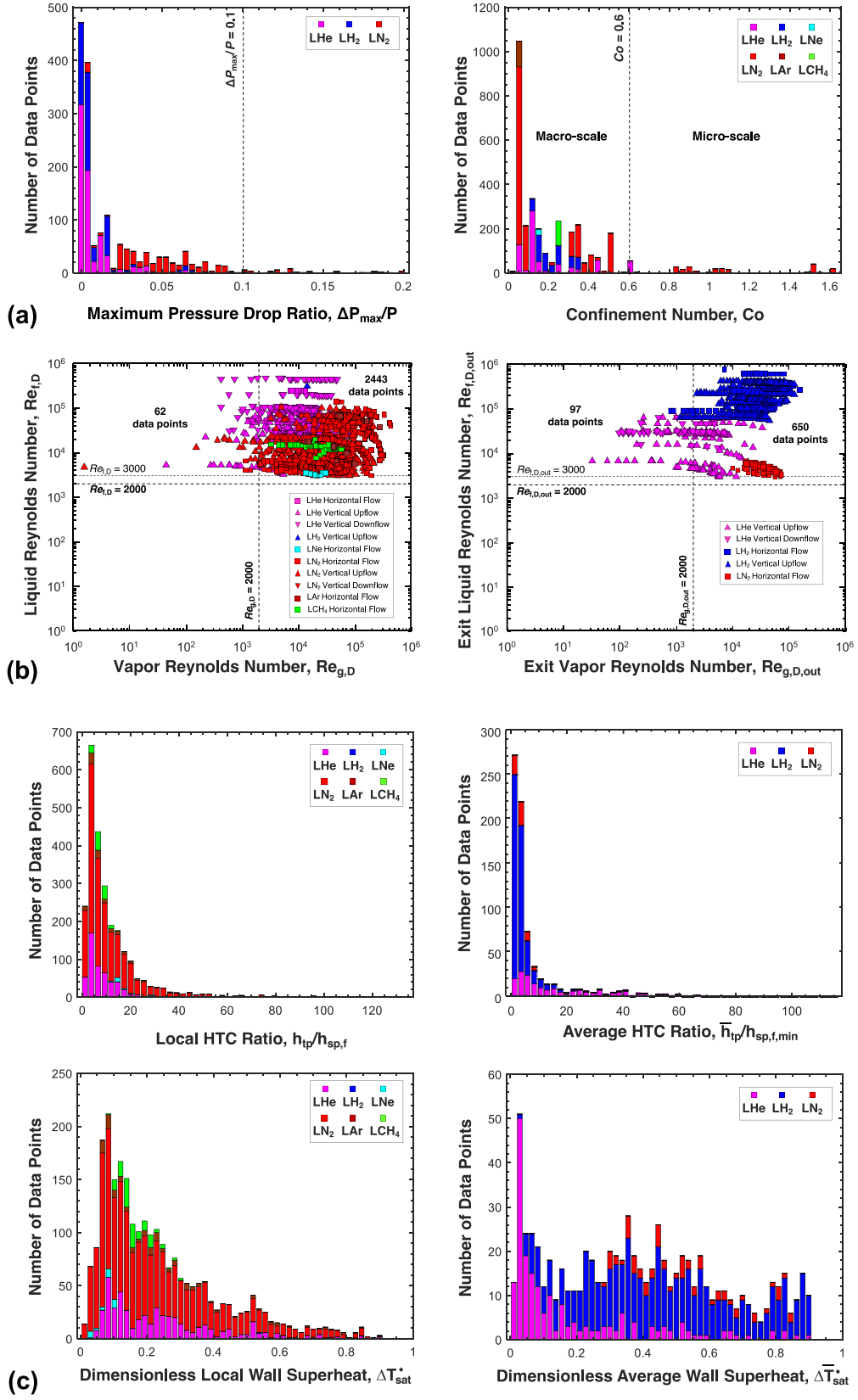

Fig. 12. Summary of accepted HTC data based on conformance to the physics-based criteria of (a) constant pressure, (b) turbulent flow, and (c) absence of non-boiling data.

Table 7
Summary of data with saturation length ratio corresponding to two-phase inlet with high vapor content, $\Delta z_{sat}/L_H > 1.1$.

Reference	Reported inlet vapor production apparatus	Reported range of inlet conditions	Number of datapoints satisfying $\Delta z_{sat}/L_H > 1.1$	Inlet Conditions $x_{e,in}$	Inlet Conditions $\Delta z_{sat}/L_H$ [a]	Local Conditions α [b]
(a) ***Liquid Helium***						
Ogata & Sato [f] [4]	Coiled preheater	Subcooled	30	0.06	1.1	0.36
		Saturated liquid				
		Two-phase mixture				
				0.78	40.38	0.93
Keilin et al. [f] [106]	1000 mm long preheater	Saturated liquid	2	0.13	1.33	0.46
		Two-phase mixture				
				0.65	4.62	0.9
Romanov et al. [f] [6]	- [c]	Saturate liquid	50	0.22	1.13	0.64
		Two-phase mixture				
				0.41	5.52	0.83
			82			
(b) ***Liquid Hydrogen***						
Wright & Walters [g] [13]	Orifice	Two-phase mixture	11	0.01	1.38 [a]	0.18 [b]
				0.02	6.39 [a]	0.36 [b]
			11			
(c) ***Liquid Neon***						
Mohr & Runge [e] [104]	Preheater along with throttle valves	Two-phase mixture	23	-	1.15	0.74
				-	71.05	0.87
			23			
(d) ***Liquid Nitrogen***						
Klimenko et al. [e] [91]	Pre-evaporator	Saturated liquid [d]	40	-	1.2	0.54
		Two-phase mixture		-	11.82	0.97
Klein [e] [88]	Evaporator	Two-phase mixture	98	-	1.11	0.63
				-	79.59	0.97
Steiner & Schlünder [e] [27]	Four pre-evaporators in series	Two-phase mixture	406	-	1.13	0.13
				-	418.98	0.98
Müller et al. [e] [105]	Four pre-evaporators in series	Saturated liquid [d]	100	-	1.11	0.1
		Two-phase mixture		-	207.38	0.96
Klimenko et al. [e] [51]	Preheater	Saturated liquid	32	-	1.27	0.28
		Two-phase mixture		-	3.28	0.63
			676			
(e) ***Liquid Argon***						
Müller et al. [e] [105]	Four pre-evaporators in series	Saturated liquid [d]	82	-	1.26	0.35
		Two-phase mixture		-	286.69	0.92
			82			
(f) ***Liquid Methane***						
Chen et al. [e] [110]	Preheater along with throttle valve	Saturated liquid	12	-	2.23	0.79
		Two-phase mixture		-	26.78	0.79
Wang et al. [e] [111]	Preheater along with throttle valve	Saturated liquid	61	-	1.17	0.36
		Two-phase mixture		-	23.18	0.78
Gong et al. [e] [112]	Preheater along with throttle valve	Saturated liquid	28	-	1.21	0.42
		Two-phase mixture		-	4.95	0.83
			101			
		Total	**975**			

[a] Saturation length ratio evaluated locally, Eq. (29), except for average HTC data of Wright and Walters [13] whose maximum saturation ratio, $\Delta z_{sat,max}/L_H$, is evaluated at tube exit substituting x_e by $x_{e,out}$ in Eq. (29).
[b] Evaluated locally using Zivi's void fraction relation, Eq. (9), except for average HTC data of Wright and Walters [13] whose outlet void fraction is evaluated at tube exit.
[c] Information not provided/accessible from original reference.
[d] Unclear from original reference.
[e] Local HTC data with prescribed local conditions (see Table 8a).
[f] Local HTC data with prescribed inlet conditions (see Table 8b).
[g] Average HTC data with prescribed inlet conditions (see Table 8c).

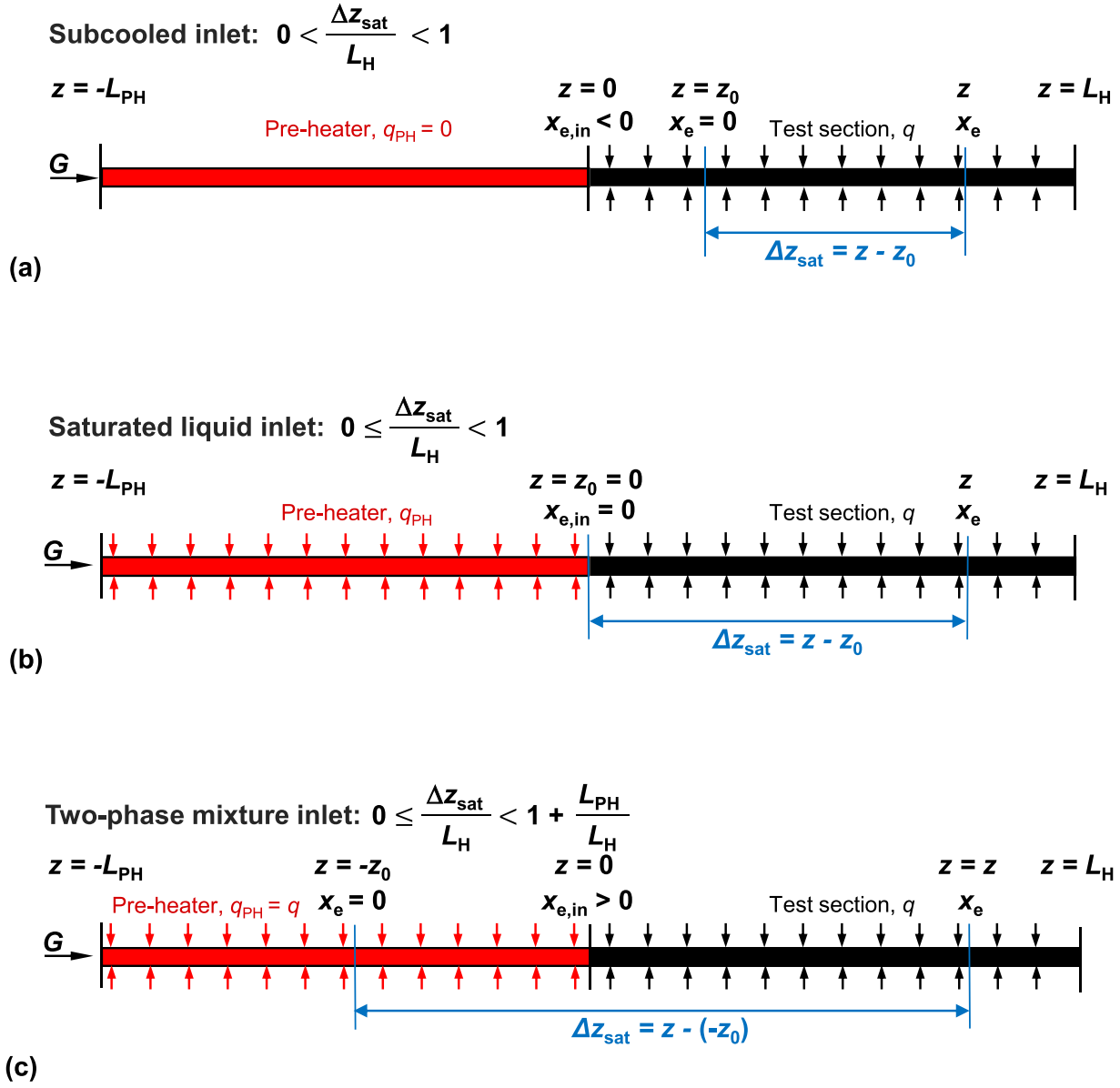

Fig. 13. Data classification based on saturation length ratio for (a) subcooled inlet, (b) saturated liquid inlet, and (c) two-phase mixture inlet.

of the tube either by pre-heating or by flashing (sudden pressure reduction).

Fig. 14(a) shows the variation of two-phase HTC, h_{tp}, with saturation length ratio for all local HTC data from the HTC database. It can be seen that although h_{tp} shows no significant trend with respect to the saturation length ratio until $\Delta z_{sat}/L_H = 1$, it begins to decrease for $\Delta z_{sat}/L_H > 1$. This confirms observations made earlier in relation to Fig. 7(c), where the nucleate boiling HTC, h_{NB}, is significantly suppressed by presence of bubbles at the inlet due to enhanced turbulence (thermal boundary layer mixing). Despite enhancement in the convective boiling HTC, h_{CB}, it is counterintuitive to see why the total HTC, h_{tp}, is decreasing with increasing saturation length ratio. This alludes to the important conclusions that *nucleate boiling is the dominant mechanism of heat transfer in all flow regimes* irrespective of inlet conditions for saturated flow boiling prior to CHF (DNB or dryout). This conclusion will be validated further in subsequent sections. Fig. 14(b) shows a histogram of $\Delta z_{sat}/L_H$ for all the local HTC data. It is obvious nearly half of the local HTC database satisfies the criteria of $\Delta z_{sat}/L_H > 1.1$, signifying its prevalence in cryogenic flow boiling literature. For average HTC, for which maximum saturation length ratio, $\Delta z_{sat,max}/L_H$, is defined by substituting x_e with $x_{e,out}$, only Wright and Walters [13] provided two-phase mixture inlet data, details of which are summarized in Table 7.

3.2.3. Phase separation parameter

It is observed from Fig. 8(b), that conduction in the annular liquid film becomes dominant when $\delta_{film}/D << 1$. This phenomenon is observed beyond the point of boiling cessation, where the boiling is completely suppressed due to the gradual thinning of the liquid film by interfacial evaporation. Therefore, within the thin film region of the annular flow regime, $h_{NB} \approx 0$ and $h_{tp} \approx h_{CB}$. Hence, using Eq. (8), a criteria of $h_{cond,\delta}/h_{sp,f}$ is proposed to identify the data points in the annular flow regime where film conduction begins to dominate or nucleate boiling is completely suppressed. As discussed earlier, the enhancement factor, F, in annular flow is a function of the liquid hold-up dimensionless term, $\Pi_{(1-\alpha)}$ (see Eq. (12)), *i.e.*,

$$\frac{h_{cond,\delta}}{h_{sp,f}} = f\left(\frac{1}{\Pi_{1-\alpha}}\right) = f\left(\frac{1}{X_{tt}}\right). \tag{30}$$

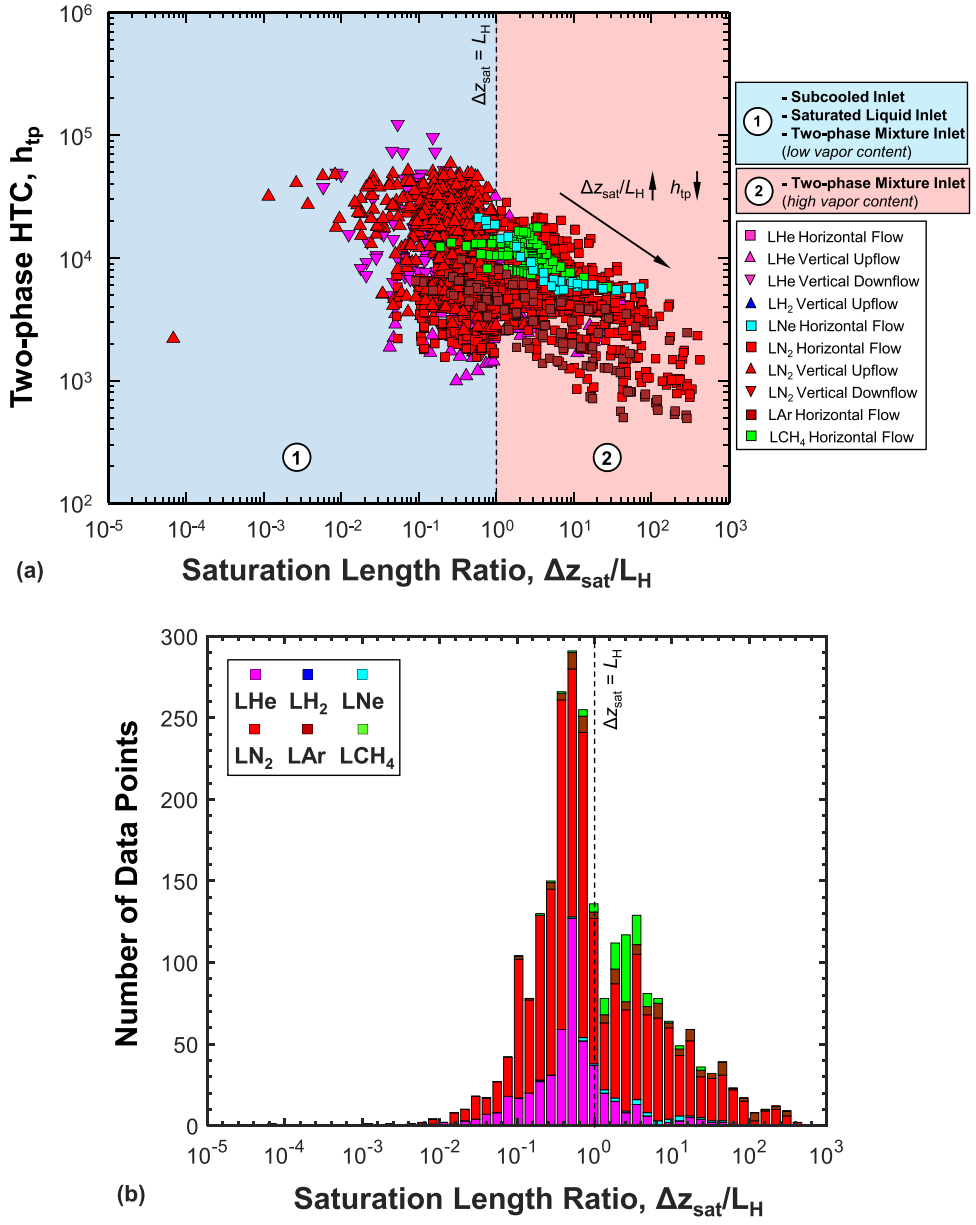

Fig. 14. Assessment of saturation length ratio classifier for local HTC data: (a) variation two-phase HTC with saturation length ratio and (b) histogram of saturation length ratio.

Fig. 15(a) shows, for local heat transfer data, the variation of $h_{cond,\delta}/h_{sp,f}$ with both void fraction, α, and $1/X_{tt}$, which is termed as the *phase separation parameter*. It is observed that beyond $\alpha = 0.8$ (transitioning to annular flows), there are few data points that exhibit $h_{cond,\delta} > h_{sp,f}$, whereas for LHe this transition is prematurely shifted to $\alpha = 0.7$. Fig. 15(a) also shows that as $1/X_{tt}$ increases, which implies increased phase separation, the slope of the curve begins to increase, from near-zero for low values of $1/X_{tt}$ to a non-zero positive value for intermediate values of $1/X_{tt}$. Beyond $1/X_{tt} = 1$, there is a sharp increase in slope, which signifies initiation of strong phase separation effects. It is also in the range $1/X_{tt} > 1$ that certain data exhibit $h_{cond,\delta}/h_{sp,f} > 1$ in the liquid film. Similar and consistent inferences are captured from Fig. 15(b) for average HTC data for which the terms are evaluated at the tube exit. Hence, the criteria of $\alpha \geq 0.8$ is chosen conservatively to segregate annular flow data from the rest. Additionally, $1/X_{tt} < 1$ is proposed to identify HTC data with both low phase separation (bubbly flow, $1/X_{tt} < 0.1$) and medium separation (intermediate flow regimes, $0.1 \leq 1/X_{tt} < 1$), as opposed to $1/X_{tt} \geq 1$ for high phase separation annular flow. The use of phase separation parameter in distinguishing flow regimes can be further justified by its applicability in developing flow regime maps based on vapor ($\rho_g j_g^2$) and liquid ($\rho_f j_f^2$) superficial momentum fluxes as their ratio, $\frac{\rho_g j_g^2}{\rho_f j_f^2} = 1/[(\frac{1-x_e}{x_e})(\frac{\rho_g}{\rho_f})^{0.5}]^2 \cong \frac{1}{X_{tt}^2}$ can be approximated to the square of phase separation parameter, $1/X_{tt}$. Hence, local HTC data with low, medium, and high phase separation, can also be approximated to satisfy the criterion $\rho_g j_g^2/\rho_f j_f^2 < 0.01$, $0.01 \leq \rho_g j_g^2/\rho_f j_f^2 < 1$, and $\rho_g j_g^2/\rho_f j_f^2 \geq 1$ respectively on a flow regime map.

3.2.4. Tube wall material

Tube material, wall thickness, surface roughness, and surface aging are all effects that can influence flow boiling heat transfer

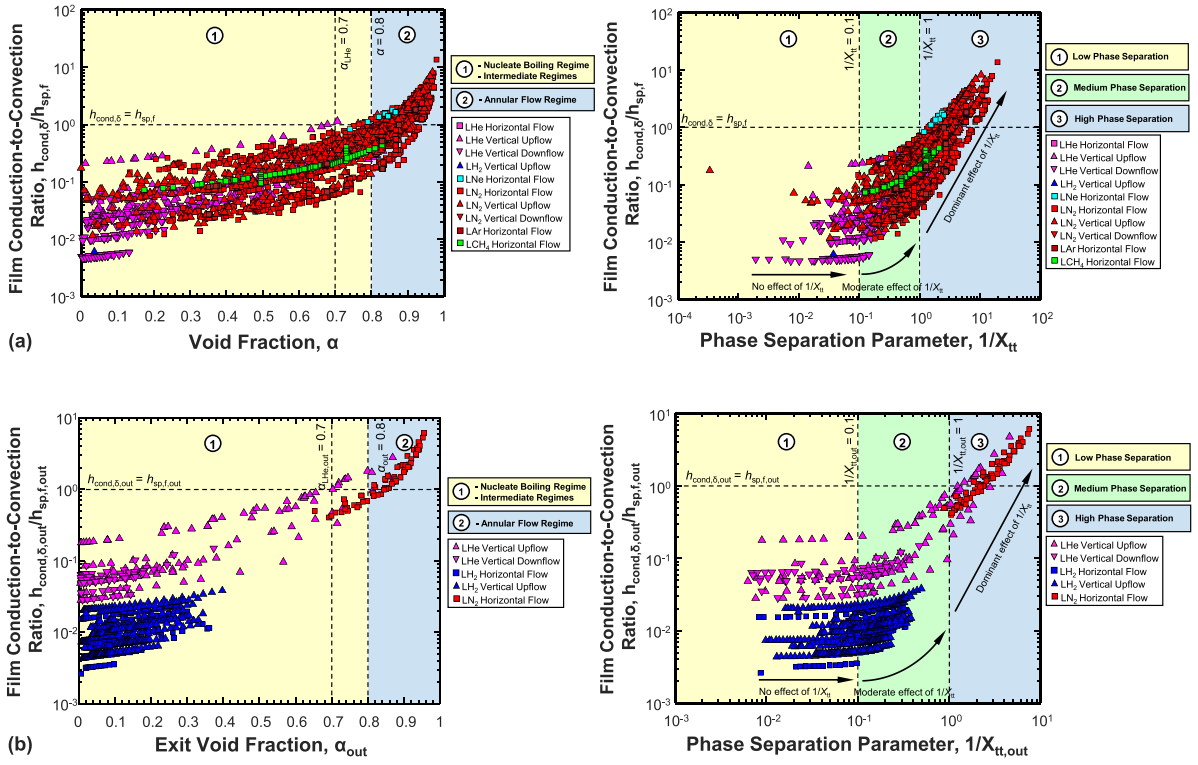

Fig. 15. Assessment of phase separation classifier by variation of film conduction-to-convection HTC ratio with void fraction, α, and phase separation term, $1/X_{tt}$, for (a) local HTC data and (b) average HTC data.

mechanism, especially the contribution of nucleate boiling. For example, as indicated in Table 3, both Cooper [50] and Gorenflo and Sokol [34] included the influence of average wall roughness in the pool boiling HTC correlation. The same two studies make distinctions in the applicability of their correlations based on tube material (copper versus stainless-steel). In fact, Cooper [50] found a 1.7-times increase in pool boiling HTC when using a copper surface as opposed to stainless-steel. This difference is clearly manifest in Fig. 3, which shows tube material plays a more significant role at cryogenic temperatures as compared to room temperature. Overall, the tube materials used in cryogenic flow boiling experiments can be segregated into two categories, stainless-steel variants (SS321, SS304, SS316, SS310S) and copper/copper alloys; other outliers include silver, used by Hildebrandt [1], and Monel, used by Johannes [86]. Increase in thermal conductivity and/or wall thickness enhance axial conduction, which influences both dominant heat transfer mechanism and transition between mechanisms. Fig. 16 shows the distribution of wall thermal conductivities of materials, evaluated using EES [28], for entire HTC database as a function of the experimentally reported wall temperature. Most obvious is the clear distinction between low conductivity stainless-steel variants ($k_w \leq 10$ $Wm^{-1}K^{-1}$) and high conductivity copper/copper alloys ($600 \leq k_w < 1500$ $Wm^{-1}K^{-1}$). An extreme exception is silver, with $k_w > 10^4$ $Wm^{-1}K^{-1}$, whose performance is also captured in Fig. 3. Hence, tube wall material is chosen as the final classifier for cryogen HTC data.

While tube material and to a lesser extent wall thickness are mentioned in most references, surface roughness is rarely described. Exceptions of studies that do provide ample description of surface roughness are works by Mohr and Runge [104], Qi et al. [103], Zhang et al. [97], Steiner and Schlünder [27], Müller et al. [105], and Hilderbrandt [1]. Given the overall lack of complete information on surface roughness and surface aging, a thorough investigation of these effect on cryogen HTC is not possible at the present time.

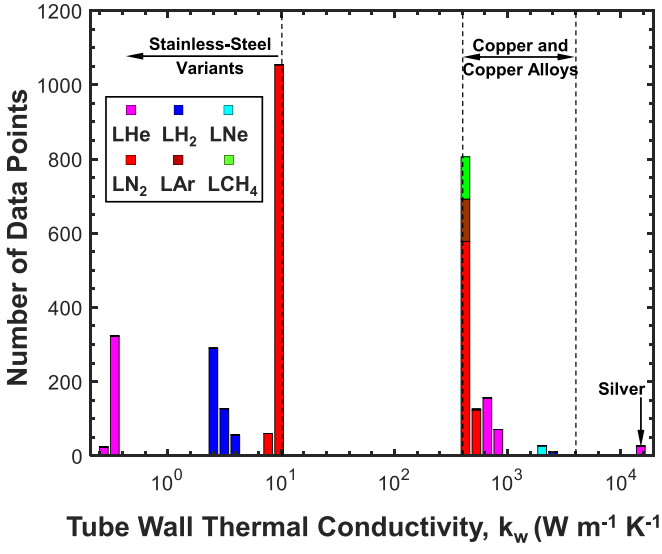

Fig. 16. Tube wall thermal conductivity distribution for entire HTC database.

3.3. Final PU-BTPFL HTC Database

The final PU-BTPFL HTC Database, which includes all data deemed acceptable for development of HTC correlations, is arrived at after applying all the data exclusion criteria outlined in the section 3.1. Complete details of the database are provided in Tables 8(a), 8(b), and 8(c). Overall, it is comprised of 3,252

Table 8a
Parameter ranges of acceptable data in the PU-BTPFL HTC Database. (a) Local HTC database with prescribed local conditions.

Reference	Acceptable HTC data	Tube dimensions		Operating Conditions			Inlet Conditions	Local Conditions		HTC Measurements		Remarks
		D x 10^3 [m]	L_H/D	P x 10^{-6} [N m^{-2}]	G [kg m^{-2} s^{-1}]	q x 10^{-3} [W m^{-2}]	$\Delta z_{sat}/L_H$ [a]	x_e	α [b]	ΔT_{sat} [K]	h_{tp} x 10^{-3} [W m^{-2} K^{-1}]	
Liquid Neon												
Horizontal flow												
Mohr and Runge [104]	27	4	25	0.15	111	0.39	0.59	0.13	0.74	0.07	5.4	SF-Copper/E-Copper Tube $t_w = 1$ mm R_p= 3.4-6.9 μm
		4	25	0.15	131	33.09	71.05	0.25	0.87	1.62	21.2	
LNe HTC data points	**27**											
Liquid Nitrogen												
(a) Vertical Upflow												
Klimenko and Sudarchikov [89]	13	10	185	0.3	310	13.75	0.05	0.01	0.09	3.36	3.65	SS Alloy Tube $t_w = 1$ mm
		10	185	0.7	490	20.32	0.4	0.09	0.52	4.78	4.84	
Klimenko et al. [91]	61	9	55.56	0.5	220	9	0.13	0.01	0.12	1.22	2.57	SS Tube
		9	55.56	0.5	220	27	11.82	0.74	0.97	5.05	9.39	
Qi et al. [103]	291	0.53	129.47	0.19	447.2	81.1	0.02	0.01	0.12	2.43	7.34	SS 304 Tube t_w = 0.16-0.49 mm R_p= 0.67-2.31 μm
		1.93	470.81	0.81	1743	135.6	0.88	0.69	0.97	14.61	41.93	
Yu [c] [113]	6	14	-	0.68	54.4	28.4	-	0	0.01	0.95	24.91	SS Tube
		14	-	1.08	107.7	28.6	-	0.12	0.54	1.14	29.91	
Xu et al. [108]	52	14	71.43	0.57	54.12	11.2	0.03	0.02	0.1	1.47	3.61	SS 304 Tube $t_w = 1$ mm
		14	71.43	1.59	107.66	31.8	0.94	0.63	0.91	5.98	13.07	
Fang et al. [114]	102	11.9	121.51	1.09	150	35	0.01	0.01	0.03	1.4	15.2	SS Alloy Tube $t_w = 0.3$ mm
		11.9	121.51	2.04	410	80.6	0.58	0.47	0.8	3.7	39.15	
Zhang et al. [97]	114	2	148.16	0.63	530	59.7	0	0	0.01	1.78	15.52	SS 321 Tube $t_w = 1$ mm R_p= 7.16 μm
		2	148.16	1	680	223.2	0.79	0.77	0.97	7.01	58.85	
	639											
(b) Horizontal flow												
Klein [88]	120	12	83.33	0.3	103	0.99	0.24	0.1	0.63	0.16	1.91	Copper Tube $t_w = 3$ mm
		12	83.33	0.3	257.4	70.41	79.59	0.7	0.97	9.64	12.68	
Steiner and Schlünder [27]	471	14	37.5	0.52	44	0.28	0.19	0.02	0.13	0.15	0.73	Copper Tube $t_w = 3$ mm R_p= 0.1 μm
		14	37.5	1.58	562	38.77	418.98	0.89	0.98	6.52	35.56	
Müller et al. [105]	110	14	37.5	0.12	44.42	0.21	0.5	0.03	0.1	0.22	0.96	Copper Tube $t_w = 3$ mm R_p= 0.1 μm
		14	37.5	2.99	457.18	62.76	207.38	0.87	0.96	4.09	28.27	
Klimenko et al. [51]	53	14.1	42.55	0.3	269.98	2.8	0.18	0.03	0.28	0.78	1.59	SS Alloy Tube
		14.1	42.55	0.3	619.05	52	3.28	0.1	0.63	6.7	9.91	
	754											
LN_2 HTC data points	**1393**											
Liquid Argon												
(a) Horizontal flow												
Müller et al. [105]	117	14	37.5	0.17	117.04	0.22	0.09	0.1	0.35	0.24	0.49	Copper Tube $t_w = 3$ mm R_p= 0.1 μm
		14	37.5	1.95	460	98.99	286.69	0.71	0.92	17.8	9.67	
LAr HTC data points	**117**											
Liquid Methane												
(a) Horizontal flow												
Chen et al. [110]	12	6	33.33	0.4	190	4.99	2.23	0.2	0.79	0.86	5.77	Copper Tube $t_w = 12$ mm
		6	33.33	0.4	190	59.83	26.78	0.2	0.79	3.66	16.33	
Wang et al. [111]	67	6	33.33	0.29	116.49	5.15	0.19	0.01	0.17	0.89	5.77	Copper Tube $t_w = 12$ mm
		6	33.33	0.59	273.89	61.99	23.18	0.19	0.78	4.1	16.49	
Gong et al. [112]	35	6	33.33	0.4	200	20	0.26	0.02	0.23	2.08	7.85	Copper Tube $t_w = 12$ mm
		6	33.33	0.4	200	50	4.95	0.24	0.83	3.81	17.79	
LCH_4 HTC data points	**114**											
Total	**1651**											

[a] Saturation length ratio evaluated locally, Eq. (29).
[b] Evaluated using Zivi's void fraction relation, Eq. (9).
[c] Data extracted from Fang et al. [114].

Table 8b
Parameter ranges of acceptable data in the PU-BTPFL HTC Database. (b) Local HTC database with prescribed inlet conditions.

Reference	Acceptable HTC data	Tube dimensions		Operating Conditions			Inlet Conditions		Local Conditions		HTC Measurements		Remarks
		D x 10^3 [m]	L_H/D [-]	P x 10^{-6} [N m^{-2}]	G [kg m^{-2} s^{-1}]	q x 10^{-3} [W m^{-2}]	$x_{e,in}$	$\Delta z_{sat}/L_H$ [a]	x_e	α [b]	ΔT_{sat} [K]	h_{tp} x 10^{-3} [W m^{-2} K^{-1}]	
Liquid Helium													
(a) Vertical Upflow													
Johannes [86]	8	2.12	139.62	0.11	130	0.53	0	0.33	0.04	0.12	0.09	2.83	Monel Tube
		2.12	139.62	0.11	130	1.52	0	0.84	0.27	0.57	0.25	8.74	$t_w = 0.11$ mm
Ogata and Sato [4]	39	1.09	77.98	0.11	82.52	0.14	-0.02	0.53	0.06	0.19	0.03	1.68	SS Tube
		1.09	77.98	0.11	162.89	2.55	0.78	40.38	0.8	0.93	0.38	7.15	$t_w = 0.26$ mm
Keilin et al. [106]	98	2	50	0.12	28	0.1	0	0.5	0.01	0.03	0.05	1.53	Copper Tube
		2	50	0.15	96	4.86	0.65	4.62	0.73	0.9	0.32	18.32	$t_w = 0.5$ mm
Grigoriev et al. [99]	29	0.67	194.03	0.1	24.93	0.05	0	0.04	0	0.01	0.03	0.99	SS Tube
		0.67	194.03	0.1	104.72	1.74	0	0.94	0.59	0.84	0.52	3.75	$t_w = 0.17$ mm
Romanov et al. [6]	56	0.47	212.77	0.1	90	0.19	0.22	0.96	0.32	0.64	0.02	2.33	-
		0.47	212.77	0.1	90	1.31	0.41	5.52	0.58	0.84	0.18	31.83	
Subbotin et al. [90]	8	1.63	110.43	0.1	85	0.68	0	0.97	0.1	0.31	0.21	2.62	SS Tube
		1.63	110.43	0.1	140	1.6	0	0.97	0.39	0.71	0.36	5.61	
Yarmak and Zhukov [107]	18	0.8	187.5	0.1	78	0.38	0	0.34	0.05	0.17	0.21	1.57	SS Tube
		0.8	187.5	0.1	235	3.96	0	0.34	0.24	0.55	0.33	13.12	$t_w = 0.1$ mm
	256												
(b) Horizontal flow													
Bredy et al. [c] [92]	7	10	15	0.1	76.39	4.47	0	0.07	0.01	0.04	0.46	9.2	SS Tube
		10	15	0.1	76.39	8.48	0	0.07	0.02	0.08	0.92	10.28	$t_w = 0.5$ mm
	7												
(c) Vertical Downflow													
Giarrantano et al. [2]	140	2.13	46.95	0.11	48	0.71	-0.1	0.01	0	0	0.06	4.08	SS Tube
		2.13	46.95	0.18	636	5.3	0.02	0.99	0.35	0.65	0.63	51.99	$t_w = 0.16$ mm
Jones and Johnson [87]	15	2	48	0.11	130	2.83	-0.07	0.02	0	0.02	0.17	7.05	-
		2	48	0.11	130	3.65	-0.07	0.51	0.11	0.29	0.48	18	
Giarrantano et al. [94]	77	2.13	46.95	0.08	45	1.63	-0.07	0.01	0	0	0.04	4.39	SS Tube
		2.13	46.95	0.2	630	6.02	0	0.96	0.32	0.64	0.74	123.3	$t_w = 0.16$ mm
	232												
LHe HTC data points	**495**												
Liquid Hydrogen													
(c) Vertical Upflow													
Core et al. [12]	1	4.25	14.93	0.63	519.57	130.74	-0.03	0.23	0.01	0.04	4.44	29.42	SS Tube
		4.25	14.93	0.63	519.57	130.74	-0.03	0.23	0.01	0.04	4.44	29.42	$t_w = 0.25$ mm
LH_2 HTC data points	**1**												
Liquid Nitrogen													
(a) Vertical Upflow													
Xu et al. [108]	17	14	71.43	0.67	27.08	6.9	-0.06	0	0	0	0.98	2.2	SS 304 Tube
		14	71.43	1.07	84.63	24.2	0	1.07	0.61	0.9	3.86	12.5	$t_w = 1$ mm
Zhang et al. [97]	20	2	148.16	0.63	680	54.98	-0.29	0.01	0	0.02	3.13	10.91	SS 321 Tube
		2	148.16	1.08	680	187.39	-0.21	0.67	0.65	0.94	9.39	22.14	$t_w = 1$ mm $R_p = 7.16$ μm
	37												
(b) Horizontal flow													
Zhang et al. [95]	197	2.92	204.97	0.23	198.98	8.3	0	0.05	0.01	0.13	4.49	1.67	SS Tube
		2.92	204.97	0.33	283.5	43.6	0	0.94	0.52	0.95	8.74	7.77	$t_w = 1.03$ mm
Chen et al. [96]	111	1.98	202.02	0.23	239.9	3.8	0	0.1	0.01	0.21	2.09	1.56	SS Tube
		1.98	202.02	0.42	506.78	44.8	0	1	0.48	0.93	7.64	7.14	$t_w = 1$ mm
	308												
(c) Vertical Downflow													
Umekawa et al. [115]	13	5	180	0.1	177	12.7	-0.01	0.12	0.03	0.5	4.53	1.67	SS 304 Tube
		5	180	0.1	177	12.7	-0.01	0.8	0.21	0.89	7.62	2.8	$t_w = 0.5$ mm
	13												
LN_2 HTC data points	**358**												
Total	**854**												

[a] Saturation length ratio evaluated locally, Eq. (29).
[b] Evaluated using Zivi's void fraction relation, Eq. (9).
[c] Tube at an orientation of 4° from the horizontal plane and considered (quasi-) horizontal in this study.

Table 8c
Parameter ranges of acceptable data in the PU-BTPFL HTC Database. (c) Average HTC database with prescribed inlet conditions.

Reference	Acceptable HTC data	Tube dimensions		Operating Conditions			Inlet Conditions		Exit Conditions		HTC Measurements		Remarks
		D x 10^3 [m]	L_H/D [-]	P x 10^{-6} [N m^{-2}]	G [kg m^{-2} s^{-1}]	q x 10^{-3} [W m^{-2}]	$x_{e,in}$	$\Delta z_{sat,max}/L_H$ [a]	$x_{e,out}$	α_{out} [b]	$\Delta \bar{T}_{sat}$ [K]	$\bar{h}_{tp}$ x 10^{-3} [W m^{-2} K^{-1}]	
Liquid Helium													
(a) Vertical Upflow													
Hilderbrandt [1]	26	1	20	0.08	22.3	0.01	0	1	0	0.01	0.02	0.64	Silver Tube
		1	20	0.08	76.3	1.8	0	1	0.29	0.65	0.13	14.75	R_p= 0.1 μm
Grigoriev et al. [99]	24	0.67	194.03	0.01	24.99	0.05	0	1	0.07	0.24	0.06	0.53	SS Tube
		0.67	194.03	0.1	105.24	1.11	0	1	0.62	0.91	0.52	2.67	t_w = 0.17 mm
Grigoriev et al. [100]	15	0.67	194.03	0.1	25.03	0.05	0	1	0.08	0.25	0.08	0.67	-
		0.67	194.03	0.1	63.82	0.9	0	1	0.53	0.81	0.26	3.6	
Petukhov et al. [5]	6	1.8	72.22	0.1	90	0.33	0	1	0.05	0.17	0.19	1.51	SS Tube
		1.8	72.22	0.1	90	1.64	0	1	0.26	0.57	0.39	4.23	t_w = 0.1 mm
Panek et al. [93]	70	6.35	0.79	0.04	7.89	0.13	0	1	0	0	0.09	0.88	OFHC Copper Tube
		6.35	0.79	0.1	31.58	9.29	0	1	0.16	0.41	1.07	16.89	
	141												
(b) Vertical Downflow													
Panek et al. [93]	59	6.35	0.79	0.04	7.89	0.1	0	1	0	0.01	0.1	0.66	OFHC Copper Tube
		6.35	0.79	0.1	31.58	8.76	0	1	0.14	0.37	0.91	16.68	
	59												
LHe HTC data points	**200**												
Liquid Hydrogen													
(a) Vertical Upflow													
Tatsumoto et al. [7]	30	3	33.33	0.7	304.17	7.52	0	1	0.01	0.02	0.37	13.17	SS 304 Tube
		3	33.33	0.7	669.63	97.87	0	1	0.09	0.26	1.13	86.25	t_w = 0.5 mm
Shirai et al. [8]	82	5.95	16.81	0.7	75.47	1.57	0	1	0	0.01	0.31	3.84	SS 304 Tube
		5.95	16.81	0.7	490.87	106.06	0	1	0.16	0.4	2.54	41.79	t_w = 0.2 mm
Tatsumoto et al. [10]	234	4	41.67	0.4	86.26	1.03	0	1	0	0.02	0.26	4.04	SS 316 Tube
		6	41.75	0.7	727.69	96.71	0	1	0.13	0.34	2.66	66.98	t_w = 0.5 mm
Matsumoto et al. [11]	56	8	25	0.7	140	10.89	0	1	0.01	0.03	0.1	27.13	SS 310S Tube
		8	25	0.7	340	59.53	0	1	0.1	0.27	0.96	225.78	
	402												
(b) Horizontal flow													
Wright and Walters [d] [13]	11	6.35	24	0.15	412.57	10	0.01	1.38	0.02	0.18	0.5	18	Copper Tube
		6.35	24	0.16	649.36	67	0.02	6.39	0.05	0.36	2.06	36.11	t_w = 6.35 mm
Tatsumoto et al. [9]	70	3	16.67	0.7	104.42	1.04	0	1	0	0.01	0.16	4.7	SS 304 Tube
		6	33.33	0.7	1787.56	133.59	0	1	0.11	0.3	3.34	81.57	t_w = 0.5 mm
	81												
LH_2 HTC data points	**483**												
Liquid Nitrogen													
(a) Horizontal flow													
Zhang et al. [95]	53	2.92	204.97	0.22	224	8.1	0	1	0.13	0.69	4.21	1.76	SS Tube
		2.92	204.97	0.33	296	35.03	0	1	0.55	0.96	7.14	5.35	t_w = 1.03 mm
Chen et al. [96]	11	1.98	202.02	0.23	290	7.28	0	1	0.11	0.65	3.78	1.93	SS Tube
													t_w = 1 mm
		1.98	202.02	0.42	290	26.28	0	1	0.4	0.91	6.02	4.65	
	64												
LN_2 HTC data points	**64**												
Total	**747**												

[a] Maximum saturation length ratio evaluated at tube exit, Eq. (29).
[b] Evaluated using Zivi's void fraction relation, Eq. (9).

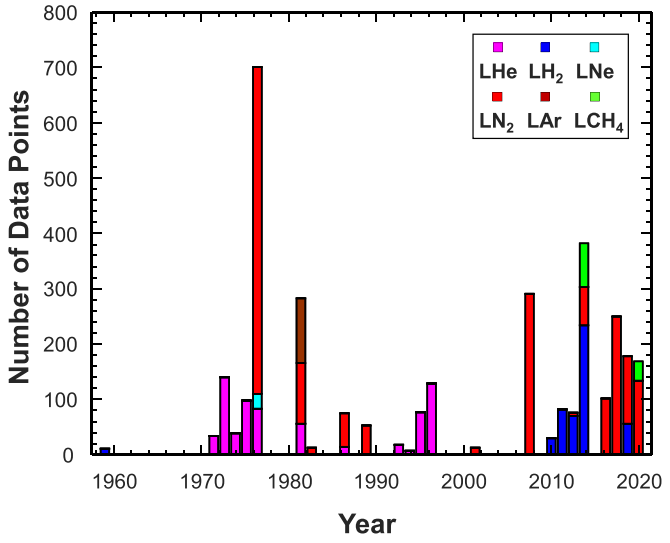

Fig. 17. Timeline for cryogen saturated flow boiling HTC data measurements spanning over past 60 years.

useable HTC data points conforming to the functional forms of Eqs. (15) and (16) and therefore acceptable for correlation development. The HTC database is divided into categories: (a) local HTC data with prescribed local conditions (1651 datapoints), (b) local HTC data with prescribed inlet conditions (854 datapoints), and average HTC data with prescribed inlet conditions (747 datapoints). Overall, the database encompasses six different fluids: liquid helium, LHe, liquid hydrogen, LH_2, liquid neon, LNe, liquid nitrogen, LN_2, liquid argon, LAr, and liquid methane, LCH_4. In Table 8, upper and lower numbers for each parameter represent minimum and maximum values, respectively, for acceptable HTC data corresponding to a particular reference. It is important to re-emphasize that the entire database (a) is for uniformly heated round tubes (with fully wetted perimeter), and (b) includes only horizontal, vertical upflow, and vertical downflow orientations, and therefore excludes other intermediate orientations.

4. Parametric Distributions of PU-BTPFL HTC Database

The PU-BTPFL HTC Database contains 3,252 HTC data points, segregated according to local/average HTC, data with/without prescribed inlet conditions, and different cryogens and flow orientations. This is the largest ever consolidated database from the literature for cryogens in the heating configuration. Fig. 17 shows a 60-year timeline during which cryogen flow boiling HTC data (from the present HTC Database) were measured. Notice how more emphasis has been placed on specific cryogens during relatively short time spans. After initial efforts in late 1950s and early 1960s in the United States by Wright and Walters [13], Core et al. [12], and Lewis et al. [14], cryogenic flow boiling research picked up in mid-1970s until the mid-1990s, with heavy focus on LHe in the former Soviet Union and on LN_2 in West Germany with sporadic research efforts on LNe [104] and LAr [105]. Thereafter, following more than a decade long gap, there was renewed interest, this time in Japan, with focus on LH_2 and LN_2 for cooling high-temperature superconducting (HTS) magnets. With more recent interest in space applications, LCH_4 gained some focus by space agencies in the United States and organizations affiliated with the Chinese Academy of Sciences [110-112]. Throughout the many decades, owing to relatively both ease of procurement and operation, LN_2 has been popular especially in academic research, which may explain why LN_2 data comprise an overwhelming fraction of the PU-BTPFL HTC database, 1815 out of the 3252 total). It must be mentioned that flow boiling research using cryogenics has not been limited to these six main fluids indicated in Fig. 17, as data for Liquid Oxygen, LOX have appeared sporadically in the literature. Unfortunately, the present authors were unable to find HTC data for this fluid in the open literature, though some data might be available in proprietary databases of national laboratories or research organizations across the globe.

Discussed next are details of controlled parameters in flow boiling experiments for data used in the PU-BTPFL HTC database. Figs. 18(a)-18(i) show histograms of data based on the following controlled parameters: (a) system pressure, P, (b) reduced pressure, P_R, (c) heat flux, q, (d) inlet quality, $x_{e,in}$, (only for HTC data with prescribed inlet conditions), (e) mass velocity, G, (f) tube inner diameter, D, (g) heated length-to-diameter ratio, L_H/D, (h) tube wall thickness, t_w, and (i) flow orientation angle, θ. For each of these parameters, the histogram is further segregated based on fluid. Fig. 18(a) shows, for cryogens (especially LHe and LH_2), far more data are available for lower pressures, and high-pressure data are limited to LN_2 and LAr. However, this might be misleading given the large variations in critical pressure for the different cryogens. The pressure distribution is better presented by plotting the data against reduced pressure, Fig. 18(b), which shows more overall uniformity in the data distribution. Nonetheless, Fig. 18(b) also shows more emphasis for LN_2, LNe, and LCH_4 on lower reduced pressures, compared to more uniform distributions for LH_2 and LHe, with highest reduced pressures associated with LHe. Fig. 18(c) shows how LHe experiments involve low heat fluxes, followed by LH_2 and LNe; all three fluids possess comparatively low critical temperatures. Owing to higher values of key thermophysical properties, LN_2 experiments operate at q values higher than all the other cryogens. Fig. 18(d) shows a majority of the data are associated with saturated liquid inlet ($x_{e,in} = 0$) and far fewer data subcooled ($x_{e,in} < 0$) or two-phase mixture ($x_{e,in} > 0$) inlets. Fig. 18(e) shows most of the data have mass velocities below G = 1,000 kg/m^{2}s, with a few higher values limited to LN_2. Fig. 18(f) shows a broad distribution of inner tube diameter, with all fluids except for LN_2 clustered towards smaller diameters of less than ~ 8 mm. The same figure shows only LHe and LN_2 data have diameters below 1 mm. Fig. 18(g) shows the vast majority of data is available for L_H/D values below ~ 100, with a small cluster of LHe and LN_2 data at ~ 200. Fig. 18(h) shows the majority of data for which wall thickness is reported have $t_w < 1.5$ mm, with only studies by Müller et al. [105], Chen et al. [110], Wang et al. [111], and Gong et al. [112] having $t_w > 2$ mm. Finally, Fig. 18(i) shows the majority of the data were obtained in vertical upflow and horizontal flow orientations, with LN_2 data available in all three orientations and LNe, LAr, and LCH_4 data only in horizontal flow orientation.

Discussed next are details of response variables in flow boiling experiments for data used in the PU-BTPFL HTC database. Figs. 19(a)-19(e), show data histograms based on the following response variables: (a) local flow quality, (b) local void fraction, (c) local wall superheat, (d) local HTC, and (e) phase separation parameter for local HTC data. Each figure also includes another distribution for average HTC data based on response variables evaluated at the tube exit, with the exception of average wall superheat and average HTC which are evaluated using the average wall temperature. Fig. 19(a) shows that a majority of LHe and LH_2 data are associated with low qualities typical of the bubbly flow regime, with only a few LHe data attaining high qualities. However, LN_2 has data spread over the entire quality range with those for LNe, LAr, and LCH_4, intermittently present. Fig. 19(b) confirms that almost all LH_2 data and majority of LHe data belong to the bubbly flow regime. On the other hand, LNe data belong to the annular flow regime and LCH_4 to intermediate flow regimes. LN_2, having a strong presence in the HTC database is found to exist in all the flow regimes. Fig. 19(c) shows that among all cryogens LHe ex-

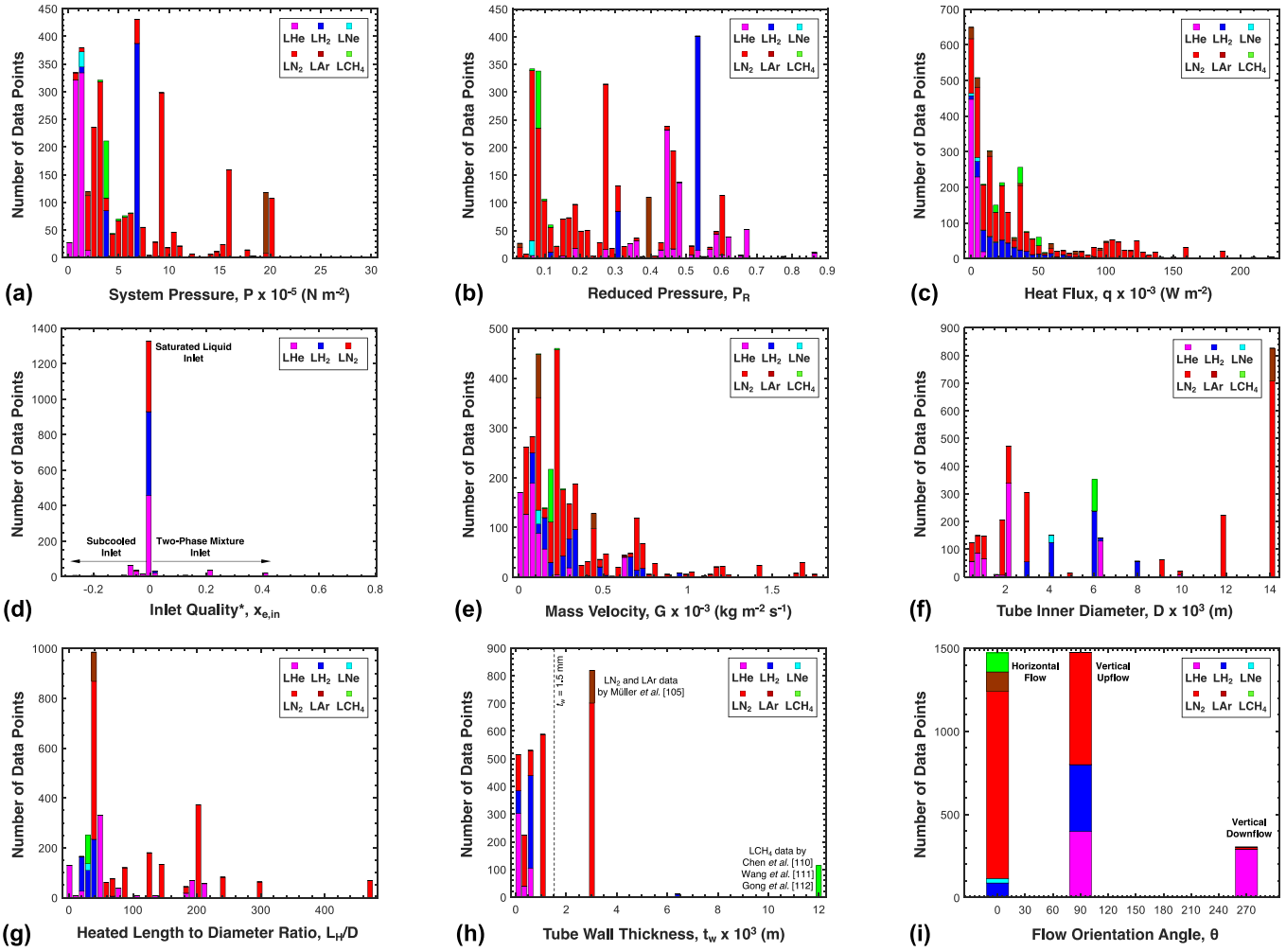

Fig. 18. Data distribution of PU-BTPFL HTC Database relative to controlled parameters: (a) system pressure, (b) reduced pressure, (c) heat flux, (d) inlet quality* (only for HTC data with prescribed inlet conditions), (e) mass velocity, (f) tube diameter, (g) heated length to diameter ratio, (h) tube wall thickness, and (i) flow orientation angle.

hibits the lowest wall superheats, followed by LH_2 and LNe, an inference that has already been alluded to in section 3.1.1. Fig. 19(d) shows that, despite lowest wall superheats, LHe exhibits the lowest HTC of all cryogens, an outcome of its low heat flux, as shown earlier in Fig. 18(c). Notice how the LH_2 data, which belong mostly to the bubbly flow regime, show the highest HTC values of all the cryogens, given the dominance of h_{NB} over h_{CB} for this fluid. Finally, Fig. 19(e) shows that, with the exception of LH_2, all fluids have some data with high phase separation ($1/X_{tt} \geq 1$), whereas the low phase separation region ($1/X_{tt} < 0.1$) is limited mostly to LHe and LH_2.

Aside from insight into details of the PU-BTPFL HTC Database, Table 8 and Figs. 17-19 serve to guide future experimental research into filling significant gaps in cryogen data in an effort to both maximize new data yield and minimize unnecessary future experimental expenditures. Following is a summary of major experimental needs based on the gaps identified in the database:

1. High priority need for Liquid Oxygen, LOX, HTC data.
2. High priority need for *accurate* local HTC data for LH_2. Although local LH_2 data are available from works by Core et al. [12] and Lewis et al. [14], very large errors and scatter in the data are found to produce exorbitantly high and sometimes even negative values of HTC, precluding the usefulness of such data in development of HTC correlations.
3. Additional data for LCH_4, LNe and LAr.
4. Additional data for vertical downflow.
5. Additional data with large heated length-to-diameter ratios leading to more annular flow and convective boiling dominant heat transfer.
6. Additional data with high mass velocities.
7. Systematic tests to investigate the parametric effects of wall thickness, wall thermal conductivity, surface roughness, and surface ageing on HTC.
8. Systematic tests to investigate the parametric effects of preheater heat flux, q_{PH}, and two-phase mixture inlet quality, $x_{e,in}$ (> 0), on flow boiling regimes and HTC.
9. In conclusion, flow visualization data for all cryogens to develop robust flow regime maps specific to cryogens with special emphasis to LHe and LH_2.

5. Development of Universal HTC Correlation

With the PU-BTPFL HTC Database now vetted against all possible physics-based violations and categorized based on physics-based classifiers, a detailed plan is adopted to develop universal

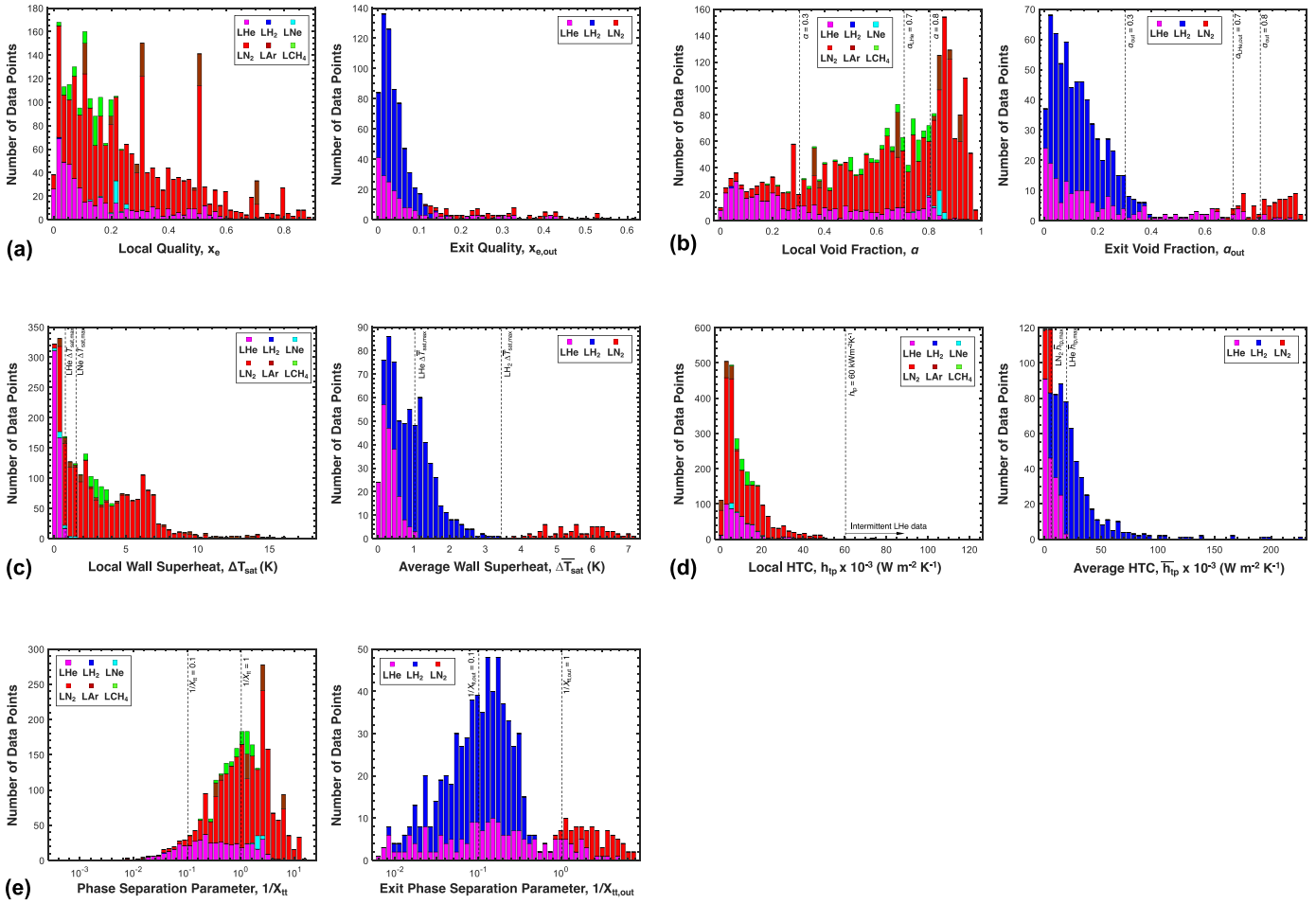

Fig. 19. Data distribution of PU-BTPFL HTC Database relative to response variables: (a) quality, (b) void fraction, (c) wall superheat, (d) two-phase heat transfer coefficient, and (e) phase separation parameter. Variables for average HTC data are evaluated at tube exit.

HTC correlations. As mentioned in section 3.2.1, three traditional classifiers: (1) fluid, (2) flow orientation, and (3) confinement number are known to affect the magnitude of HTC because of flow physics unique to each classifier. As seen from Fig. 19(d), HTC values of LHe are lower than that those for LN_2 which in turn are orders of magnitude lower than for LH_2, hence the need to use fluid as a primary classifier. At low mass velocities or low liquid-only Froude number, the convective boiling heat transfer mechanism is affected only in horizontal flow, whereas the nucleate boiling heat transfer mechanism is unaffected. Although, in general, cryogens tend to exhibit high values of $Fr_{fo,D}$ (*i.e.,* weak gravity effects), flow orientation classifier is retained initially to prove or disprove the aforementioned claim. As seen from Fig. 12(a), it was determined that almost the entire PU-BTPFL HTC Database is within the category of macro-channels ($Co < 0.6$), thereby making the confinement number classifier inconsequential for cryogenic flow boiling. Hence, only the former two classifiers, fluid and orientation, are retained during development of HTC correlations. However, the discussion in sections 3.2.2 and 3.2.3 emphasized the need for two additional important classifiers: (4) saturation length ratio, $\Delta z_{sat}/L_H$, and (5) phase separation parameter, $1/X_{tt}$. Special attention is also given to the last classifier: (6) tube wall material, because of the strong dependency of wall thermal conductivity on temperature at cryogenic temperatures, and potential for strong axial conduction effects.

Hence, these selected classifiers are used throughout the development of universal cryogen HTC correlations by distinguishing the fluid physics for nucleate boiling and convective boiling.

5.1. Assessment of Seminal HTC Correlations

Using the traditional classifiers of fluid and flow orientation, and newly proposed classifiers of saturation length ratio, $\Delta z_{sat}/L_H$, phase separation parameter, $1/X_{tt}$, and tube wall material, the performance of seminal flow boiling HTC correlations, Table 2, and pool boiling HTC correlations, Table 3, are tested for both local HTC and average HTC in Tables 9(a) and 9(b) respectively, by evaluating the mean absolute error (MAE), which is defined for local HTC as

$$MAE = \frac{1}{N}\sum \frac{\left|h_{tp,pred} - h_{tp,exp}\right|}{h_{tp,exp}} \times 100\%, \tag{31}$$

With h_{tp} replaced with $\bar{h}_{tp}$ for average HTC. Here, all the five classifiers are treated as mutually independent to pursuit of a first approximate guess regarding roles of the classifiers. It can be seen from Tables 9(a) that pool boiling correlations in general, especially those of Forster and Zuber [35] and Cooper [50] perform better than almost all of the flow boiling correlations despite being compared to local flow boiling HTC data. This peculiar behavior will be studied further in subsequent sections. Nonetheless, it does point

Table 9a
Performance of seminal local flow and pool boiling HTC correlations using the PU-BTPFL HTC Database, segregated by different classifiers. (a) Local HTC database [a] with both prescribed local and inlet conditions.

Author(s)	MAE (%) for traditional classifiers							MAE (%) for additional proposed classifiers					
	Fluid (data points)					Flow orientation (data points)		Saturation length ratio [b] (data points)		Phase separation parameter [c] (data points)		Tube wall material [d] (data points)	
	LHe (495)	LNe (27)	LN_2 (1751)	LAr (117)	LCH_4 (114)	Vertical Flows (1178)	Horizontal Flow (1327)	Two-phase mixture inlet (with high vapor content) $\Delta z_{sat}/L_H$ > 1.1 (964)	Other inlet conditions $\Delta z_{sat}/L_H \leq$ 1.1 (1541)	High phase separation $1/X_{tt} \geq$ 1 (1348)	Low-to-medium phase separation $1/X_{tt}$ < 1 (1157)	SS variants (1440)	Cu/Cu alloys (1057)
Flow boiling correlation													
Schrock & Grossman [e,f] [40]	61.6	57.5	58.8	80.1	45.1	61.4	58.2	47.3	67.5	67.4	50.7	66.6	50.6
Chen [e,f] [41]	43.4	37.5	53.5	77.6	24.0	44.9	56.6	39.1	58.7	53.9	47.9	60.4	38.7
Shah [43]	43.2	53.7	64.7	24.5	29.7	55.3	58.4	43.6	65.3	62.3	50.7	67.8	42.4
Gungor & Winterton [e] [42]	59.3	48.5	69.5	37.0	22.3	66.0	61.6	40.3	78.3	67.0	59.8	81.5	39.6
Klimenko [g] [44]	55.4	15.4	41.7	216	5.7	37.3	61.4	55.7	47.3	58.9	40.9	33.8	72.1
Liu & Winterton [e] [48]	35.7	60.5	40.5	95.4	17.0	34.4	47.6	35.0	45.4	45.5	36.6	41.5	41.4
Steiner & Taborek [f] [31]	69.6	17.7	77.5	122	16.1	81.1	68.9	48.6	90.9	82.6	65.3	94.8	47.4
Kim & Mudawar [e] [49]	142	65.4	49.7	80.2	42.7	92.7	48.8	45.5	84.4	61.8	78.4	83.5	49.9
Pool boiling correlation													
Forster & Zuber [e] [35]	34.3	49.1	34.6	113	30.9	31.5	44.2	33.5	41.1	38.7	37.6	40.1	35.8
Cooper [50]	34.5	73.3	34.2	136	8.9	30.8	45.2	38.2	38.6	42.7	33.4	35.2	42.9
Gorenflo & Sokol [34]	37.3	70.0	43.4	331	19.3	36.9	71.0	61.9	50.6	67.2	40.6	35.9	81.2

[a] Evaluated using 2505 local HTC data points.
[b] Based on criterion developed in Section 3.2.2.
[c] Based on criterion developed in Section 3.2.3.
[d] Based on criterion developed in Section 3.2.4.
[e] Correlation not applicable to cryogens.
[f] Correlation not applicable to horizontal flows.
[g] Evaluated only for data points with known wall thermal conductivities, k_w, at local wall temperature.

Table 9b
Performance of seminal local flow and pool boiling HTC correlations using the PU-BTPFL HTC Database, segregated by different classifiers. (b) Average HTC database [a,b] with prescribed inlet conditions.

Author(s)	MAE (%) for traditional classifiers					MAE (%) for additional proposed classifiers					
	Fluid (data points)			Flow orientation (data points)		Saturation length ratio [c] (data points)		Phase separation [d] (data points)		Tube wall material [e] (data points)	
	LHe (200)	LH_2 (483)	LN_2 (64)	Vertical Flows (602)	Horizontal Flow (145)	Two-phase mixture inlet (with high vapor content) $\Delta z_{sat,max}/L_H$ > 1.1 (11)	Other inlet conditions $\Delta z_{sat,max}/L_H \leq 1.1$ (736)	High phase separation $1/X_{tt,out} \geq$ 1 (88)	Low-to-medium phase separation $1/X_{tt,out}$ < 1 (659)	SS variants (566)	Cu/Cu alloys (140)
Flow boiling correlation											
Schrock & Grossman [f,g] [40]	100	35.9	75.4	56.1	58.3	50.0	56.6	77.4	53.7	41.9	117
Chen [f,g] [41]	43.3	32.8	144	36.9	79.6	51.7	45.1	127	34.2	48.0	29.3
Shah [43]	42.0	52.2	130	45.9	98.7	12.8	56.8	119	47.8	64.4	22.2
Gungor & Winterton [f] [42]	81.3	52.4	152	58.7	110	10.4	69.5	140	59.1	68.1	74.1
Klimenko [h] [44]	131	32.1	64.9	61.7	53.1	21.0	60.6	58.7	60.1	35.8	164
Liu & Winterton [f] [48]	21.5	94.3	86.5	66.1	107	12.1	75.1	69.8	74.7	91.3	12.3
Steiner & Taborek [g] [31]	58.3	28.3	169	36.9	95.8	32.5	48.6	173	31.8	52.0	23.0
Kim & Mudawar [f] [49]	114	113	81.9	105	133	25.6	112	111	111	116	100
Pool boiling correlation											
Forster & Zuber [f] [35]	45.5	37.7	89.1	39.2	64.8	41.7	44.2	80.2	39.4	44.8	39.7
Cooper [50]	30.8	152	58.3	105	137	30	113	51.8	119	137	24
Gorenflo & Sokol [34]	53.3	62.6	29.7	55.5	64.5	41.8	57.5	37.8	59.9	59.2	51.8

[a] Evaluated using 747 average HTC data points.
[b] Average HTC is determined using harmonic average given by Eq. (17).
[c] Based on criterion developed in Section 3.2.2 for average HTC data.
[d] Based on criterion developed in Section 3.2.3 for average HTC data.
[e] Based on criterion developed in Section 3.2.4.
[f] Correlation not applicable to cryogens.
[g] Correlation not applicable to horizontal flows.
[h] Evaluated only for data points with known wall thermal conductivities, k_w, at average wall temperature.

to dominance of the nucleate boiling heat transfer mechanism for cryogens, as discussed earlier in section 1.3. The next step is to examine MAE trends relative to individual classifiers. For the fluid classifier, only LAr shows very large deviations from predictions of most correlations. As to flow orientation, no particular trend is observed for flow boiling correlations whereas pool boiling correlations perform better for vertical flows. Excepting the correlations by Klimenko [44] and Gorenflo and Sokol [34], all other flow boiling and pool boiling correlations show better MAE in predicting local HTC data with high-quality two-phase mixture inlet ($\Delta z_{sat}/L_H > 1.1$) than those with nominal inlet conditions ($\Delta z_{sat}/L_H \leq 1.1$). Similarly, with the exception of the Kim and Mudawar [49] correlation, all other flow boiling and pool boiling correlations show better MAE for local HTC data with low-to-medium phase separation ($1/X_{tt} < 1$) than those with high phase separation ($1/X_{tt} \geq 1$). As to tube wall material, no conclusions can be made from the results in the absence of a clear trend.

Table 9(b) also shows different trends in the performance of pool boiling and flow boiling correlations based on specific classifiers. With respect to the fluid classifier, the LHe data (which span the entire spectrum of void fractions, as seen in Fig. 19(b)) are best predicted by Liu and Winterton's correlation [48]. As to the LH_2 data, the pool boiling correlation of Cooper [50] shows the poorest predictions, despite this data being dominated by the nucleate boiling mechanism, and by the fact that the same correlation shows reasonable predictions for the other fluids. Overall, best predictions of the LH_2 data are achieved with by the correlation of Steiner and Taborek [32], which does not account for boiling suppression. For the LN_2 data, having the highest exit void fraction of all fluids, best predictions are achieved by Gorenflo and Sokol's pool boiling correlation [34]. In terms of the flow orientation classifier, both flow boiling and pool boiling correlations perform better for the vertical than the horizontal orientation, with the exception of Klimenko's [44]. Similar to local HTC data, average HTC data with high-quality two-phase mixture inlet ($\Delta z_{sat,max}/L_H > 1.1$) are predicted better than those with nominal inlet conditions ($\Delta z_{sat,max}/L_H \leq 1.1$) by both flow boiling and pool boiling correlations except Chen's [41]. Also similar to local HTC data, average HTC data with low-to-medium phase separation ($1/X_{tt,out} < 1$) are predicted better than those with high phase separation ($1/X_{tt,out} \geq 1$) by both flow boiling and pool boiling correlations except Klimenko's [44] and Liu and Winterton's [48]. The exorbitant increase in MAE observed for Cooper [50] with low-to-medium phase separation data is due to the error propagated by its poor prediction for LH_2 data, which constitutes a major portion of data with $1/X_{tt,out} < 1$. With regards to tube wall material, here too no distinct trend is observed, hence no conclusions can be drawn from the results.

While results from Tables 9(a) and 9(b) provide a first order assessment of the influence of individual classifiers, they are both based on the assumption that these classifiers are mutually independent. However, in reality, all four classifiers (fluid, flow orientation, saturation length ratio, phase separation parameter) are coupled. To allow for interdependence of classifiers, the local HTC data are segregated into four categories instead based on fluid physics, and predictions of all seminal flow boiling HTC correlations, Table 2, are assessed in a separate figure for each category:

(1) Nominal inlet conditions ($\Delta z_{sat}/L_H \leq 1.1$) and low-to-medium phase separation ($1/X_{tt} < 1$): Fig. 20.
(2) Nominal inlet conditions ($\Delta z_{sat}/L_H \leq 1.1$) and high phase separation ($1/X_{tt} \geq 1$): Fig. 21.
(3) High quality two-phase mixture inlet ($\Delta z_{sat}/L_H > 1.1$) and low-to-medium phase separation ($1/X_{tt} < 1$): Fig. 22.
(4) High quality two-phase mixture inlet ($\Delta z_{sat}/L_H > 1.1$) and high phase separation ($1/X_{tt} \geq 1$): Fig. 23.

For each category, the corresponding figure provides detailed statistical assessment of predictive accuracy in terms of (i) MAE, (ii) root mean squared error (RMS), and (iii) data points predicted within ±30% (θ) and ±50% (ξ), where RMS for local and average HTC is defined as

$$RMS = \sqrt{\frac{1}{N}\sum\left(\frac{h_{tp,pred} - h_{tp,exp}}{h_{tp,exp}}\right)^2} \times 100\%, \quad (32)$$

and h_{tp} is replaced with $\bar{h}_{tp}$ for average HTC data. In addition to comparing the performance metrics, the predicted transition of two-phase HTC ($h_{tp,pred}/h_{CB,pred}$) from nucleate boiling dominant ($h_{CB,pred}/h_{NB,pred} < 1$) to convective boiling dominant ($h_{CB,pred}/h_{NB,pred} > 1$) for each correlation, denoted by black symbols, is qualitatively compared with the true transitional behavior using experimental two-phase HTC data ($h_{tp,exp}/h_{CB,pred}$).

Fig. 20 compares predictions of the different seminal correlations with local PU-BTPFL HTC data with nominal inlet conditions and low-to-medium phase separation (Category 1). It can be seen that all correlations provide reasonable prediction trends and agreement with the data, confirming the majority of data in this category are nucleate boiling dominant, one obvious exception is large deviations of LHe data using Chen's [41] correlation. Fig. 21 shows that, for local PU-BTPFL HTC data with nominal inlet conditions and high phase separation (Category 2), the data continue to be nucleate boiling dominant despite the correlations predicting them to be in the convective boiling dominant region. Notice in this case the difference between predicted trends (black symbols) and experimental trends for all the correlations. As the value of $h_{CB,pred}/h_{NB,pred}$ approaches unity, the *predicted* trends for almost all correlations change slope as they transition, either asymptotically or sharply, to the convective boiling dominant region, while the experimental values tend to maintain the same slope as the nucleate boiling dominant region, even for values of $h_{CB,pred}/h_{NB,pred}$ well above unity. This implies that h_{CB} is being over-predicted for these higher $h_{CB,pred}/h_{NB,pred}$ values which include annular flow data ($\alpha \geq 0.8$). Fig. 22 shows that, for local PU-BTPFL HTC data with high quality two-phase mixture inlet and low-to-medium phase separation (Category 3), all correlations correctly predict deviation towards the convective boiling dominant region. This points to enhanced convection due to presence of high-vapor-content bubbles from inlet onward enhancing both macro-layer evaporation and turbulence in the thermal boundary layer due to bubble motion. Finally, Fig. 23 shows that, for local PU-BTPFL HTC data with high quality two-phase mixture inlet and high phase separation (Category 4), all correlations predict appreciable data penetration into the convective boiling region with reasonable accuracy excepting Liu and Winterton's [48] correlation. Hence, in conclusion, it is observed that for nominal inlet conditions ($\Delta z_{sat}/L_H \leq 1.1$, Categories 1 and 2), irrespective of the magnitude of phase separation parameter, $1/X_{tt}$, the HTC data are predicted as almost always nucleate boiling dominant, with convective boiling being present but insignificant. However, for high quality two-phase mixture inlet conditions ($\Delta z_{sat}/L_H > 1.1$), data with low-to-medium phase separation ($1/X_{tt} < 1$, Category 3) incur partial suppression of nucleate boiling and partial enhancement of convective boiling due to presence of high-vapor-content bubbles from inlet onward. But for high phase separation ($1/X_{tt} \geq 1$, Category 4), both suppressed nucleate boiling and maximum convective boiling (still comparatively lesser in magnitude than nucleate boiling) will contribute to the HTC. A similar exercise is done using average HTC data by segregating the data based on saturation length ratio and phase separation parameter and seeing if the results are consistent with the aforementioned inferences.

As indicated earlier, the average HTC coefficient, $\bar{h}_{tp}$, is obtained by harmonic averaging. Since the harmonic averaging operator is

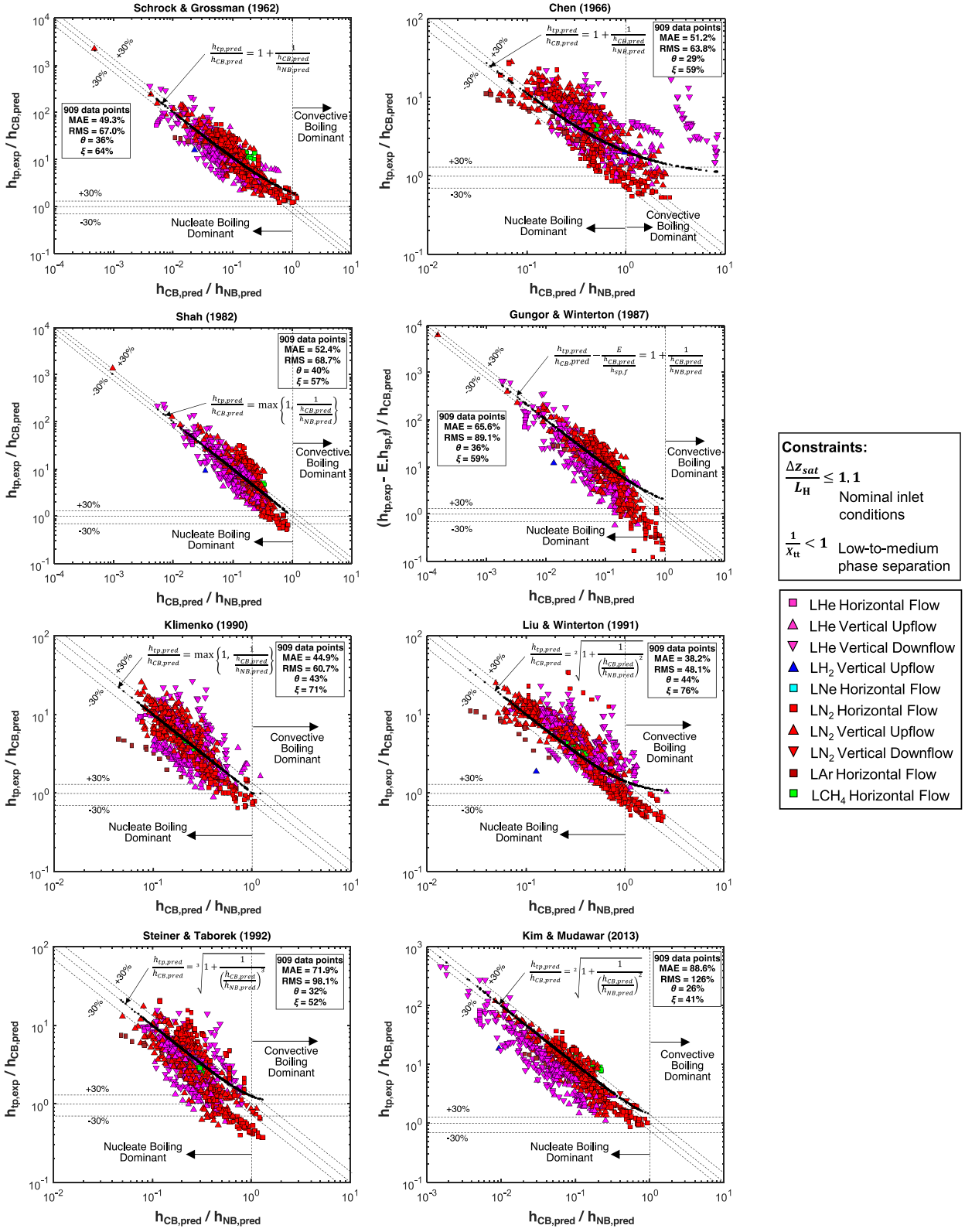

Fig. 20. Performance of seminal flow boiling HTC correlations against local PU-BTPFL HTC Database corresponding to Category 1: nominal operating conditions ($\Delta z_{sat}/L_H \leq 1.1$) and low-to-medium phase separation data ($1/X_{tt} < 1$). Solid black symbols represent information predicted by equation shown corresponding to each data point.

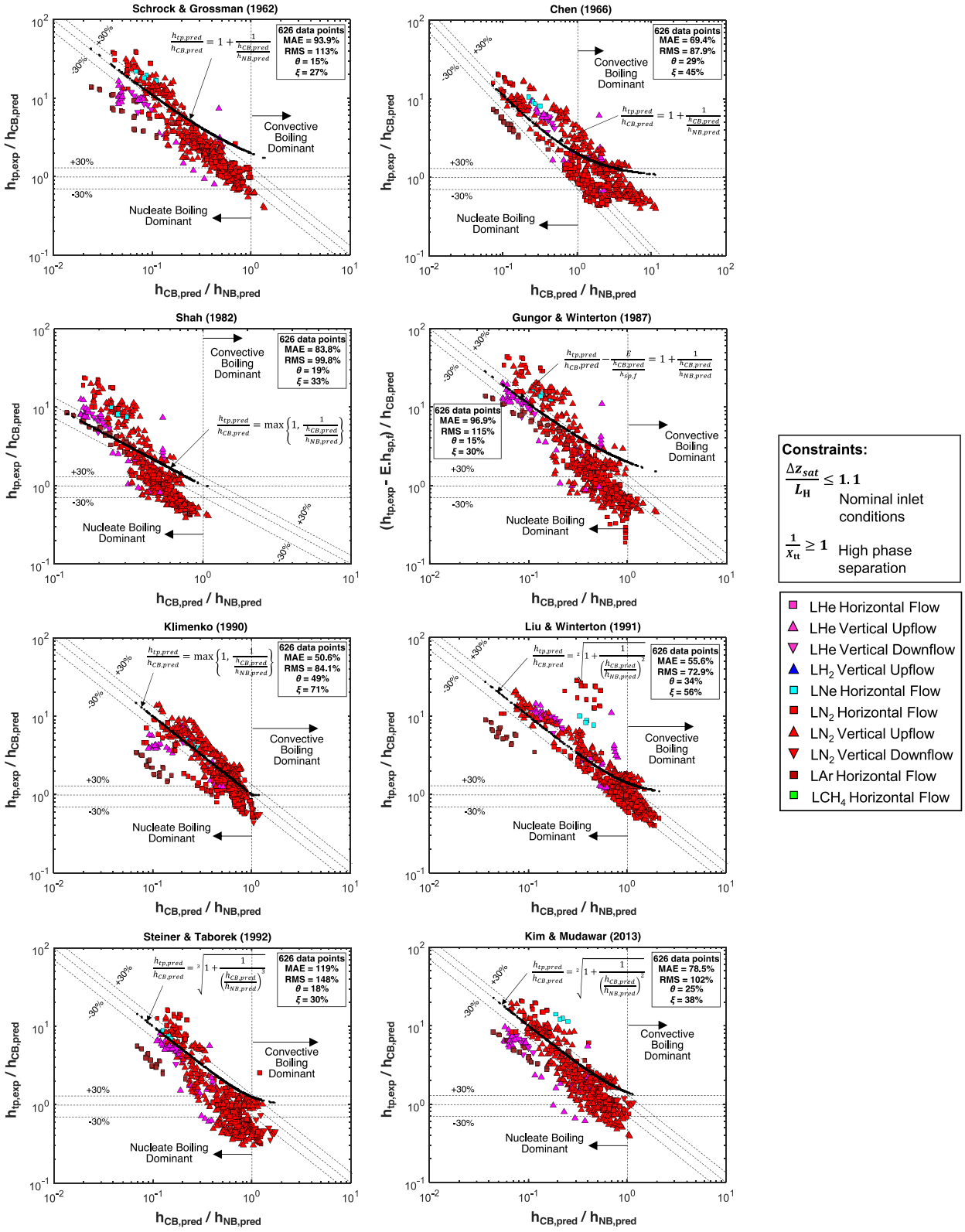

Fig. 21. Performance of seminal flow boiling HTC correlations against local PU-BTPFL HTC Database corresponding to Category 2: nominal operating conditions ($\Delta z_{sat}/L_H \leq 1.1$) and high phase separation data ($1/X_{tt} \geq 1$). Solid black symbols represent information predicted by equation shown corresponding to each data point.

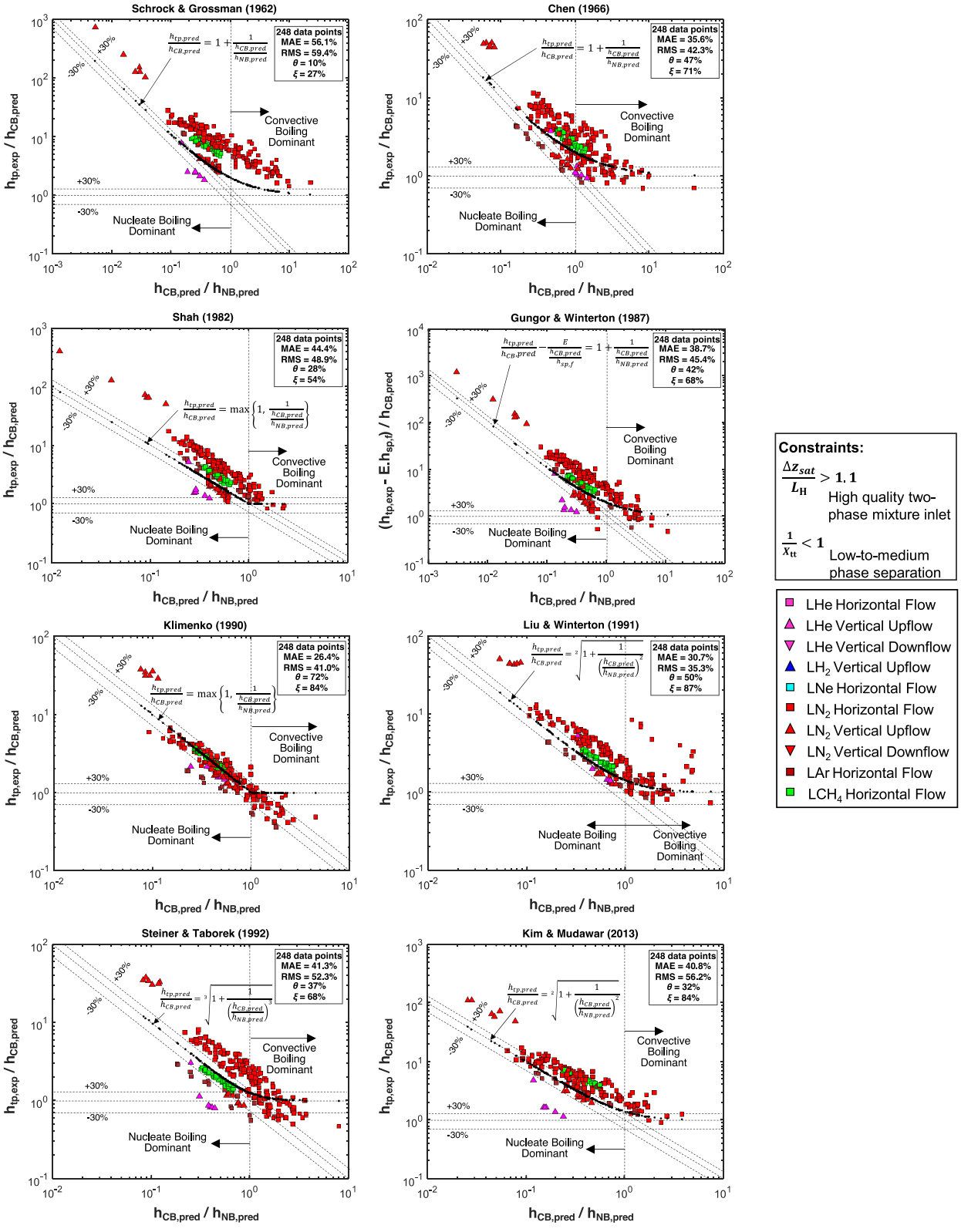

Fig. 22. Performance of seminal flow boiling HTC correlations against local PU-BTPFL HTC Database corresponding to Category 3: high quality two-phase mixture inlet ($\Delta z_{sat}/L_H > 1.1$) and low-to-medium phase separation data ($1/X_{tt} < 1$). Solid black symbols represent information predicted by equation shown corresponding to each data point.

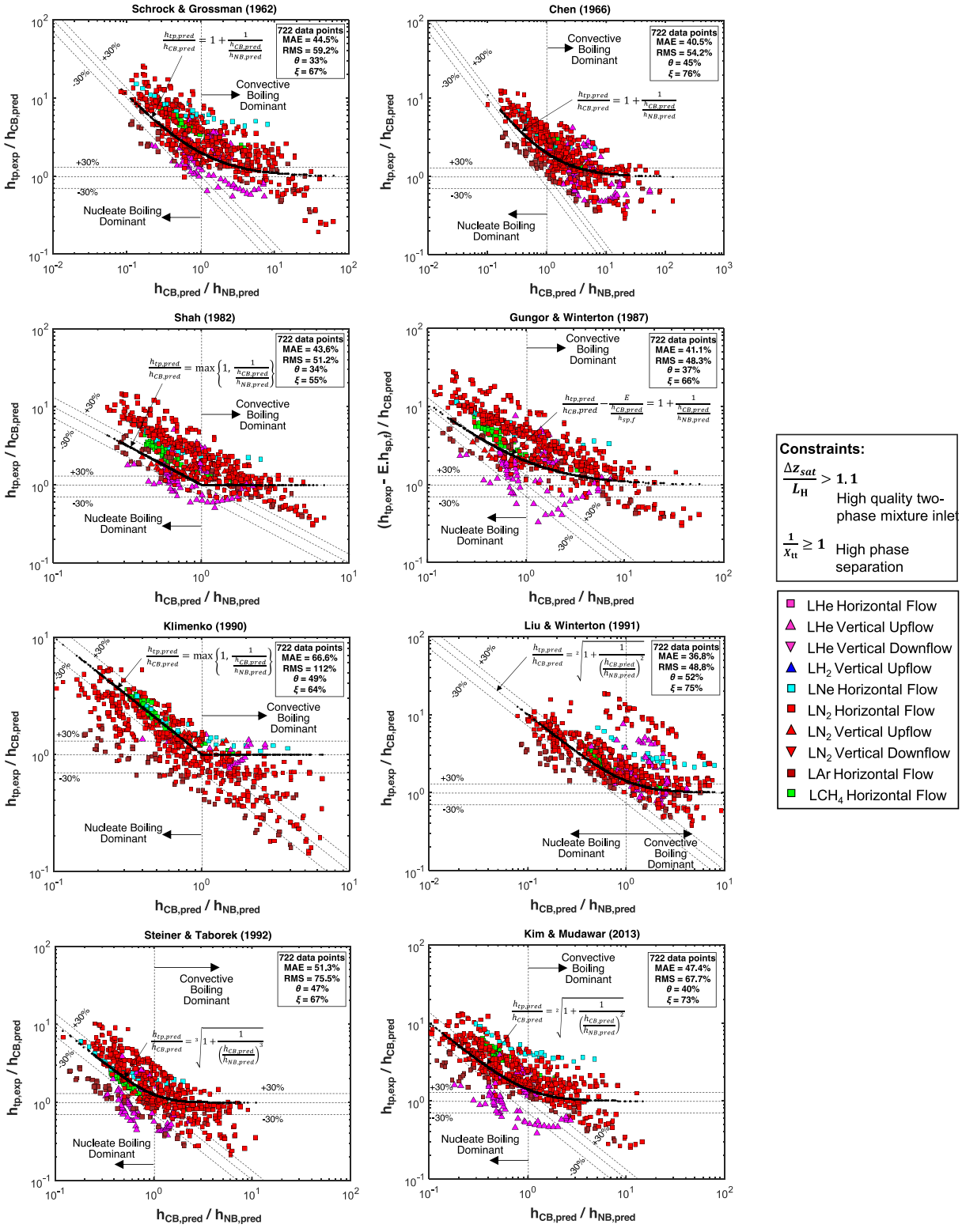

Fig. 23. Performance of seminal flow boiling HTC correlations against local PU-BTPFL HTC Database corresponding to Category 3: high quality two-phase mixture inlet ($\Delta z_{sat}/L_H > 1.1$) and high phase separation data ($1/X_{tt} \geq 1$). Solid black symbols represent information predicted by equation shown corresponding to each data point.

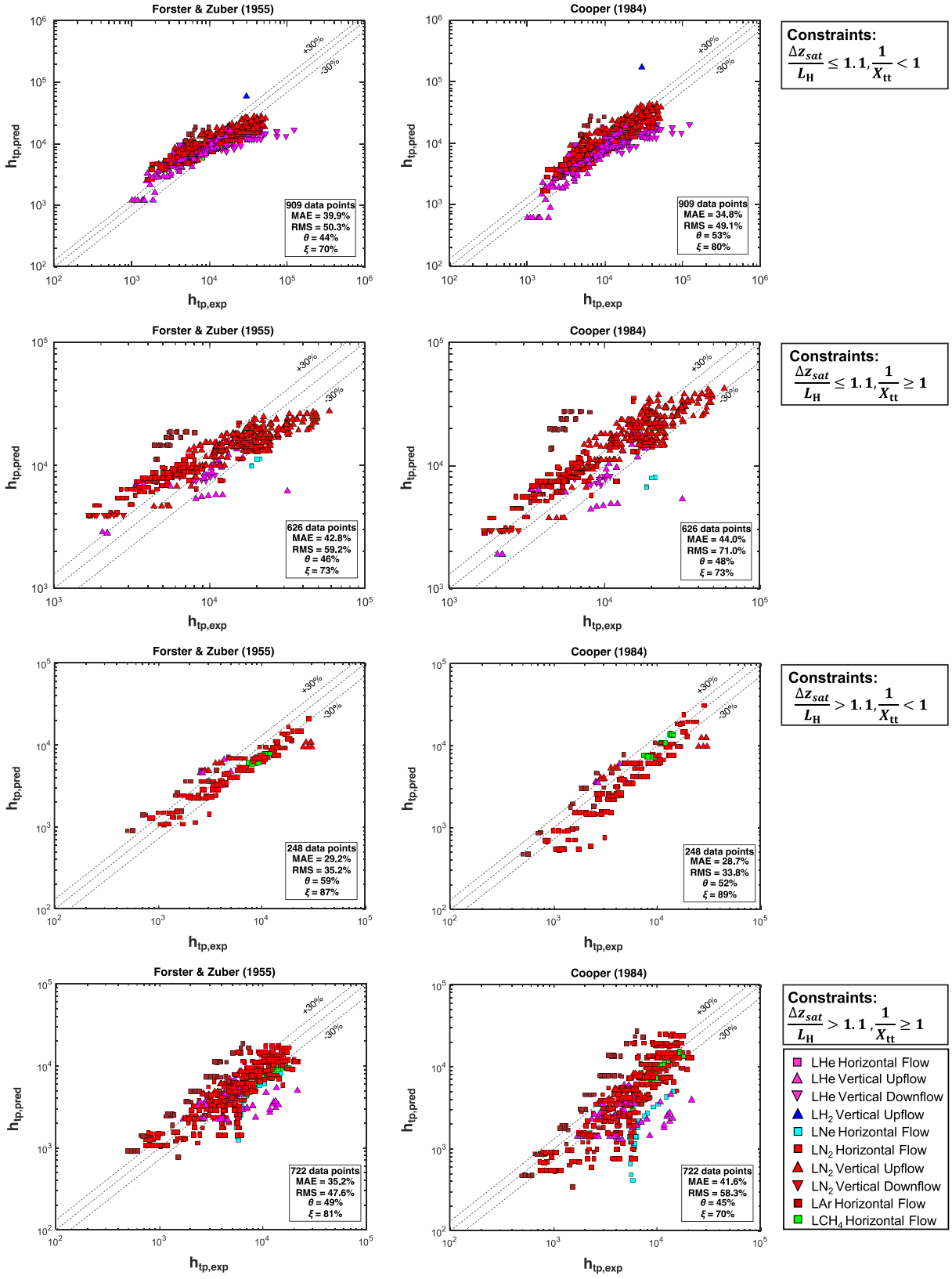

Fig. 24. Performance of pool boiling HTC correlations by Forster and Zuber [35] (implicit correlation) and Cooper [50] (explicit correlation) against local PU-BTPFL HTC Database corresponding to four data categories.

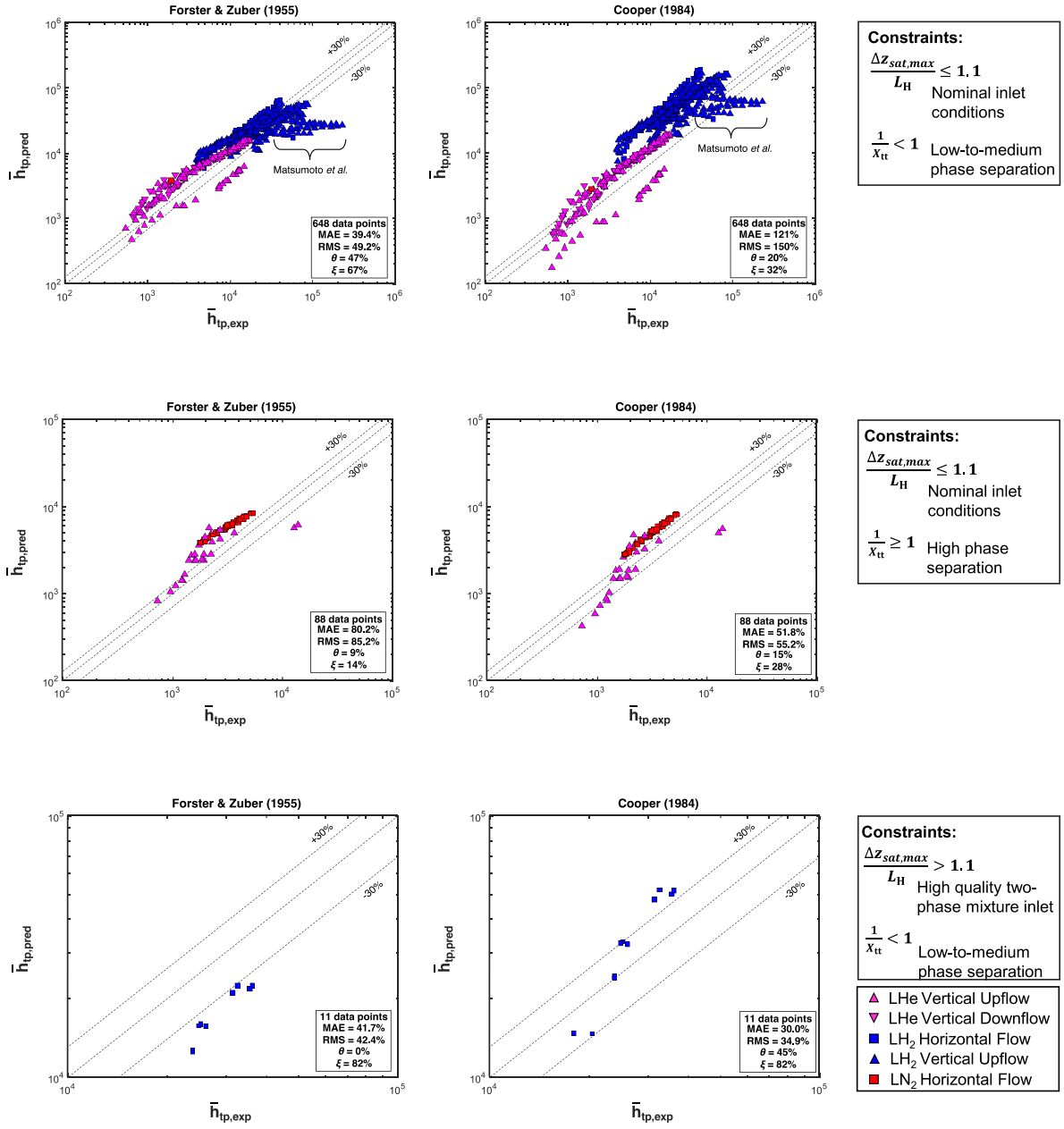

Fig. 25. Performance of pool boiling HTC correlations by Forster and Zuber [35] (implicit correlation) and Cooper [50] (explicit correlation) against average PU-BTPFL HTC Database corresponding to three data categories. Indicated are LH_2 data by Matsumoto et al. [11] showing appreciable departure from other LH_2 data.

not additive in nature, $\bar{h}_{tp}$ is represented as the sum of $\bar{h}_{NB}$ and $\bar{h}_{CB}$ by assuming an arithmetic average operation since the increase in the MAE due to the operation was found to be only 0.2% for Chen's [41] correlation, which showed the best MAE of all the flow boiling correlations. The results for average HTC data are consistent with those of local HTC data for nominal inlet conditions (Categories 1 and 2), as the HTC data are found to be nucleate boiling dominant, with experimental data maintaining the same slope as the nucleate boiling dominant region, even for values of $\bar{h}_{CB,pred}/\bar{h}_{NB,pred}$ well above unity. Interesting observations are made for LH_2, which could not be made earlier for local HTC data due to its absence from the local HTC Database. At values $\bar{h}_{CB,pred}/\bar{h}_{NB,pred} > 1$, few LH_2 data points obey the predicted trends and start to asymptotically transition into convective boiling regime. This trend was not observed for any other cryogenic HTC data with nominal inlet conditions and low-to-medium phase separation. For high quality two-phase mixture inlet conditions ($\Delta z_{sat,max}/L_H > 1.1$) with low-to-medium phase separation ($1/X_{tt,out} < 1$, Category 3), LH_2 data show transitioning into the convective boiling regime, which is consistent with results for local HTC data.

Because of the strong presence of nucleate boiling heat transfer component under all possible operating conditions, the PU-BTPFL HTC data are now compared to the pool boiling HTC correlations by Forster and Zuber [35], having an implicit functional form, and Cooper [50], having an explicit functional form. Figs. 24 and 25 show comparisons based on local and average HTC data, respectively, under all possible combinations of saturation length ratio, $\Delta z_{sat}/L_H$, and phase separation parameter, $1/X_{tt}$. Fig. 24 shows for local data that, Cooper's [50] correlation performs slightly better for data with low-to-medium phase separation ($1/X_{tt} < 1$) irrespective of inlet conditions, whereas Forster and Zuber's [35] provides slightly more superior predictions for data with high phase separa-

Table 10a
New universal saturated flow boiling HTC correlations for cryogens using local PU-BTPFL data. (a) Correlation for data with nominal inlet conditions, including subcooled, saturated liquid, and two-phase mixture (with low vapor content).

Correlation	Equation(s)	Constants
MAE (%) = 26.4 RMS (%) = 36.1 θ (%) = 68 ξ (%) = 86 Fluids: LHe, LH_2, LNe, LN_2, LAr, LCH_4 Flow Orientations: Vertical upflow Vertical downflow Horizontal flow Constraints: $\Delta z_{sat}/L_H \le 1.1$ [a] $\Delta P_{max}/P < 0.2$ $Re_{f,D} > 3000$ $\Delta T^*_{sat} < 1$ (-10%)	$h_{tp}^2 = h_{NB}^2 + h_{CB}^2$ $\frac{h_{NB}}{h_{sp.f}} = [c_1 Bo^{c_2} P_R^{c_5} (1-x_e)^{-c_8} Co^{-c_9}]$ $\frac{h_{CB}}{h_{sp.f}} = [c_3 \left(\frac{1}{X_{tt}}\right)^{c_4} \left(\frac{\rho_f}{\rho_g}\right)^{-c_6} Co^{-c_7}]$ where $h_{sp.f} = \frac{(4f_{sp.f}/8)(Re_{f,D}-1000)Pr_f}{1+12.7(4f_{sp.f}/8)^{0.5}(Pr_f^{2/3}-1)} \frac{k_f}{D}$ $4f_{sp.f} = [0.7904 \ln Re_{f,D} - 1.64]^{-2}$	$C_1 = 1226$ $C_6 = 0.37$ $C_2 = 0.81$ $C_7 = 1.39$ $C_3 = 0.55$ $C_8 = 0.67$ $C_4 = 0.39$ $C_9 = 0.06$ $C_5 = -0.05$ Transition of HTC mechanism: Eq. (10) $n = 2$ (asymptotic) Convective boiling (annular flow): Eq. (12) $F\left(\frac{1}{\Pi_{1-\alpha}}\right) \sim \frac{1}{X_{tt}} = \left(\frac{x_e}{1-x_e}\right)^{0.9} \left(\frac{\rho_f}{\rho_g}\right)^{0.5} \left(\frac{\mu_g}{\mu_f}\right)^{0.1}$ Nucleate boiling (bubbly flow): Eq. (14) $\frac{1}{\Pi'_{1-x_e}} = \frac{1}{1-x_e}$ Effect of G on h_{NB} [c]: $h_{NB} \sim G^{-0.01}$ Effect of x_e on h_{NB} [c]: $h_{NB} \sim (1-x_e)^{0.13}$

D x 10^3 [m]	P x 10^{-6} [N m^{-2}]	P_R	G [kg m^{-2} s^{-1}]	q x 10^{-3} [W m^{-2}]	x_e	α [b]	ΔT_{sat}	h_{tp} x 10^{-3} [W m^{-2} K^{-1}]
0.47	0.08	0.03	24.93	0.05	0	0	0.03	0.99
14.1	2.04	0.86	1743	223.2	0.77	0.97	17.8	123.3

[a] Saturation length ratio evaluated locally, Eq. (29).
[b] Evaluated using Zivi's void fraction relation, Eq. (9).
[c] $h_{sp,f,GN} = h_{sp,f,DB}$ ($\pm$ 30%) $\sim G^{0.8}$ $(1\text{-}x_e)^{0.8}$ based on Fig. 10.

Table 10b
New universal saturated flow boiling HTC correlations for cryogens using local PU-BTPFL data. (b) Correlation for data with high-quality two-phase mixture nominal inlet conditions.

Correlation	Equation	Constants
MAE (%) = 34.5 RMS (%) = 48.5 θ (%) = 53 ξ (%) = 81 Fluids: LHe, LNe, LN_2, LAr, LCH_4 Flow Orientations: Vertical upflow Horizontal flow Constraints: $\Delta z_{sat}/L_H > 1.1$ [a] $\Delta P_{max}/P < 0.2$ $Re_{f,D} > 3000$ $\Delta T^*_{sat} < 1$ (-10%)	$h_{tp}^2 = h_{NB}^2 + h_{CB}^2$ $\frac{h_{NB}}{h_{sp.f}} = [c_1 Bo^{c_2} P_R^{c_5} (1-x_e)^{-c_7}]$ $\frac{h_{CB}}{h_{sp.f}} = [c_3 \left(\frac{1}{X_{tt}}\right)^{c_4} \left(\frac{\rho_f}{\rho_g}\right)^{-c_6}]$ where $h_{sp.f} = \frac{(4f_{sp.f}/8)(Re_{f,D}-1000)Pr_f}{1+12.7(4f_{sp.f}/8)^{0.5}(Pr_f^{2/3}-1)} \frac{k_f}{D}$ $4f_{sp.f} = [0.7904 \ln Re_{f,D} - 1.64]^{-2}$	$C_1 = 562$ $C_6 = -0.42$ $C_2 = 0.57$ $C_7 = 0.76$ $C_3 = 0.51$ $C_4 = 0.41$ $C_5 = 0.02$ Transition of HTC mechanism: Eq. (10) $n = 2$ (asymptotic) Convective boiling (annular flow): Eq. (12) $F\left(\frac{1}{\Pi_{1-\alpha}}\right) \sim \frac{1}{X_{tt}} = \left(\frac{x_e}{1-x_e}\right)^{0.9} \left(\frac{\rho_f}{\rho_g}\right)^{0.5} \left(\frac{\mu_g}{\mu_f}\right)^{0.1}$ Nucleate boiling (bubbly flow): Eq. (14) $\frac{1}{\Pi'_{1-x_e}} = \frac{1}{1-x_e}$ Effect of G on h_{NB} [c]: $h_{NB} \sim G^{0.23}$ Effect of x_e on h_{NB} [c]: $h_{NB} \sim (1-x_e)^{0.04}$

D x 10^3 [m]	P x 10^{-6} [N m^{-2}]	P_R	G [kg m^{-2} s^{-1}]	q x 10^{-3} [W m^{-2}]	x_e	α [b]	ΔT_{sat}	h_{tp} x 10^{-3} [W m^{-2} K^{-1}]
0.47	0.1	0.03	39.79	0.14	0.02	0.1	0.02	0.49
14.1	2.99	0.88	619	97.22	0.89	0.98	15.3	28.27

[a] Saturation length ratio evaluated locally, Eq. (29).
[b] Evaluated using Zivi's void fraction relation, Eq. (9).
[c] $h_{sp,f,GN} \approx h_{sp,f,DB}$ ($\pm$ 30%) $\sim G^{0.8}$ $(1\text{-}x_e)^{0.8}$ based on Fig. 10.

tion ($1/X_{tt} \ge 1$), again irrespective of inlet conditions. Nonetheless, differences between predictive accuracy of the two correlations are relatively minor. For average HTC data, Fig. 25, shows that Cooper's [50] correlation fails to capture the bulk of LH_2 data, but does a better job than Forster and Zuber's [35] for the other fluids (LHe and LN_2) under all operating conditions.

5.2. New Universal HTC correlations

Using the functional form for the HTC given earlier in Eq. (16), and using $n = 2$ (chosen based on providing lower MAE than $n = 1$) for asymptotic transition of the HTC from bubbly flow to annular flow, the local HTC correlation is expressed as

$$\frac{h_{tp}^2}{h_{sp.f}^2} = \left[f\left(Bo, P_R, \frac{1}{\Pi'_{1-x_e}}\right)\right]^2 + \left[F\left(\frac{1}{\Pi_{1-\alpha}}\right)\right]^2, \quad (33)$$

where, $h_{sp,f}$ is found using the Eqs. (4) and (5), substituting $Re_{fo,D}$ with $Re_{f,D}$. The dependence of the ratio $h_{tp}/h_{sp,f}$ on the parameters in Eq. (33) was ascertained empirically in two separate steps:

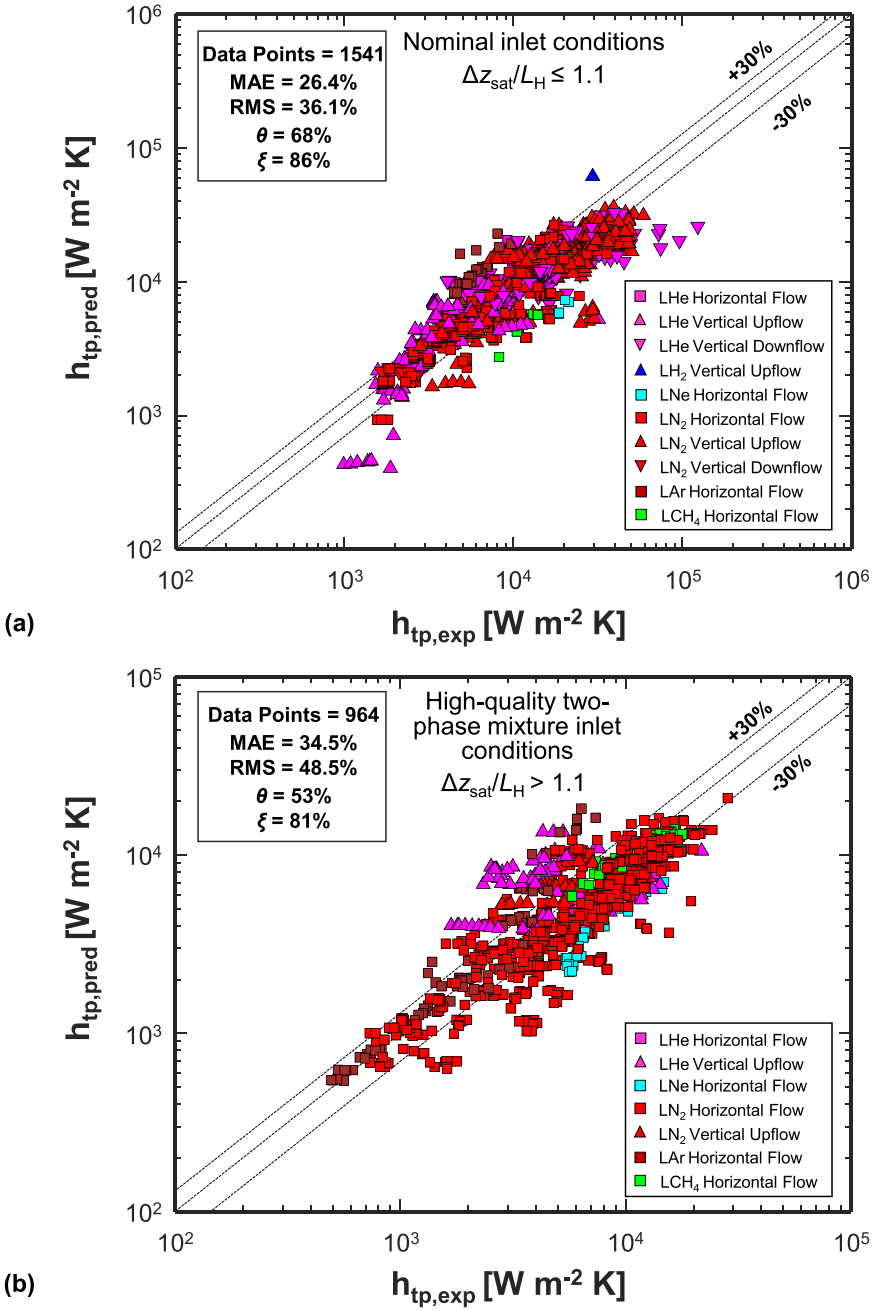

Fig. 26. Comparison of predictions of new universal cryogen HTC correlations against local data in the PU-BTPFL HTC Database corresponding to (a) nominal inlet conditions, $\Delta z_{sat}/L_H \leq 1.1$, including subcooled, saturated liquid, and low-quality two-phase mixture, and (b) high-quality two-phase mixture inlet conditions ($\Delta z_{sat}/L_H > 1.1$).

(1) Determining functional dependence on enhancement factor, F, for high phase separation ($1/X_{tt} \geq 1$) data alone (corresponding to annular flow ($\alpha \geq 0.8$)).
(2) Determining functional dependence on boiling number, Bo, for low-to-medium phase separation ($1/X_{tt} < 1$) data alone.

For the dependence on F for high phase separation ($1/X_{tt} \geq 1$) data, three different enhancement factor formulations of Chen [41], $F = 1/X_{tt}$, Shah [43], $F = 1/N_{conv.}$, and Liu and Winterton [48], $F = 1 + x_e Pr_f(\frac{\rho_f}{\rho_g} - 1)$, showed similar power law trends (slope on a log-log scale) of $h_{tp}/h_{sp,f}$ versus F for all nominal inlet ($\Delta z_{sat}/L_H \leq 1.1$) and both local and average HTC data. For these same data, defining the enhancement factor as $F = 1/X_{tt}$, in accordance with Chen's [41] correlation, the ratio $h_{tp}/h_{sp,f}$ ratio provided proportional to $1/X_{tt}$. However, similar plots for high quality two-phase mixture inlet ($\Delta z_{sat}/L_H > 1.1$) showed appreciable scatter, making it difficult to determine a clear trend.

In the second part of the data trend analysis, the dependence of $h_{tp}/h_{sp,f}$ on Bo was examined for both local and average HTC data with low-to-medium phase separation ($1/X_{tt} < 1$). The trends were different for nominal inlet versus high-quality two-phase mixture inlet conditions. For the nominal inlet conditions ($\Delta z_{sat}/L_H \leq 1.1$), the analysis showed $h_{tp}/h_{sp,f} \sim Bo$ for local HTC data and $Bo^{0.8}$ for average HTC data. The reduction in the exponent of Bo for average HTC data can be attributed to the peculiar behavior of LH_2, which comprises the majority of the average HTC data. On the other hand, analysis of the high quality two-phase mixture inlet conditions ($\Delta z_{sat}/L_H > 1.1$) showed $h_{tp}/h_{sp,f} \sim Bo^{0.5}$ for both local and average HTC data. The smaller exponent for the latter high

quality is indicative of the appreciable boiling suppression due to high vapor content at the inlet.

Given the significant differences in the exponents to *Bo* and $1/X_{tt}$ for high quality two-phase mixture inlet data as opposed to other inlet conditions, two distinct HTC correlations are developed, one for local HTC data with nominal inlet ($\Delta z_{sat}/L_H \leq 1.1$) and a second for local HTC data high quality two-phase mixture inlet ($\Delta z_{sat}/L_H > 1.1$).

Table 10(a) shows details of the new universal saturated boiling HTC correlation for local data with nominal operating conditions, $\Delta z_{sat}/L_H \leq 1.1$, including subcooled, saturated liquid, and two-phase mixture (with low vapor content).

$$\frac{h_{tp}^2}{h_{sp,f}^2} = \left[1226 Bo^{0.81} P_R^{-0.05} (1-x_e)^{-0.67} Co^{-0.06}\right]^2 + \left[0.55\left(\frac{1}{X_{tt}}\right)^{0.39}\left(\frac{\rho_f}{\rho_g}\right)^{-0.37} Co^{-1.39}\right]^2 \quad (34)$$

Fig. 26(a) compares predictions of this correlation against local HTC data. With a MAE of 26.4% *irrespective of fluid or flow orientation*, and with this correlation provides very good predictive accuracy. Notice also, that 68% and 86% of the data are captures within 30% and 50%, respectively, of the predicted values.

Table 10(b) shows similar details for the new universal saturated boiling HTC correlation for data with high quality two-phase mixture inlet conditions, $\Delta z_{sat}/L_H > 1.1$.

$$\frac{h_{tp}^2}{h_{sp,f}^2} = \left[562 Bo^{0.57} P_R^{0.02} (1-x_e)^{-0.76}\right]^2 + \left[0.51\left(\frac{1}{X_{tt}}\right)^{0.41}\left(\frac{\rho_f}{\rho_g}\right)^{0.42}\right]^2 \quad (35)$$

Fig. 26(b) compares predictions against relevant local HTC data. With a MAE of 34.5%, and 53% an 81% of the data captured within 30% and 50%, respectively, of predictions, the predicted values, this correlation also shows very good predictive accuracy for data with $\Delta z_{sat}/L_H > 1.1$.

It should be noted that the above universal correlations as well as details provided in Tables 10(a) and 10(b), were found using the genetic algorithm-based optimization tool in the MATLAB Global Optimization Toolbox [116] which iteratively varies both coefficient and exponents to find global minimum as opposed to local minimum. The error being sought in the minimization is the MAE, Eq. (31).

5.3. Recommendations for Future Work

Despite the success of the new correlations as new robust predictive tools for saturated boiling HTC for cryogen, findings from this study point to the need for future work to further the understanding of the underlying fluid physics and improve predictive accuracy. For example, aside from the data voids outlined earlier, more focused study of the effects of body force is essential, not only in terms of flow orientations effects, but also by performing experiments in reduced gravity [117,118] in order to simulate the true environment important to many new space applications employing cryogens. Future work must also capitalize of the successes of recent theoretical, semi-empirical and computational modeling tools, which have shown significant advances in understanding interfacial behavior in both boiling [119,120] and condensing [121,122] flows to provide a more systematic basis for predicting void fraction.

6. Conclusions

The present study was motivated by the absence of a large, reliable, error-free saturated flow boiling HTC database for developing and validating HTC correlations as well as future analytic and computational models. An exhaustive literature search identified 3252 useful local and average HTC data points for six different fluids, LHe I, para-LH_2, LNe, LN_2, LAr, and LCH_4, comprising a new consolidated PU-BTPFL HTC database. An exhaustive parametric study of the database was performed to gain insight into the fluid physics unique to cryogens, and to aid future investigators into important operating conditions for which there is a dearth of data. Finally, using the database, universal cryogen HTC correlations were constructed for two distinct inlet conditions, nominal and high-quality two-phase mixture inlet, which required careful physics-based classification of the data. Key inferences/recommendations from the study are as follows:

1. Cryogens generally exhibit stronger nucleate boiling heat transfer mechanism as compared to the convective boiling heat transfer mechanism, with LHe I exhibiting very poor convective boiling heat transfer in the annular flow regime as compared to other cryogens.
2. It is recommended to treat LHe I data separately from other cryogens when developing predictive tools for HTC. This inference is based on the observation that LHe I behaves as an outlier in terms of all three dominant heat transfer mechanisms (liquid convection, nucleate boiling, convective boiling).
3. It is recommended to treat saturated flow boiling with high-vapor-content two-phase mixture inlet conditions separately from subcooled or saturated liquid inlet conditions, given large differences in dominant flow regimes.
4. Wall temperatures are likely to exceed the critical temperature for cryogens like LHe I, para-LH_2, and LNe, possessing extremely low critical temperatures of 5.2 K, 33.1 K, and 44.4 K, respectively. Corresponding data should therefore be excluded from consideration when developing correlations for saturated boiling HTC.
5. Almost all of the world HTC data for cryogens are from experiments carried out in tubes exhibiting macro-channel fluid physics ($Co \leq 0.6$) with negligible pressure drop.
6. In case of missing inlet quality information, it is recommended to use the saturation length ratio (defined in Eq. (29)) to identify saturated flow boiling HTC data with high-vapor-content two-phase mixture inlet (alluded to in point 4) using the criterion $\Delta z_{sat}/L_H > 1$.
7. Seminal pool boiling HTC correlations by Forster and Zuber [35] and Cooper [50] perform better than seminal flow boiling correlations for cryogenic saturated flow boiling data. This is proof of the stronger nucleate boiling heat transfer mechanism as compared to the convective boiling heat transfer mechanism for cryogens as compared to other fluid classes.
8. New universal cryogen HTC correlations are developed, segregated based on inlet conditions, which show superior performance in terms of both trend and predictive accuracy.

Declaration of Competing Interest

The authors declare that they have no known competing financial interests or personal relationships that could have appeared to influence the work reported in this paper.

Acknowledgements

The authors are grateful for financial support provided by the National Aeronautics and Space Administration (NASA) under grant no. 80GRC018C0055. The authors would also like to acknowledge the services provided by Purdue Libraries, especially its Interlibrary Loan (ILL) service, for helping acquire literature from across the world.

Appendix 1

Given the unique manner in which the Chen [41] correlation is used to determine the nucleate boiling HTC, h_{NB}, the method used is summarized in this Appendix. In the Chen correlation, the expression for h_{NB} in presented in terms the pool boiling model of Forster and Zuber [35] modified with a suppression factor, S,

$$h_{NB} = 0.00122\left(\frac{k_f^{0.79}c_{p,f}^{0.45}\rho_f^{0.49}}{\sigma^{0.5}\mu_f^{0.29}h_{fg}^{0.24}\rho_g^{0.24}}\right)(\Delta T_{sat})^{0.24}(\Delta P_{sat})^{0.75}S. \tag{A1.1}$$

Rearranging and introducing terms of density ratio, ρ_f/ρ_g, Jacob number, Ja, and saturated liquid Prandtl number, Pr_f, reduce Eq. (A1.1) to

$$h_{NB} = 0.00122\left(\frac{k_f^{0.5}c_{p,f}^{0.5}\rho_f^{0.25}}{\sigma^{0.5}}\right)Pr_f^{-0.29}\left(\frac{\rho_f}{\rho_g}Ja\right)^{0.24}(\Delta P_{sat})^{0.75}S. \tag{A1.2}$$

Using the definition of bubble radius [35], R_b, from Eq. (6), the corresponding Nusselt number is defined as

$$Nu_{NB} = \frac{h_{NB}R_b}{k_f} = \left(0.00122\sqrt{2\pi}\right)Pr_f^{-0.29}\left(\frac{\rho_f}{\rho_g}Ja\right)^{1.24}S. \tag{A1.3}$$

Finally, substituting the definition of bubble Reynolds number [35],

$$Re_b = \frac{\pi}{Pr_f}\left(\frac{\rho_f}{\rho_g}Ja\right)^2, \tag{A1.4}$$

into Eq. (A1.3) gives

$$Nu_{NB} = \frac{h_{NB}R_b}{k_f} = 0.0015Re_b^{0.62}Pr_f^{0.33}S. \tag{A1.5}$$

Appendix 2

In literature, such as Klimenko et al. [51], there are references to a common misconception regarding the definition of average HTC, $\bar{h}$, when defined using local HTC, h, values. The average HTC has often been misinterpreted as arithmetic average of local HTCs. However, this inference is contingent on the boundary condition being isothermal. But, for constant heat flux boundary condition, the average HTC is the harmonic average of local HTCs.

In case of saturated flow boiling with constant wall heat flux, q, the surface energy balance integrated over a differential area element dA gives,

$$q\iint dA = \iint qdA = \iint h(T_w - T_{sat})dA. \tag{A2.1}$$

Hence, assuming the saturation temperature, T_{sat}, to be constant, the average HTC is defined as,

$$q\iint dA = \bar{h}A\left(\bar{T}_w - T_{sat}\right). \tag{A2.2}$$

Should average HTC be assumed the arithmetic average of local HTC values, $\bar{h} = \frac{1}{A}\iint hdA$, substituting into Eq. (A2.2) and combining with Eq. (A2.1) give the following relation for average wall temperature:

$$\bar{T}_w = \frac{\iint hT_w dA}{\iint hdA}. \tag{A2.3}$$

However, Eq. (A2.3) is the incorrect definition of average wall temperature. The correct definition is

$$\bar{T}_w = \frac{\iint T_w dA}{\iint dA}. \tag{A2.4}$$

Hence, for a constant heat flux boundary condition, such as in cryogen experiments, Eq. (A2.4) is used as the starting point to a correct relation for average HTC. Substituting the definition of local wall temperature, $T_w = T_{sat} + (q/h)$, in Eq. (A2.4),

$$\bar{T}_w\iint dA = \iint\left(T_{sat} + \frac{q}{h}\right)dA. \tag{A2.5}$$

On re-arranging, Eq. (A2.5) simplifies to

$$\left(\bar{T}_w - T_{sat}\right)\frac{\iint dA}{\iint \frac{1}{h}dA} = q. \tag{A2.6}$$

Hence, comparing Eq. (A2.6) to Eq. (A2.2), the relationship between average HTC and local HTCs is found to be a harmonic average as opposed to arithmetic average.

$$\frac{1}{\bar{h}} = \frac{\iint \frac{1}{h}dA}{\iint dA} \tag{A2.7}$$

Hence, in case of saturated flow boiling with constant heat flux, the average HTC in the present study is treated as harmonic average of local HTCs.

References

[1] G. Hildebrandt, Heat transfer to boiling helium-I under forced flow in a vertical tube, in: Proc. 4th Int. Cryo. Eng. Conf., 1972, pp. 295–300.
[2] P.J. Giarratano, R.C. Hess, M.C. Jones, Forced convection heat transfer to subcritical helium I, National Bureau of Standards, 1973 Report 73-322.
[3] H. Ogata, S. Sato, Critical heat flux for two-phase flow of helium I, Cryogenics 13 (1973) 610–611.
[4] H. Ogata, S. Sato, Forced convection heat transfer to boiling helium in a tube, Cryogenics 14 (1974) 375–380.
[5] B.S. Petukhov, V.M. Zhukov, S.B. Anisimov, Cryogenic liquids forced boiling heat transfer in a rotating channel, Cryogenics 26 (1986) 226–233.
[6] V.I. Romanov, A.L. Sevryugin, Yu.M. Pavlov, V.I. Antipov, Investigating burnouts with helium boiling in a channel, Teploenergetika 28 (1981) 620–622.
[7] H. Tatsumoto, Y. Shirai, M. Shiotsu, K. Hata, H. Kobayashi, Y. Naruo, Y. Inatani, T. Kato, K. Kinoshita, Forced convection heat transfer of subcooled liquid hydrogen in a small tube, in: Proc. of ICEC23-ICMC, 2010, pp. 491–496.
[8] Y. Shirai, H. Tatsumoto, M. Shiotsu, K. Hata, H. Kobayashi, Y. Naruo, Y. Inatani, K. Kinoshita, Forced flow boiling heat transfer of liquid hydrogen for superconductor cooling, Cryogenics 51 (2011) 295–299.
[9] H. Tatsumoto, Y. Shirai, M. Shiotsu, K. Hata, Y. Naruo, H. Kobayashi, Y. Inatani, K. Kinoshita, Forced convection heat transfer of subcooled liquid hydrogen in horizontal tubes, in: AIP Conference Proceedings, 1434, 2012, pp. 747–754.
[10] H. Tatsumoto, Y. Shirai, M. Shiotsu, K. Hata, Y. Naruo, H. Kobayasi, Y. Inatani, Forced convection heat transfer of saturated liquid hydrogen in vertically–mounted heated pipes, in: AIP Conference Proceedings, 1573, 2014, pp. 44–51.
[11] T. Matsumoto, Y. Shirai, M. Shiotsu, K. Fujita, Y. Iwami, Y. Naruo, H. Kobayashi, S. Nonaka, Y. Inatani, Film boiling heat transfer properties of liquid hydrogen flowing inside of heated pipe, IOP Conference Series: Materials Science and Engineering 502 (2019) 012090.
[12] T.C. Core, J.F. Harkee, B. Misra, K. Sato, Heat-transfer studies, Aerojet-General Corporation Technical Document, 1959 TID/SNA-164.
[13] C.C. Wright, H.H. Walters, Single tube heat transfer tests—Gaseous and liquid hydrogen, Wright Air Development Center, 1959 Technical Report 59-423.
[14] J.P. Lewis, J.H. Goodykoontz, J.F. Kline, Boiling heat transfer to liquid hydrogen and nitrogen in forced flow, National Aeronautics and Space Administration Technical Note D-1314, 1962.
[15] H. Tatsumoto, Y. Shirai, K. Hata, T. Kato, M. Futakawa, M. Shiotsu, Forced convection heat transfer of subcooled liquid nitrogen in a vertical tube, In Journal of Physics: Conference Series 234 (2010) 032057.
[16] H. Tatsumoto, Y. Shirai, K. Hata, T. Kato, M. Shiotsu, Forced convection heat transfer of subcooled liquid nitrogen in horizontal tube, AIP Conference Proceedings 985 (2008) 665–672.
[17] J. Van Noord, A heat transfer investigation of liquid and two-phase methane, National Aeronautics and Space Administration Technical Memorandum, 2010 2010-216918.
[18] A. Trejo, M.J. Galvan, A.G. Trujillo, A.R. Choudhuri, Experimental investigation of liquid methane convection and boiling in rocket engine cooling channels, in: 50th AIAA/ASME/SAE/ASEE Joint Propulsion Conference, 2014, pp. 4007–4022.
[19] A. Trejo, C. Garcia, A. Choudhuri, Experimental investigation of transient forced convection of liquid methane in a channel at high heat flux conditions, Exp. Heat Transf. 29 (2016) 97–112.
[20] A. Trejo, A. Trujillo, M. Galvan, A. Choudhuri, J.C. Melcher, J.J. Bruggemann, Experimental investigation of methane convection and boiling in rocket engine cooling channels, J. Thermophys. Heat Transf. 30 (2016) 937–945.

[21] M.L. Meyer, L.A. Arrington, J.E. Kleinhenz, W.M. Marshall, Testing of a liquid oxygen/liquid methane reaction control thruster in a new altitude rocket engine test facility, National Aeronautics and Space Administration Technical Memorandum, 2012 2012-217643.
[22] W.H. Robbins, H.B. Finger, An historical perspective of the NERVA nuclear rocket engine technology program, National Aeronautics and Space Administration Contractor Report 187154 (1991).
[23] J.L. Felder, H.D. Kim, G.V. Brown, Turboelectric distributed propulsion engine cycle analysis for hybrid-wing-body aircraft, in: 47th AIAA Aerospace sciences meeting including the new horizons forum and aerospace exposition, 2009, pp. 1132–1156.
[24] D. Chen, Y. Shi, Experimental study on flow boiling heat transfer of LNG in a vertical smooth tube, Cryogenics 57 (2013) 18–25.
[25] D. Chen, Y. Shi, Study on two-phase pressure drop of LNG during flow boiling in a 8 mm horizontal smooth tube, Exp. Therm. Fluid. Sci. 57 (2014) 235–241.
[26] E.W. Lemmon, I.H. Bell, M.L. Huber, M.O. McLinden, NIST standard reference database 23: Reference fluid thermodynamic and transport properties-REFPROP, version 10.0, Standard Reference Data Program, National Institute of Standards and Technology, Gaithersburg, 2018.
[27] D. Steiner, E.U. Schlünder, Heat transfer and pressure drop for boiling nitrogen flowing in a horizontal tube: 1. Saturated flow boiling, Cryogenics 16 (1976) 387–398.
[28] S.A. Klein, EES – Engineering Equation Solver, Version 10.834-3D, [2020-05-27].
[29] V. Ganesan, R. Patel, J. Hartwig, I. Mudawar, Universal critical heat flux (CHF) correlations for cryogenic flow boiling in uniformly heated tubes, Int. J. Heat Mass Transfer 166 (2021) 120678.
[30] F.W. Dittus, L.M.K Boelter, Heat transfer in automobile radiators of the tubular type, Int. Comm. Heat Mass Transfer 12 (1985) 3–22.
[31] D. Steiner, J. Taborek, Flow boiling heat transfer in vertical tubes correlated by an asymptotic model, Heat Transfer Eng 13 (1992) 43–69.
[32] D. Steiner, Wärmeübertragung beim sieden gesättigter flüssigkeiten, Sect. Hbb, VDI Wärmeatlas: VDI Verlag Düsseldorf, 1988.
[33] V. Gnielinski, Forced convection in ducts, Hemisphere Handbook of Heat Exchanger Design, Hemisphere, New York, 1990.
[34] D. Gorenflo, P. Sokol, Prediction method of pool boiling heat transfer with cryogenic liquids, Int. J. Refrig. 11 (1988) 315–320.
[35] H.K. Forster, N. Zuber, Dynamics of vapor bubbles and boiling heat transfer, A.I.Ch.E. J. 1 (1955) 531–535.
[36] S.M. Zivi, Estimation of steady-state steam void-fraction by means of the principle of minimum entropy production, ASME J. Heat Transfer 86 (1964) 247–252.
[37] R.W. Lockhart, R.C. Martinelli, Proposed correlation of data for isothermal two-phase, two-component flow in pipes, Chem. Eng. Progr. 45 (1949) 39–48.
[38] Y. Qiu, D. Garg, L. Zhou, C.R. Kharangate, S.M. Kim, I. Mudawar, An artificial neural network model to predict mini/micro-channels saturated flow boiling heat transfer coefficient based on universal consolidated data, Int. J. Heat Mass Transfer 149 (2020) 119211.
[39] W.M. Rohsenow, A method of correlating heat transfer data for surface boiling of liquids, ASME Trans 74 (1952) 969–976.
[40] V.E. Schrock, L.M. Grossman, Forced Convection Boiling in Tubes, Nucl. Sci. Eng. 12 (1962) 474–481.
[41] J.C. Chen, Correlation for boiling heat transfer to saturated fluids in convective flow, Ind. Eng. Chem. Process Des. Dev. 5 (1966) 322–329.
[42] K.E. Gungor, R.H.S. Winterton, Simplified general correlation for saturated flow boiling and comparisons of correlations with data, Chem. Eng. Res. Des. 65 (1987) 148–156.
[43] M.M. Shah, Chart correlation for saturated boiling heat transfer: equations and further study, ASHRAE Trans 88 (1982) 185–196.
[44] V.V. Klimenko, A generalized correlation for two-phase forced flow heat transfer—second assessment, Int. J. Heat Mass Transfer 33 (1990) 2073–2088.
[45] M.M. Shah, Prediction of heat transfer during boiling of cryogenic fluids flowing in tubes, Cryogenics 24 (1984) 231–236.
[46] M.M. Shah, A new correlation for heat transfer during boiling flow through pipes, ASHRAE Trans 82 (1976) 66–86.
[47] K.E. Gungor, R.H.S. Winterton, A general correlation for flow boiling in tubes and annuli, Int. J. Heat Mass Transfer 29 (1986) 351–358.
[48] Z. Liu, R.H.S. Winterton, A general correlation for saturated and subcooled flow boiling in tubes and annuli, based on a nucleate pool boiling equation, Int. J. Heat Mass Transfer 34 (1991) 2759–2766.
[49] S.M. Kim, I. Mudawar, Universal approach to predicting saturated flow boiling heat transfer in mini/micro-channels – Part II. Two-phase heat transfer coefficient, Int. J. Heat Mass Transfer 64 (2013) 1239–1256.
[50] M.G. Cooper, Saturation nucleate pool boiling – a simple correlation, I. Chem. Eng. Symp. Ser. 86 (1984) 785–793.
[51] V.V Klimenko, M.V. Fyodorov, Y.A. Fomichyov, Channel orientation and geometry influence on heat transfer with two-phase forced flow of nitrogen, Cryogenics 29 (1989) 31–36.
[52] L.E. Dean, L.M. Thompson, K.R. Stehling, T.F. Reinhardt, W.M. Smith, Heat transfer characteristics of liquid nitrogen, Bell Aircraft Corporation, 1955 Report No. 56-982-035.
[53] H.H. Walters, Single-tube heat transfer tests with liquid hydrogen, Adv. Cryog. Eng. 6 (1961) 509–516.
[54] J.H. Jones, M. Altman, Two-phase flow and heat transfer for boiling liquid nitrogen in horizontal tubes, In Chem. Eng. Prog. Symp. Ser. 61 (1965) 205–212.
[55] J.W.H. Chi, Forced convective boiling heat transfer to hydrogen, J. Spacecr. Rockets 3 (1966) 150–152.
[56] M.R. Glickstein, R.H. Whitesides, Forced-convection nucleate and film boiling of several aliphatic hydrocarbons, in: ASME-AIChE Heat Transfer Conference and Exhibit, 1967, pp. 1–8. 67-HT-7.
[57] V.E. Keilin, E.Y. Klimenko, I.A. Kovalev, Device for measuring pressure drop and heat transfer in two-phase helium flow, Cryogenics 9 (1969) 36–38.
[58] S.J. Hynek, W.M. Rohsenow, A.E. Bergles, Forced-convection dispersed-flow film boiling, Office of Scientific, 1969 and Technical Information Report DSR 70586-63.
[59] M. Jergel, R. Stevenson, Heat transfer to liquid helium in narrow channels with laminar and turbulent flow, Appl. Phys. Lett. 17 (1970) 125–127.
[60] M. Jergel, R. Stevenson, Static heat transfer to liquid helium in open pools and narrow channels, Int. J. Heat Mass Transfer 14 (1971) 2099–2107.
[61] M. Jergel, K. Hechler, R. Stevenson, The effect of forced circulation on heat transfer with liquid helium in narrow channels, Cryogenics 10 (1970) 413–417.
[62] M. Jergel, I. Hlasnik, A few remarks on the heat transfer in helium liquid—gas flow, Cryogenics 13 (1973) 676–678.
[63] V.I. Antipov, V.A. Grigoriev, J.I. Krokhin, A.S. Kulikov, Heat transfer with nitrogen boiling in capillaries, Proc. of 14th International Congress of Refrigeration 14 (1975) 337–351.
[64] S.S. Papell, R.C. Hendricks, Boiling incipience and convective boiling of neon and nitrogen, National Aeronautics and Space Administration Technical Memorandum X-73615, 1977.
[65] S.S. Papell, R.C. Hendricks, Boiling incipience and convective boiling of neon and nitrogen, Adv. Cryog. Eng. 23 (1978) 284–294.
[66] B.S. Petukhov, V.M. Zhukov, V.M. Shieldcret, Investigation of heat transfer and hydrodynamics in the helium two-phase flow in a vertical channel, in: Advanced Course in Heat Exchangers: Theory and Practice, ICHMT Symposium, 1981, pp. 251–262.
[67] V.I. Subbotin, V.I. Deev, A.I. Pridantsev, V.K. Andreev, V.V. Arkhipov, V.N. Novikov, A.N. Savin, V.V. Solodovnikov, Heat transfer and hydrodynamics in cooling channels of superconducting devices, Cryogenics 25 (1985) 261–265.
[68] D. Steiner, Heat transfer during flow boiling of cryogenic fluids in vertical and horizontal tubes, Cryogenics 26 (1986) 309–318.
[69] H. Umekawa, N. Ishida, Dryout and post-dryout heat transfer in a natural circulation loop of liquid nitrogen, Heat Transfer—Japanese Research 26 (1997) 449–458.
[70] W. Lu, Forced convective boiling in liquid nitrogen from discrete heat sources, University of Kentucky, 1998 Ph.D. Thesis.
[71] A.V. Klimenko, A.M. Sudarchikov, Investigation of hydrodynamic instability at a forced flow boiling of nitrogen in a channel at high pressures, in: Proc. of International Heat Transfer Conference, 2002, p. 12.
[72] L. Benkheira, B. Baudouy, M. Souhar, Heat transfer characteristics of two-phase He I (4.2 K) thermosiphon flow, Int. J. Heat Mass Transfer 50 (2007) 3534–3544.
[73] S.L. Qi, P. Zhang, R.Z. Wang, L.X. Xu, Flow boiling of liquid nitrogen in micro-tubes: Part I–The onset of nucleate boiling, two-phase flow instability and two-phase flow pressure drop, Int. J. Heat Mass Transfer 50 (2007) 4999–5016.
[74] R. Yun, J.S. Hwang, J.T. Chung, Y. Kim, Flow boiling heat transfer characteristics of nitrogen in plain and wire coil inserted tubes, Int. J. Heat Mass Transfer 50 (2007) 2339–2345.
[75] X. Fu, S.L. Qi, P. Zhang, R.Z. Wang, Visualization of flow boiling of liquid nitrogen in a vertical mini-tube, Int. J. Multiph. Flow 34 (2008) 333–351.
[76] P. Zhang, X. Fu, Two-phase flow characteristics of liquid nitrogen in vertically upward 0.5 and 1.0 mm micro-tubes: visualization studies, Cryogenics 49 (2009) 565–575.
[77] X. Fu, P. Zhang, C.J. Huang, R.Z. Wang, Bubble growth, departure and the following flow pattern evolution during flow boiling in a mini-tube, Int. J. Heat Mass Transfer 53 (2010) 4819–4831.
[78] X. Fu, P. Zhang, Q. Bao, R.Z. Wang, Heat transfer characteristics of convective boiling of liquid nitrogen in microchannel heat sinks, Journal of Engineering Thermophysics 32 (2011) 811–815.
[79] S. Mustafi, High Reynolds number vertical up-flow parameters for cryogenic two-phase helium I, University of Maryland, 2014 Ph.D. Thesis.
[80] D. Deng, S.W. Xie, X.D. Li, R.S. Wang, Flow boiling heat transfer of liquid nitrogen in heated U-tubes, J. Heat Transfer 136 (2014) 024501.
[81] K. Yoneda, Y. Shirai, M. Shiotsu, Y. Oura, Y. Horie, T. Matsuzawa, H. Shigeta, H. Tatsumoto, K. Hata, Y. Naruo, H. Kobayashi, Y. Inatani, Forced flow boiling heat transfer properties of liquid hydrogen for manganin plate pasted on one side of a rectangular duct, Physics Procedia 67 (2015) 637–642.
[82] H. Tatsumoto, Y. Shirai, M. Shiotsu, Y. Naruo, H. Kobayashi, Y. Inatani, Transient heat transfer from a wire inserted into a vertically mounted pipe to forced flow liquid hydrogen, Physics Procedia 67 (2015) 649–654.
[83] A.M. Sudarchikov, Onset of boiling of liquid in channel, High Temperature 54 (2016) 873–877.
[84] X. Liu, X. Chen, Q. Zhang, S. Wang, Y. Hou, L. Chen, Investigation on CHF of saturated liquid nitrogen flow boiling in a horizontal small channel, Appl. Therm. Eng. 125 (2017) 1025–1036.
[85] T. An, Y. Wang, W.Q. Liu, Experimental investigation of heat transfer characteristics of liquid nitrogen flow boiling in a mini-channel, Int. Heat Transfer Conf, Digital Library (2018) 6479–6485.

[86] C. Johannes, Studies of forced convection heat transfer to helium I, Adv. Cryog. Eng. 17 (1972) 352–360.
[87] M.C. Jones, W.W Johnson, Heat transfer and flow of helium in channels–practical limits for applications in superconductivity, 675, National Bureau of Standards Technical Note, 1976.
[88] G. Klein, Heat transfer for evaporating nitrogen streaming in a horizontal tube, in: Proc. 6th Int. Cryo. Eng. Conf, 1976, pp. 314–318.
[89] V.V. Klimenko, A.M. Sudarchikov, Investigation of forced flow boiling of nitrogen in a long vertical tube, Cryogenics 23 (1983) 379–385.
[90] V.I. Subbotin, V.I. Deev, V.V. Solodovnikov, V.V. Arkhipov, Heat transfer in two-phase flow of helium, Int. Heat Transfer Conf, Digital Library (1986) 2343–2348.
[91] V.V. Klimenko, Y.A. Fomichev, A.V. Grigor'ev, An experimental investigation of heat transfer with evaporation of liquid nitrogen in a vertical channel, Teploenergetika 34 (1987) 45–48.
[92] P. Bredy, D. Neuveglise, M.X. Francois, C. Meuris, R. Duthil, Test facility for helium I two phase flow study, Cryogenics 34 (1994) 361–364.
[93] J. Panek, X. Huang, S.W. Van Sciver, Localized heat transfer to vertical forced flow two-phase helium, Adv. Cryog. Eng. 41 (1996) 173–177.
[94] P.J. Giarratano, R.C. Hess, M.C. Jones, Forced convection heat transfer to subcritical helium I, Adv. Cryog. Eng. 19 (1995) 404–416.
[95] Q. Zhang, J. Chen, J. Li, J. Cao, L. Chen, Y. Hou, Experimental study on saturated flow boiling heat transfer of nitrogen in a small-diameter horizontal heated tube, Exp. Therm. Fluid. Sci. 86 (2017) 257–271.
[96] S. Chen, X. Chen, L. Chen, Q. Zhang, Y. Hou, Experimental study on the heat transfer characteristics of saturated liquid nitrogen flow boiling in small-diameter horizontal tubes, Exp. Therm. Fluid. Sci. 101 (2019) 27–36.
[97] B.C. Zhang, Q.L. Li, Y. Wang, J.Q. Zhang, J. Song, F.C. Zhuang, Experimental investigation of nitrogen flow boiling heat transfer in a single mini-channel, Journal of Zhejiang University-SCIENCE A 21 (2020) 147–166.
[98] U.H. von Glahn, J.P. Lewis, Nucleate-and film-boiling studies with liquid hydrogen, Adv. Cryog. Eng. 5 (1960) 262–269.
[99] V.A. Grigoriev, Yu.M. Pavlov, E.V. Ametistov, V.I. Antipov, Heat transfer in boiling helium to superconducting elements in power generating equipment, Future energy production systems. Heat and mass transfer processes, Volume I (1976) 261–268.
[100] V.A. Grigor'ev, V.I. Antipov, Y.M. Pavlov, A.V. Klimenko, Experimental investigation of heat transfer with boiling of nitrogen and helium in tubes, Teploenergetika 24 (1977) 11–14.
[101] Y. Katto, S. Yokoya, Critical heat flux of forced convective boiling in uniformly heated vertical tubes with special reference to very large length-to-diameter ratios, Int. J. Heat Mass Transfer 30 (1987) 2261–2269.
[102] C.F. Coolebrook, Turbulent flow in pipes with particular reference to the transition region between the smooth and rough pipes laws, J. Inst. Civ. Eng. 11 (1939) 133–156.
[103] S.L. Qi, P. Zhang, R.Z. Wang, L.X. Xu, Flow boiling of liquid nitrogen in micro–tubes: Part II–Heat transfer characteristics and critical heat flux, Int. J. Heat Mass Transfer 50 (2007) 5017–5030.
[104] V. Mohr, R. Runge, in: Forced convection boiling of neon in horizontal tubes, Hemisphere Publishing Corporation, New York, 1977, pp. 307–343.
[105] H.M. Muller, W. Bonn, D. Steiner, Heat transfer and critical heat flux at flow boiling of nitrogen and argon within a horizontal tube, in: Advanced Course in Heat Exchangers: Theory and Practice. ICHMT Symposium, 1981, pp. 233–250.
[106] V.E. Keilin, I.A. Kovalev, V.V. Likov, M.M. Pozvonkov, Forced convection heat transfer to liquid helium I in the nucleate boiling region, Cryogenics 15 (1975) 141–145.
[107] I.L. Yarmak, V.M. Zhukov, Forced liquid helium flow transient heat transfer in a narrow channel under step heat flux, Cryogenics 32 (1992) 729–736.
[108] B. Xu, Y. Shi, D. Chen, Z. Yu, Heat transfer characteristics during flow boiling of liquid nitrogen in vertical tube, CIESC Journal 65 (2014) 460–467.
[109] P.A. Kew, K. Cornwell, Correlations for the prediction of boiling heat transfer in small-diameter channels, Appl. Therm. Eng. 17 (1997) 705–715.
[110] G.F. Chen, M.Q. Gong, S. Wang, J.F. Wu, X. Zou, New flow boiling heat transfer model for hydrocarbons evaporating inside horizontal tubes, in: AIP Conference Proceedings, 1573, 2014, pp. 1092–1098.
[111] S. Wang, M.Q. Gong, G.F. Chen, Z.H. Sun, J.F. Wu, Flow boiling heat transfer characteristics of methane in a horizontal tube, in: AIP Conference Proceedings, 1573, 2014, pp. 1512–1518.
[112] M. Gong, Q. Song, G. Chen, X. Zhuang, Z. Yang, Y. Yao, Boiling heat transfer characteristics for methane, ethane and their binary mixtures, Heat Transf. Eng. 41 (2020) 1–16.
[113] Z.J. Yu, Study on flow friction and characteristics of heat transfer of liquid nitrogen boiling, Shanghai Jiao Tong University, 2012 Master's Thesis.
[114] X. Fang, A.M. Sudarchikov, Y. Chen, A. Dong, R. Wang, Experimental investigation of saturated flow boiling heat transfer of nitrogen in a macro-tube, Int. J. Heat Mass Transfer 99 (2016) 681–690.
[115] H. Umekawa, M. Ozawa, T. Yano, Boiling two-phase heat transfer of LN_2 downward flow in pipe, Exp. Therm. Fluid. Sci. 26 (2002) 627–633.
[116] MATLAB Global Optimization Toolbox, The MathWorks Inc., Natick, MA, 2018 R2018b, Version 9.5.0.944444.
[117] H. Zhang, I. Mudawar, M.M. Hasan, Experimental and theoretical study of orientation effects on flow boiling CHF, Int. J. Heat Mass Transfer 45 (2002) 4463–4478.
[118] C. Konishi, I. Mudawar, Review of flow boiling and critical heat flux in microgravity, Int. J. Heat Mass Transfer 80 (2015) 469–493.
[119] S.M. Kim, I. Mudawar, Universal approach to predicting saturated flow boiling heat transfer in mini/micro-channels – Part I. Dryout incipience quality, Int. J. Heat Mass Transfer 64 (2013) 1226–1238.
[120] D. Mikielewicz, J. Mikielewicz, J. Tesmar, Improved semi-empirical method for determination of heat transfer coefficient in flow boiling in conventional and small diameter tubes, Int. J. Heat Mass Transfer 50 (2007) 3949–3956.
[121] S.M. Kim, I. Mudawar, Theoretical model for annular flow condensation in rectangular micro-channels, Int. J. Heat Mass Transfer 55 (2012) 958–970.
[122] H. Lee, C.R. Kharangate, N. Mascarenhas, I. Park, I. Mudawar, 2015 I., Experimental and computational investigation of vertical downflow condensation, Int. J. Heat Mass Transfer 85 (2015) 865–879.